V. L. Mironov

The textbook for students of the senior courses
of higher educational institutions

Fundamentals of the scanning probe microscopy

THE RUSSIAN ACADEMY OF SCIENCES
INSTITUTE OF PHYSICS OF MICROSTRUCTURES

Nizhniy Novgorod

2004

V. L. Mironov
The textbook for students of the senior courses of higher educational institutions

THE RUSSIAN ACADEMY OF SCIENCES INSTITUTE
OF PHYSICS OF MICROSTRUCTURES

Nizhniy Novgorod
2004

Abstract

This work is a text-book for senior and magistracy students, dedicated to one of the most modern solid-state body surface research techniques – Scanning Probe Microscopy (SPM). The book considers the basic SPM types: Scanning Tunnel Microscopy (STM), Atomic Force Microscopy (AFM), Electric Force Microscopy (EFM), Magnetic Force Microscopy (MFM), Near-field Optical Microscopy (NOM), which have found the most widespread application in scientific research activities.

Foreword 4

Introduction 5

1. The scanning probe microscopy technique 6
   1.1. Principles of work of scanning probe microscopes 6
   1.2. Scanning elements (scanners) of probe microscopes 7
   1.3. Devices for precise movements a tip and a sample 13
   1.4. Protection of probe microscopes against external influences 17
   1.5. Formation and processing of SPM images 22

2. Modes of the scanning probe microscopy 37
   2.1. Scanning tunnel microscopy 37
   2.2. Atomic force microscopy 53
   2.3. Electric force microscopy 76
   2.4. Magnetic force microscopy 79
   2.5. Near-field optical microscopy 87

Conclusion 94

Basic stages of STM development 95

REFERENCES 97

Foreword

This textbook is written on the basis of the course of lectures read by the author in 2002 – 2003 to students of the senior courses of radio-physical faculty and "Higher school of the general and applied physics" faculty of Nizhniy Novgorod State University. One of the reasons to write this book was the full absence of the educational literature on methods of the scanning probe microscopy in Russian language. While there are many educational textbooks in English (here, first of all, I would like to mention D.Sarida's [Lit. 1] excellent book, which has been partially used when writing the given textbook), only few domestic works of survey character [Lit. 2-Lit. 8], which can be used to train students, are known at present. Mainly, the textbooks issued in Bashkiria State University [Lit. 11] and materials on Internet sites [Lit. 12, Lit. 13] can be used for the educational purposes.

The textbook has been written in short terms (actually, in two months) by request of the "NT-MDT" company (Zelenograd), making scanning probe microscopes for scientific researches and special SPM complexes to train students on the probe microscopy modes. Probably, due to the so short term allocated for writing, this book has some drawbacks. I will be grateful to everyone who will inform about the noticed mistakes, inaccuracies and other possible lacks.

The writing of the given textbook, in many respects, was inspired by S.V.Gaponov - the director of Institute of physics of microstructures of the Russian Academy of Science, corresponding member of the Russian Academy of Science. Taking an opportunity, I express gratitude to IPM RAS employees D.G.Volgunov, S.A.Treskov and O.G.Udalov for numerous fruitful discussions; V.N.Rjabokon ("NT-MDT") for critical and constructive reviewing of the given work; G.V.Mironova for a careful proof-reading of the manuscript. I express also the sincere gratitude to the "NT-MDT" company (Zelenograd), especially to V.A.Bykov and A.V.Bykov, for ideological and material support of the publishing project.

V.L.Mironov

Introduction

The scanning probe microscopy (SPM) is one of powerful modern research techniques of morphology and local properties of the solid body surface with high spatial resolution. During last 10 years the scanning probe microscopy has turned from an exotic technique accessible only to a limited number of research groups, to a widespread and successfully used research tool of surface properties. Currently, practically every research in the field of physics of surface and thin-film technologies applies the SPM techniques. Development of the scanning probe microscopy has formed also a basis for development of new methods in the nanotechnology – technology of creation of structures with nanometric scales.

The scanning tunnel microscope (STM) is the first in the probe microscopes family; it was invented in 1981 by the Swiss scientists Gerd Binnig and Heinrich Rohrer [Lit. 14, Lit. 15]. In their works they have shown, that this is a quite simple and rather effective way of research of a surface with the spatial resolution down to atomic one. The given technique was truly recognized after visualization of the atomic structure of a surface of some materials and, particularly, the reconstructed surface of silicon. In 1986, G.Binnig and H.Rohrer were awarded the Nobel Prize on physics for creation of a tunnel microscope.

After the tunnel microscope creation, atomic force microscope (AFM), magnetic force microscope (MFM), electric force microscope (EFM), near-field optical microscope (NOM) and many other devices having similar principles of work and named as scanning probe microscopes have been created in a short period of time. Now the probe microscopy is a rapidly developing area of technology and applied scientific researches.

1. The scanning probe microscopy technique

1.1. Principles of work of scanning probe microscopes

Research of a surface microrelief and its local properties is performed by scanning probe microscopes using specially prepared tips in the form of needles. The working part of such tips (the apex) has the size about ten nanometers. The characteristic distance between a tip and a surface of samples in probe microscopes makes about 0.1 – 10 nanometers. Various types of interaction of a tip with a surface lay in the basis of probe microscopes work. So, work of a tunnel microscope is based on the phenomenon of a tunnel current flowing between a metal needle and a conducting sample; various types of force interaction underlie the work of atomic force, magnetic force and electric force microscopes. We will consider the common features inherent to various probe microscopes. Let the interaction of a tip with a surface be characterized by some parameter P. If there is a sharp enough and biunique dependence of the parameter P on the tip-sample distance $P = P(z)$, then the given parameter can be used organize the feedback system (FS) supervising the distance between a tip and a sample. The general principle of feedback organization of a scanning probe microscope is schematically shown on Fig. 1.

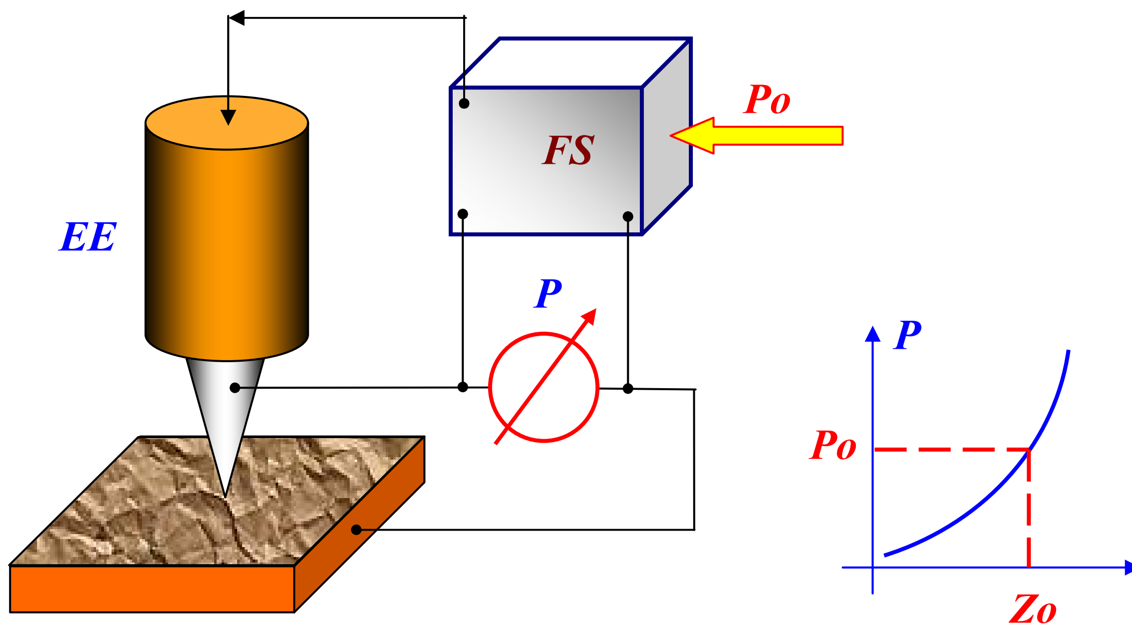

Fig. 1. The feedback system organization circuit of a probe microscope

The feedback system keeps the P parameter value constant and equal to Po value, set by the operator. If the tip-sample distance changes (for example, increases), there is a change (increase) in parameter P. In the feedback system a differential signal is formed proportional to $\Delta P = P - P_o$ value, which increases up to the necessary value and is passed to the executive element EE. The executive element executes this differential signal, approaching the tip to the surface or retracting it until the differential signal does not become equal to zero. Thus it is possible to support the tip-sample distance with high accuracy. In existing probe microscopes the accuracy of keeping the tip-surface distance reaches the value of ~ 0.01 Å. During tip movement along the sample surface there is a change of the P parameter of interaction, caused by the topography of a surface. The feedback

system executes these changes so that when the tip is moved in X, Y planes, the signal on the executive element appears proportional to the topography of a surface. The specially organized process of sample scanning is performed in order to obtain the SPM image. During scanning the tip first moves above a sample along the certain line (line scan), thus the value of a signal on the executive element, proportional to the topography of a surface, is recorded in memory of a computer. Then the tip comes back to the initial point and passes to the next scanning line (frame scan), and the process repeats again. The feedback signal recorded in this manner during scanning is processed by a computer, and then the SPM image of surface topography $Z = f(x, y)$ is plotted by means of computer graphics. Alongside with research of the topography of a surface, probe microscopes allow to study various properties of a surface: mechanical, electric, magnetic, optical and many others.

1.2. Scanning elements (scanners) of probe microscopes

It is necessary to supervise the working tip-sample distance and to move the tip in the plane of a sample with high accuracy (at a level of Angstrem fractions) so that probe microscopes would work properly. This problem is solved with the help of special manipulators - scanning elements (scanners). Scanning elements of probe microscopes are made of piezoelectric materials – the materials having piezoelectric properties. Piezoelectric materials change their sizes in an external electric field. The inverse piezoeffect equation for crystals is as follows:

$$u_{ij} = d_{ijk} E_k ,$$

where u_{ij} - deformation tensor, E_k - components of an electric field, d_{ijk} - tensor components of piezoelectric coefficients. The tensor type of piezoelectric coefficients is defined by the type of crystals symmetry.

Converters made from piezoceramic materials are widely used in various technical applications. The piezoceramics represent the polarized polycrystalline material obtained by methods of powders sintering from crystal ferroelectrics. Polarization of ceramics is performed as follows. The ceramics is heated up above the Curie temperature (for the majority of piezoceramics this temperature is less than 300°C), and then is slowly cooled in a strong electric field (about 3 kV/cm). After cooling, piezoceramic has the induced polarization and gets the ability to change its sizes (increase or reduce depending on a mutual direction of a polarization vector and a vector of an external electric field). The basic characteristics of ceramic materials used in technical equipment can be found in the book [Lit. 16]. Piezoceramics represent the piezoelectric structures. The tensor type of piezoelectric constants for piezoceramics becomes essentially simpler – only three factors d_{33}, d_{31}, d_{15}, describing longitudinal, cross (in relation to a polarization vector) and shift deformations are not equal to zero. We shall consider a flat plate from piezoceramics (Fig. 2) in an external field. Let the polarization vector $\vec{P}$ and a vector of an electric field $\vec{E}$ be directed along the X axis. Then, designating $d_{\parallel} = d_{33}$ and $d_{\perp} = d_{31}$, we get that the deformation of piezoceramics in a direction parallel to a field is equal to $u_{xx} = d_{\parallel} E_x$, and in a direction perpendicular to a field it is $u_{rr} = d_{\perp} E_x$.

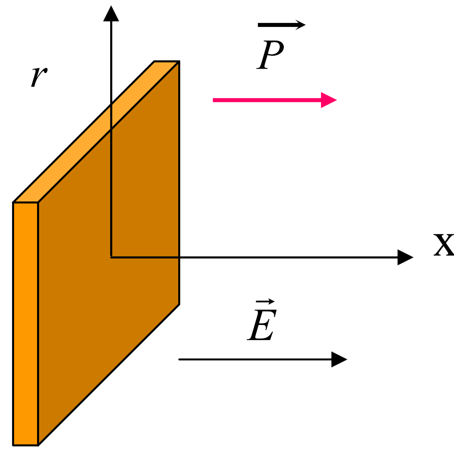

Fig. 2. Piezoceramic plate in an external electric field

Tubular piezoelements (Fig. 3) are widely used in the scanning probe microscopy. They allow obtaining big enough movements of objects at rather small control voltages. Tubular piezoelements represent hollow thin-walled cylinders made from piezoceramic materials. Usually electrodes, as thin layers of metal, are applied on external and internal surfaces of a tube, and end faces of a tube remain uncovered.

Fig. 3. Tubular piezoelement

Under the influence of a potential difference between internal and external electrodes the tube changes its longitudinal sizes. In this case the longitudinal deformation under influence of a radial electric field can be written down as:

$$u_{xx} = \frac{\Delta x}{l_0} = d_{\perp} E_r ,$$

where l_0 - length of a tube in an undeformed state. Absolute lengthening of the piezo-tube is equal to

$$\Delta x = d_{\perp} \frac{l_0}{h} V ,$$

where h – thickness of a piezo-tube wall, V - potential difference between internal and external electrodes. Thus, at the same V voltage the lengthening of a tube will be more with its length being more and its wall thickness being less.

Assembly of three tubes into one unit (Fig. 4) allows to organize precise movements of a tip of a microscope in three mutually perpendicular directions. Such scanning element is referred to as tripod.

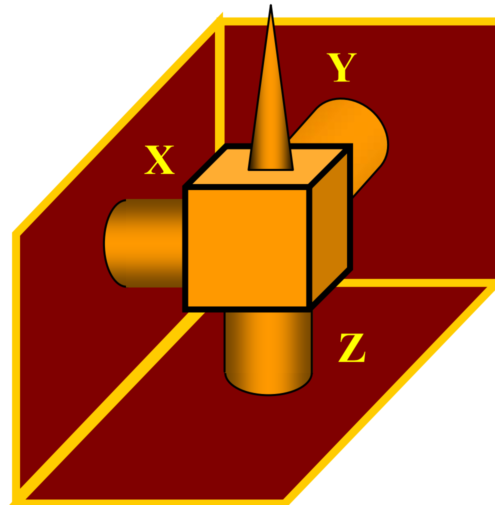

Fig. 4. Scanning element as tripod, assembled on tubular piezoelements

The drawbacks of such scanner are the complexity of manufacturing and strong asymmetry of its construction. For today the scanners made on the basis of one tubular element are most widely used in the scanning probe microscopy. The general view of a tubular scanner and arrangement of electrodes are presented on Fig. 5. The material of a tube has a radial direction of a polarization vector.

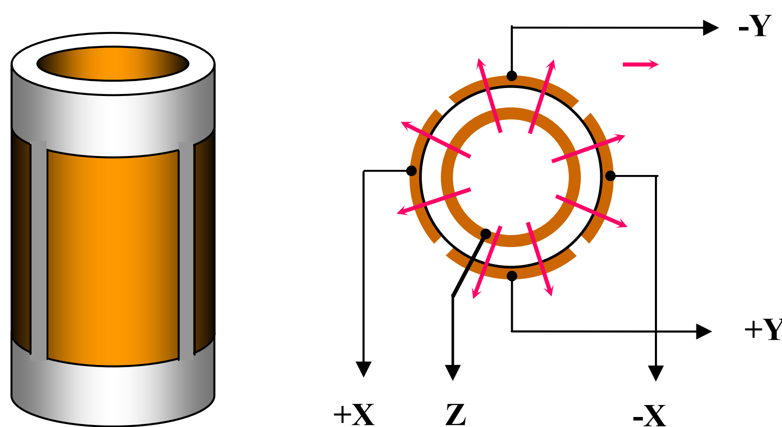

Fig. 5. Tubular piezo-scanner

The internal electrode is usually continuous. The external electrode of the scanner is divided by cylinder generatrixes into four sections. When differential-mode voltage is applied on opposite sections of an external electrode (in regard to internal electrode) part of a tube reduces in length in the place where the direction of a field coincides with the polarization direction, and increases where these directions are opposite to each other. This leads to a bend of a tube in a corresponding direction. Scanning in the X, Y plane is done in this manner. Change of an internal electrode potential relatively to all external sections results in lengthening or reduction of a tube on Z axis. Thus, it is possible to implement the three-coordinate scanner on the basis of one piezo-tube. Real

scanning elements frequently have a more complex construction; however principles of their work remain the same.

Scanners on the basis of bimorph cells are also widely used. Bimorph represents two plates of piezoelectric material which have been glued together in such a manner that polarization vectors in each of them are directed to the opposite sides (Fig. 6). If a voltage is applied on bimorph electrodes, as shown on Fig. 6, one of the plates will extend, and another one will be compressed, which will result in a bend of the whole element. In real constructions of bimorph elements the potential difference between the internal common electrode and external electrodes is created so that in one element the field coincides with the direction of a polarization vector, and in another element it is oppositely directed.

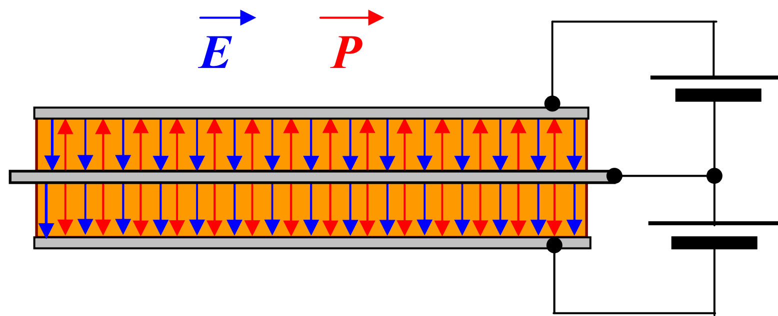

Fig. 6. Construction of a bimorph cell

The bimorph bend under influence of electric fields lies in the basis of bimorph piezo-scanners work. Combining three bimorph elements in one construction it is possible to implement a tripod on bimorph elements (Fig. 7).

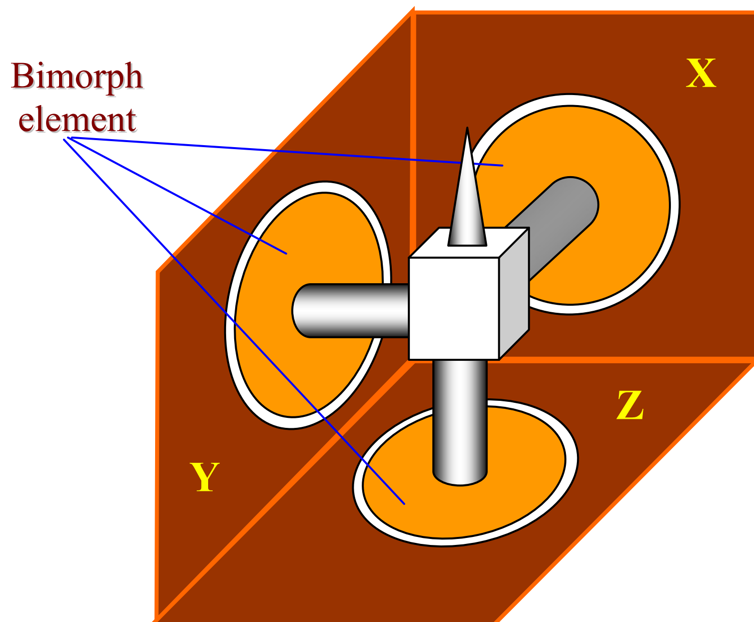

Fig. 7. Three-coordinate scanner on three bimorph elements

If external electrodes of a bimorph element are divided into four sectors, then it is possible to organize movement of a tip along the Z axis and in the X, Y plane on one bimorph element (Fig. 8).

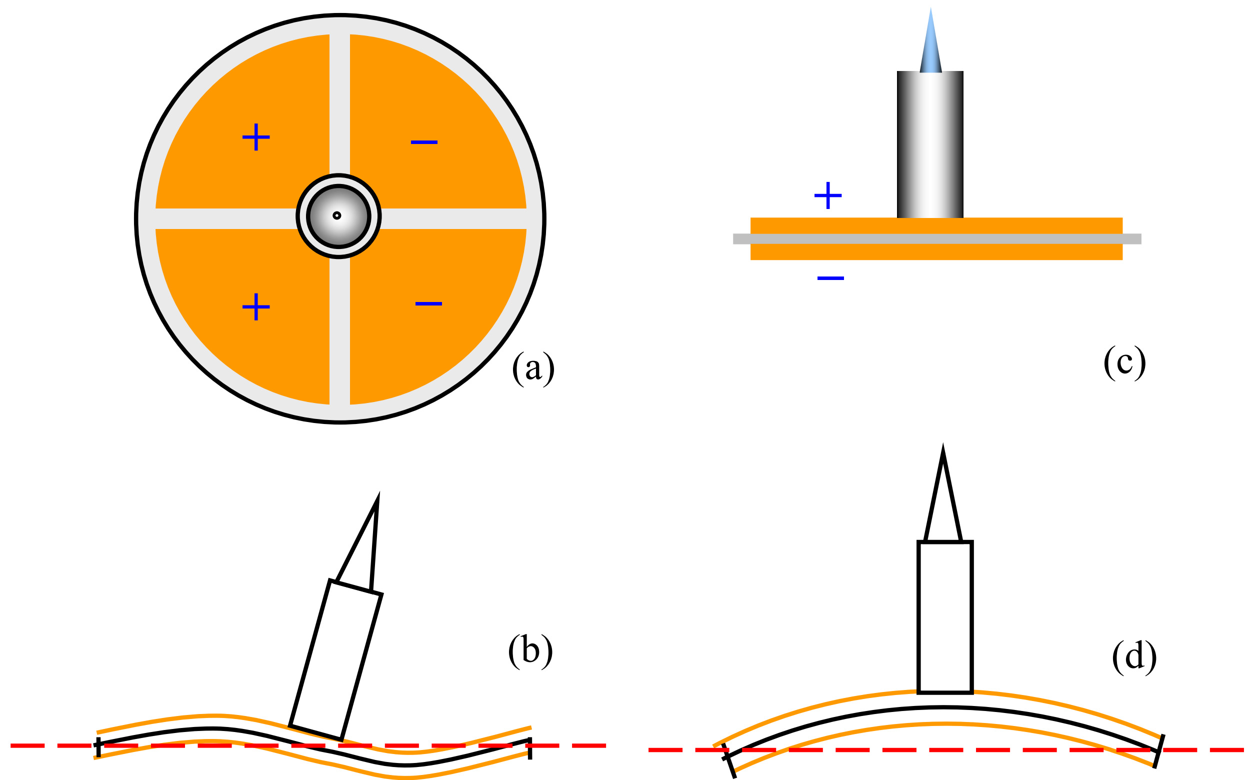

Fig. 8. Schematic representation of a bimorph piezo-scanner work

Indeed, applying a differential-mode voltage on opposite pairs of external electrodes sections makes it is possible to bend a bimorph so that the tip will move in the X, Y plane (Fig. 8 (a, b)). And changing the potential of an internal electrode in relation to all sections of external electrodes, it is possible to bend the bimorph, moving the tip in the Z axis direction (Fig. 8 (c, d)).

Piezoceramics nonlinearity

Despite of a number of technological advantages over crystals, piezoceramics have some deficiencies affecting negatively the work of scanning elements. One of such lacks is the nonlinearity of piezoelectric properties. Dependence of the piezo-tube shift size in Z direction on the value of the applied field is presented on Fig. 9 as an example. Generally (especially at large control fields) the piezoceramics are characterized by nonlinear dependence of deformation on the field (or on the control voltage). Thus, deformation of piezoceramics is a complex function of an external electric field:

$$u_{ij} = u_{ij}(\vec{E}).$$

For small control fields the given dependence can be represented in the following way:

$$u_{ij} = d_{ijk} E_k + \alpha_{ijkl} E_k E_l + ...,$$

where d_{ijk} and α_{ijkl} are linear and square-law modules of a piezoelectric effect.

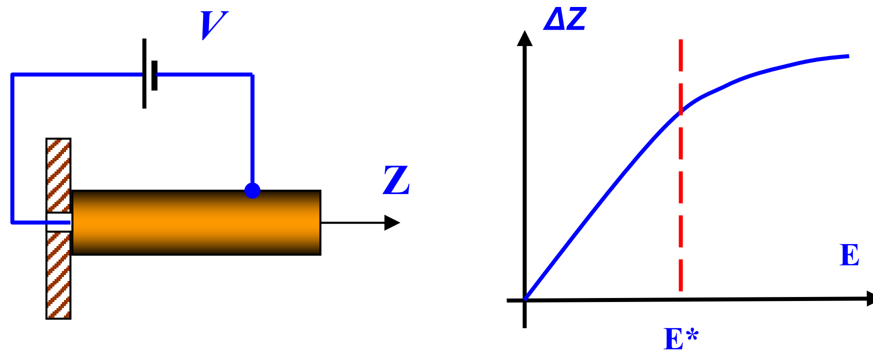

Fig. 9. Schematic representation of dependence of ceramics shift on the size of applied electric field

Typical values of E* fields, at which nonlinear effects start to affect, make about 100 V/mm. Therefore for the correct work of scanning elements the control fields are usually used in the area of ceramics linearity (E <E*).

Piezoceramics creep

Another drawback of piezoceramics is the so-called creep –delay of a reaction on the change of the control electric field value. Time diagrams of control fields change and corresponding shifts of the scanner along the Z axis and in the X, Y plane are schematically shown on Fig. 10.

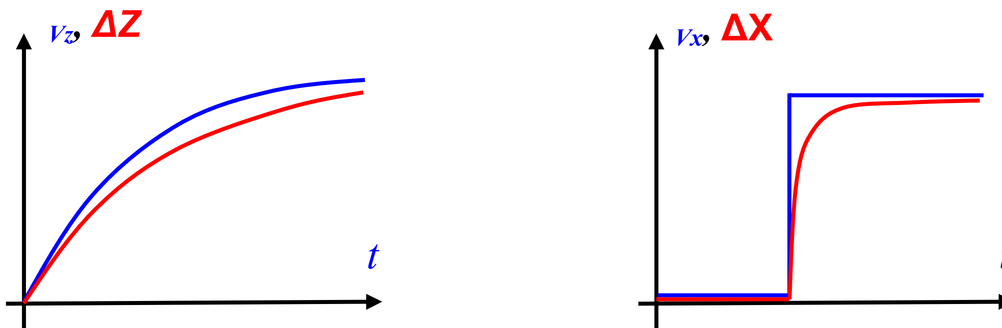

Fig. 10. Schematic time diagrams of change of a control field on a Z-electrode in a feedback circuit and on an X-electrode during scanning (shown in dark blue color). Red color schematically shows the dependences corresponding to reaction of the scanner on change of control voltages

The creep results in appearance of geometrical distortions in SPM images due to this effect. Specifically strong influence of the creep occurs when the scanner is moved to a reference point for conduction of local measurements and on initial stages of the scanning process. Time delays are used to reduce the ceramics creep influence on the specified processes, allowing partially to compensate the scanner delay.

Piezoceramics hysteresis

Another drawback of piezoceramics is the ambiguity of the lengthening dependence on a direction of electric field change (hysteresis).

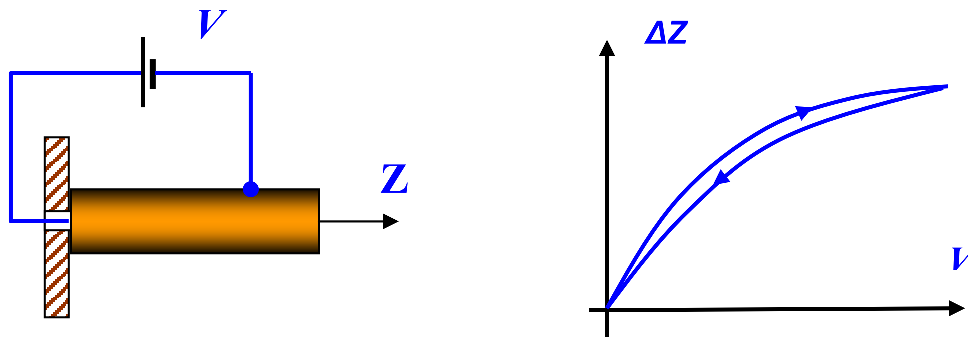

Fig. 11. Dependence of the piezo-tube shift size on the size and direction of the applied voltage

It leads to a situation when the piezoceramic appears in various points of a trajectory, with the same control voltages, depending on a direction of movement (Fig. 11). For exclusion of distortions in the SPM images caused by a piezoceramics hysteresis, registration of information during samples scanning is done only on one of the dependence branches $\Delta Z = f(V)$.

1.3. Devices for precise movements a tip and a sample

One of the important technical problems in the scanning probe microscopy is the necessity of precise moving of a tip and a sample with the purpose to create a working interval of a microscope and select a surface area to research. Various types of devices performing movements of objects with high accuracy are applied to solve this problem. Various mechanical reducers, in which coarse initial movements of a mover correspond to fine movements of a movable object, became widely spread. Ways of a reduction of movements can be various. Lever devices, in which the reduction of movement is performed due to a difference of length of shoulders of levers, are widely applied. The lever reducer is schematically presented on Fig. 12.

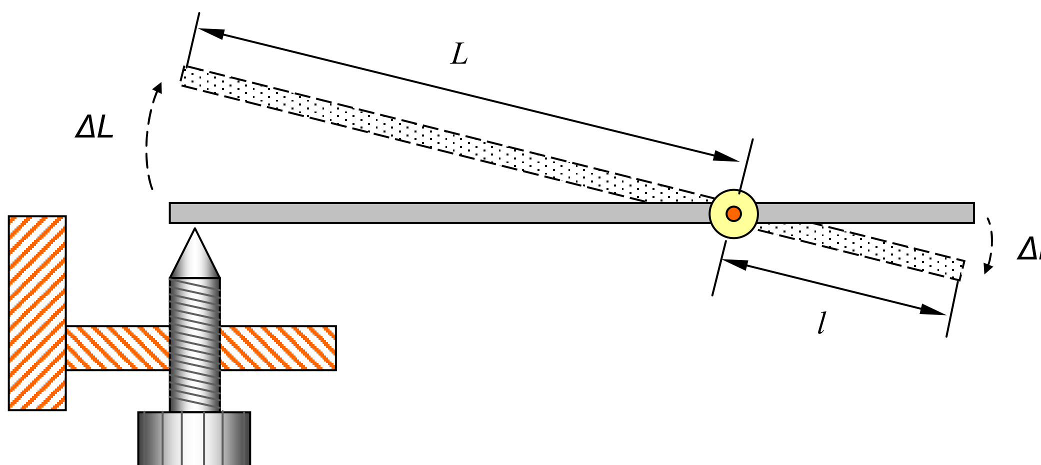

Fig. 12. Lever movement reducer schematic

The mechanical lever allows to receive reduction of moving with the following factor:

$$R = \frac{\Delta L}{\Delta l} = \frac{L}{l} \ .$$

Thus, the more is the relation of the *L* shoulder to the *l* shoulder, the more precisely the process of a tip approach to a sample can be controlled.

Mechanical reducers are also widely used in constructions of microscopes, in which the reduction of movements is achieved due to the difference of stiffness coefficients of two concatenated elastic elements (Fig. 13) are widely used. The construction consists of rigid base, spring and elastic beam. The *k* spring force and the *K* elastic beam stiffness are selected so that the following condition is satisfied: $k < K$.

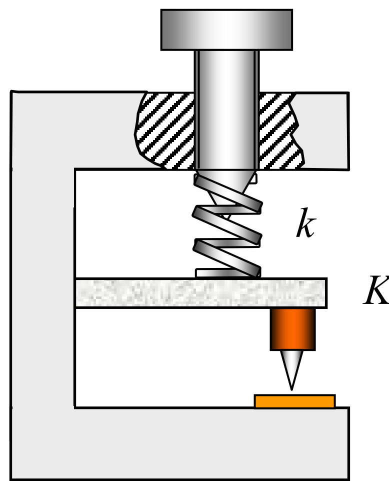

Fig. 13. Spring reducer of movements schematic

From the equilibrium condition it follows, that

$$F_{elast} = k \cdot \Delta l = K \cdot \Delta L \ ,$$

where Δl and ΔL - displacements of a spring and an elastic beam. In this case the reduction coefficient is equal to the relation of stiffness coefficients of elastic elements:

$$R = \frac{\Delta l}{\Delta L} = \frac{K}{k} \ .$$

Thus, the more is the relation of beam stiffness to spring force, the more precisely it is possible to control the displacement of a working element of a microscope.

Step-by-step electric motors

Step-by-step electric motors (SEM) represent electromechanical devices, which transform the electric pulses to discrete mechanical movements (discrete rotation of a rotor). The important advantage of step-by-step electric motors is that they provide unequivocal dependence of position of a rotor on input pulses of a current so that the rotation angle of a rotor is defined by the number

of actuating pulses. In SEM the rotating moment is created by magnetic streams created by the stator and rotor poles, which are oriented relative to each other in appropriate way. Stator is made of a material with high magnetic permeability and has several poles. The magnetic conductors are assembled from separate plates, similarly to the core of the transformer, to reduce the losses by whirling currents. The rotating moment is proportional to the value of a magnetic field, which is defined by the current in windings and the number of coils. If one of the windings of the step-by-step electric motor is fed, the rotor takes a certain position. Switching off the current in one winding and switching it on in another one, it is possible to move the rotor to the next position, etc. Thus, controlling the current in windings, it is possible to rotate the SEM rotor in a step-by-step mode. It will remain in this position until the external applied moment does not exceed some value called the holding moment. After that the rotor will turn and try to take one of the following positions of equilibrium.

Motors with constant magnets have the simplest construction. They consist of a stator with windings and a rotor with constant magnets. Fig. 14 shows the simplified construction of a step-by-step electric motor. Interchanging poles of a rotor have the rectilinear form and are located in parallel to the motor axis. The engine shown on figure has 3 pairs of poles of a rotor and 2 pairs poles of a stator. The engine has 2 independent windings, with each of them reeled up on two opposite poles of a stator. A motor shown on Fig. 14 has the incrementation parameter of 30 grad. When a current in one of the windings is switched on, the rotor tends to take such position, at which the unlike poles of rotor and stator are opposite to each other. To realize the continuous rotation it is necessary to switch on the windings alternatively.

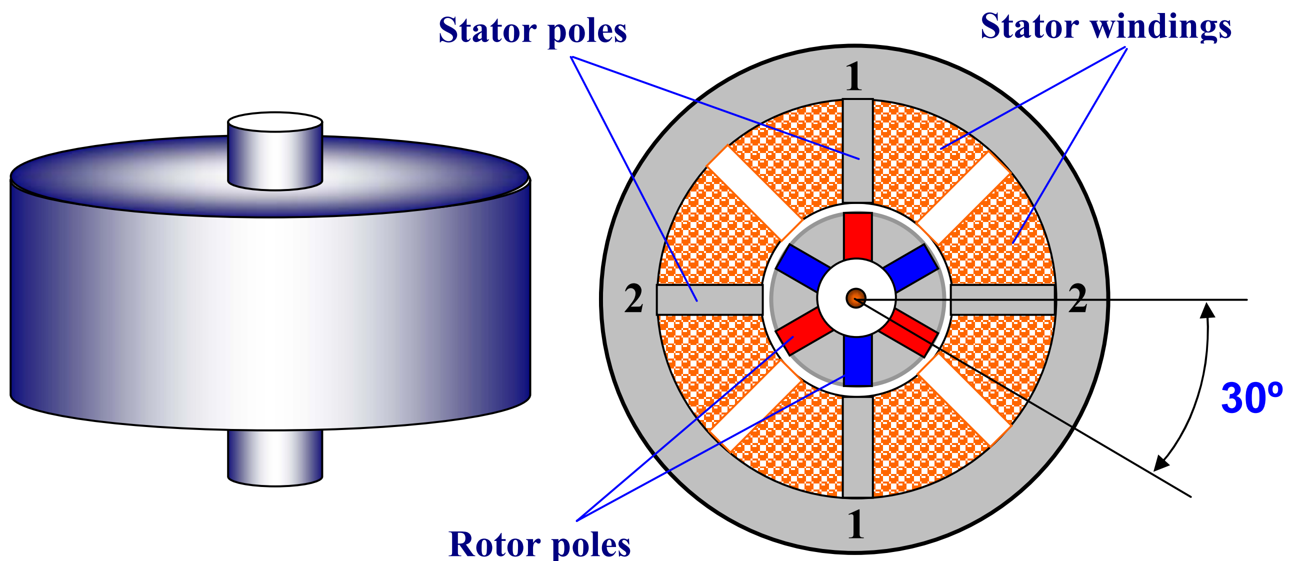

Fig. 14. Step-by-step electric motor with constant magnets

Step-by-step electric motors having more complex construction and providing from 100 up to 400 steps per one revolution of a rotor (angles of a step 3.6 – 0.9 grad) are used in practice. If such motor runs together with threaded connection, then the accuracy of object positioning of about 0.25 - 1 micron is provided at a step of a groove about 0.1 mm. Additional mechanical reducers are applied to increase the accuracy. The possibility of electric control allows to use effectively SEMs in automated systems of approach of a tip to a sample in scanning probe microscopes.

Step-by-step piezoelectric motors

Requirements of good isolation of devices from external vibrations and necessity of work of the probe microscopes in conditions of vacuum impose serious restrictions on application of purely mechanical devices for tip and sample movements. In this respect, devices on the basis of the piezoelectric converters, allowing to perform remote control of objects movement, became widely used in probe microscopes.

One of the constructions of a step-by-step inertial piezoelectric motor is presented on Fig. 15. This device contains the base (1) on which the piezoelectric tube (2) is fixed. The tube has electrodes (3) on external and internal surfaces. The split spring (4), representing the cylinder with separate springing petals, is fixed on the end of a tube. The object holder (5) – a cylinder with polished surface, massive enough - is established in a spring. The moved object can be fixed to the holder with the help of a spring or a captive nut that allows the device to work at any orientation in space.

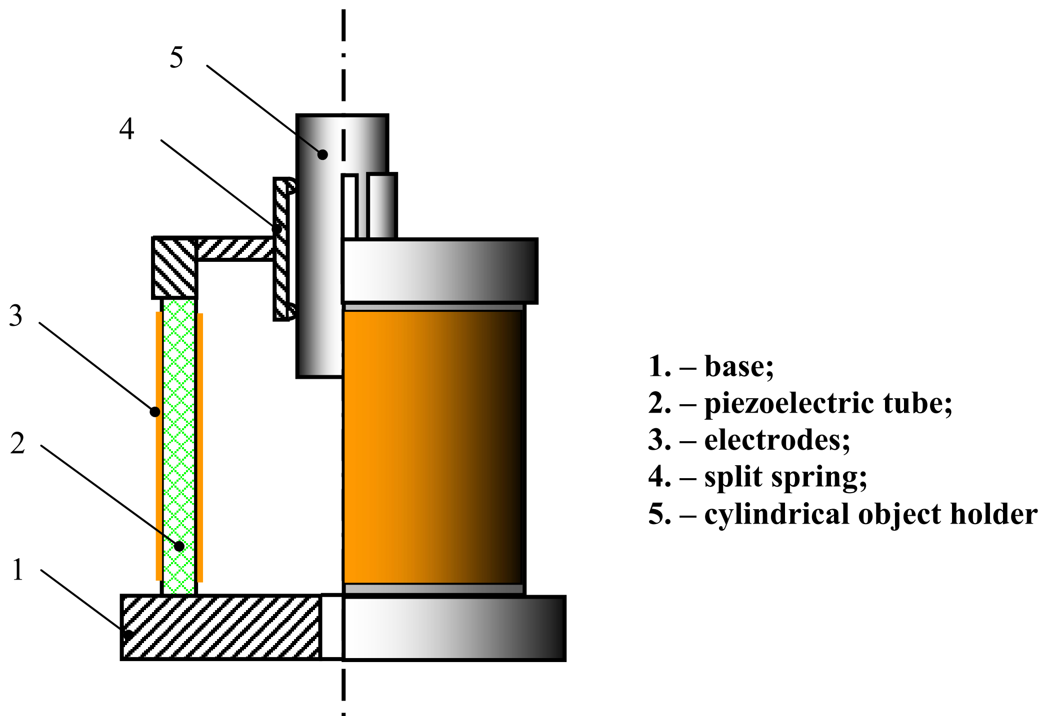

Fig. 15. – Step-by-step piezoelectric motor

The device works as follows. To move the object holder in the *Z* axis direction the pulse voltage of the sawtooth configuration is applied to electrodes of a piezo-tube. The characteristic form of a control voltage pulse is presented on Fig. 16.

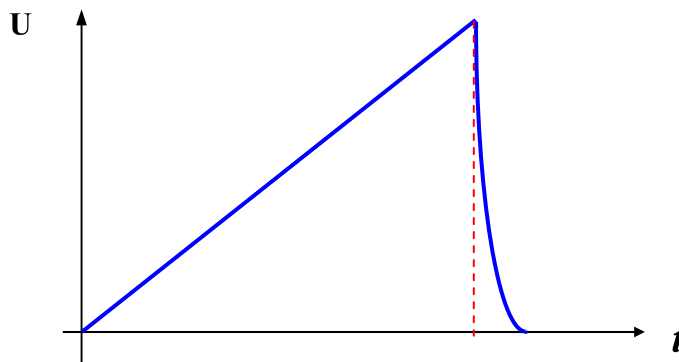

Fig. 16. Control voltage pulse form of a step-by-step inertial piezoelectric motor

The tube is smoothly extended or compressed on the low-angle front of a sawtooth voltage, depending on the polarity of voltage, and its end, together with the spring and the object holder, is shifted on the following distance:

$$\Delta l = d_{31} \frac{l}{h} U .$$

At the moment of a sawtooth voltage dump the tube returns to the starting position with the a acceleration, which has its maximal size in the beginning:

$$a = \Delta l \omega^2 ,$$

where ω - resonant frequency of longitudinal fluctuations of a tube. If the following condition is satisfied -

$$F_{mp} < ma$$

(m -weight of the object holder, F_{mp} - friction force between the object holder and the split spring) - the object holder, due to its inertia, slides relatively to the split spring. As a result, the object holder takes some $K \Delta l$ step in relation to the starting position. The K factor is defined by the ratio of construction details weights and stiffness of a split spring. When the polarity of pulses of a control voltage is alternated, the object movement direction changes. Thus, applying a sawtooth voltage of various polarities on the piezo-tube electrodes, it is possible to move the object in space and to approach the tip to a sample in a scanning probe microscope.

1.4. Protection of probe microscopes against external influences

Protection against vibrations

Any construction of a scanning probe microscope represents the oscillatory system having the whole set of own resonant frequencies ω_k. External mechanical influences on the frequencies coinciding with ω_k, cause the phenomena of a resonance in the measuring heads construction, which results in fluctuations of a tip relatively to a sample and is perceived as a parasitic periodic noise, which is deforming and dithering the SPM images of samples surface. To reduce the influence of external vibrations the measuring heads are made of massive metal details having high (more than 100 kHz) frequencies. Scanning elements of probe microscopes have the least resonant frequencies. It is necessary to temporize between the size of the maximal field of view of a scanning element and its resonant frequency in constructions of modern microscopes. Resonant frequencies in a range of 10 - 100 kHz are typical for scanners.

Various types of vibration-isolating systems are applied to protect devices against external vibrations. Conditionally the vibration-isolating systems can be distinguished as passive and active ones. The basic idea incorporated in passive vibration-isolating systems consists in the following. The amplitude of forced oscillations of a mechanical system quickly falls down at increase in the difference between the frequency of the excitation force and own resonant frequency of a system (typical amplitude-frequency characteristic (AFC) of an oscillatory system is presented on Fig. 17).

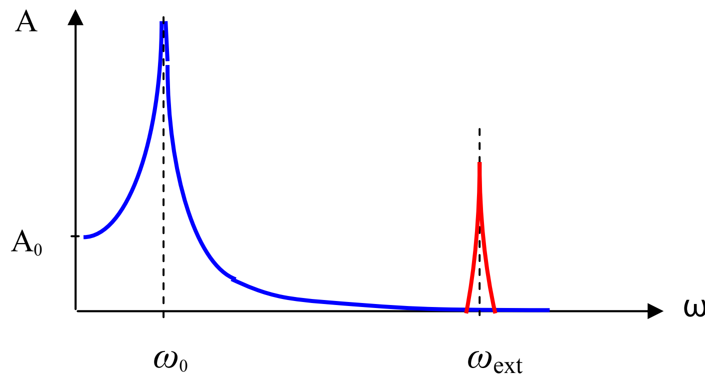

Fig. 17. AFC schematic image of an oscillatory system Red color shows spectrum of external vibrations

Therefore external influences with frequencies $\omega_{EXT} >> \omega_0$ practically do not render appreciable influence on the oscillatory system. Hence, if a measuring head of a probe microscope is placed on the vibration-isolating platform or on the elastic suspension (Fig. 18), then only external fluctuations with frequencies close to the resonant frequency of a vibration-isolating system will pass onto the case of a microscope. Since own frequencies of SPM heads make 10 - 100 kHz, choosing the resonant frequency of vibration-isolating systems low enough (about 5 - 10 Hz), it is possible to protect the device from external vibrations rather effectively. In order to quench oscillations on own resonant frequencies, dissipative elements with viscous friction are introduced into vibration-isolating systems.

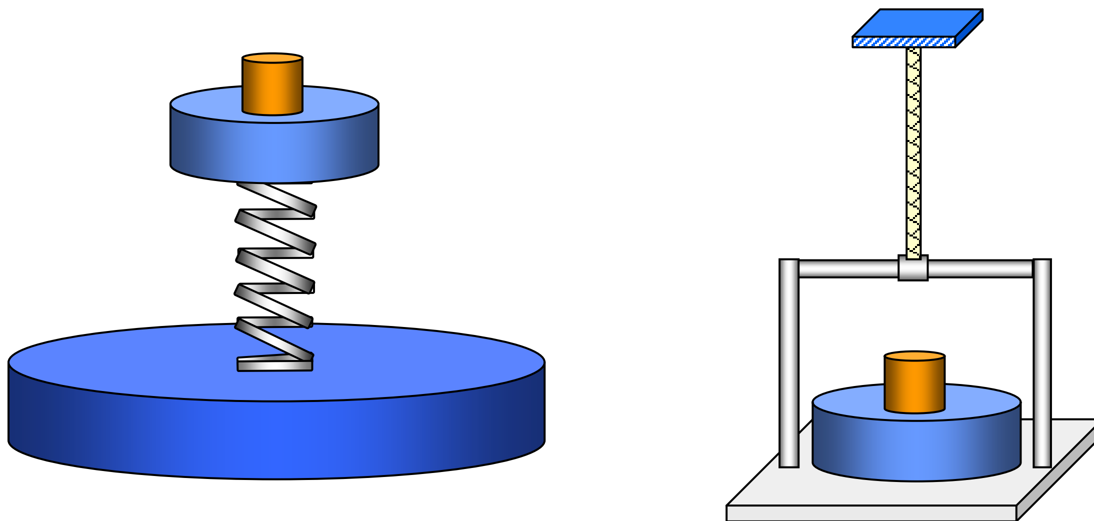

Fig. 18. Passive vibration-isolating systems

Thus, for maintenance of effective protection it is necessary, that the resonant frequency of a vibration-isolating system was as small as possible. However, it is difficult to realize in practice very low frequencies. For spring platforms and elastic suspensions the resonant frequency is equal to

$$\omega_0 = \sqrt{\frac{k}{m}},$$

where k –spring force (or elastic suspension stiffness), m - weight of vibration-isolating platforms together with the SPM head. We shall estimate parameters of the vibration-isolating system providing suppression of high-frequency vibrations. From a condition of equilibrium it follows, that

$$mg = k\Delta l\ ,$$

where Δl - lengthening (or compression) of an elastic element, g - gravitational acceleration. Then, for the size of lengthening:

$$\Delta l = \frac{gm}{k} = \frac{g}{\omega_p^2} = \frac{g}{(2\pi\nu)^2} \cong 0.25 \cdot \frac{1}{\nu^2}\ .$$

Thus, in order to obtain the resonant frequency of vibration-isolating systems of about 1 Hz, it is necessary that lengthening (or compression) of an elastic element made 25 cm. Such lengthening can be realized in a most simple way with the help of spring or rubber suspensions. Taking into account, that the stretching of springs can achieve 100 %, for realization of 1 Hz resonant frequency of a suspension, the length of an elastic element should make also 25 cm, and, hence, the total size of the vibration-isolating system will make 50 cm. If resonant frequency requirements are less stringent, it is possible to achieve essential compactification of the vibration-isolating system. So, for realization of 10 Hz frequency the compression of an elastic element should make only 2,5 mm. Such compression is done in practice easily enough with the help of a pile of metal plates with rubber linings, which considerably reduces the dimensions of vibration-isolating systems.

Active systems of suppression of external vibrations are also successfully applied to protect the SPM heads. Such devices represent electromechanical systems with a negative feedback, which provides stable position of the vibration-isolating platform in space (Fig. 19).

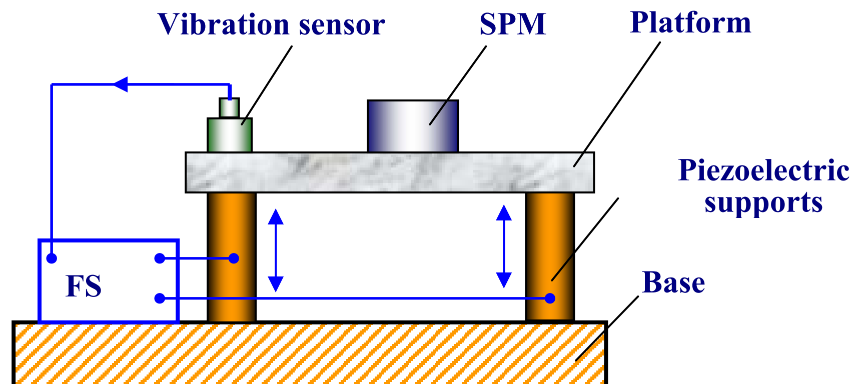

Fig. 19. Active vibration-isolating system schematic

The principle of work of active systems can be examined on the following simple example. The vibration sensor (accelerometer) – the device reacting to acceleration, going through a platform – is installed on a platform. The signal from the sensor acts in the feedback system (FS) where it is amplified and transmitted in an antiphase to the piezoelectric support which, shifting to the opposite side, extinguish the acceleration going through the platform. This is the so-called proportional adjustment. In fact, let the platform oscillate with the ω frequency under action of external force, so that its shift is

$$u = u_0 Sin(\omega t).$$

Then the acceleration experienced by a platform will be equal to

$$\ddot{u} = -\omega^2 u_0 Sin(\omega t).$$

The feedback system in this case supplies an antiphase signal to the supports; therefore displacement of a platform will represent the superposition of two shifts:

$$u = u_0 Sin(\omega t) - aSin(\omega t) = (u_0 - a)Sin(\omega t).$$

Thus, the feedback system will increase the a amplitude of a signal until acceleration of a platform is equal to zero:

$$\ddot{u} = -\omega^2 (u_0 - a)Sin(\omega t).$$

The working frequencies band of active systems is defined by a frequencies band of stable operation of electromechanical feedback system. In case of nonharmonic vibrations $u = u(t)$ the accelerometer signal is integrated twice by the hardware and is transmitted in an antiphase to the piezoelectric supports, so that the amplitude of oscillations of a platform tends to zero:

$$u = u(t) - \alpha \iint \ddot{u}(t)dt \Rightarrow 0.$$

Multistage constructions of vibration-isolating systems of various types are applied in practice, allowing to increase essentially the degree of protection of devices against external vibrations.

Protection against acoustic noise

Another source of vibrations of elements of probe microscopes construction are acoustic noises of various nature.

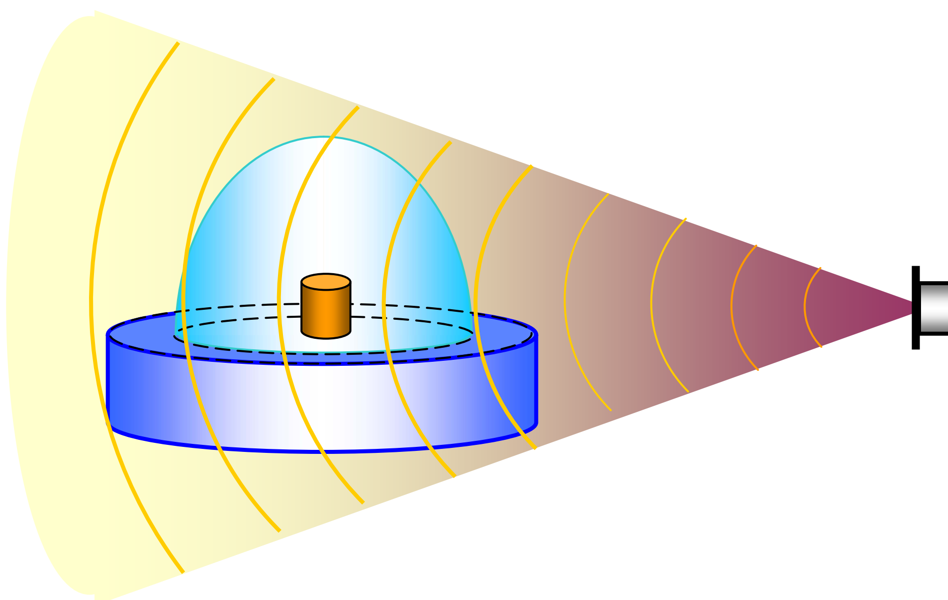

Fig. 20. SPM protection against acoustic noise

The specifics of an acoustic noise are that acoustic waves influence directly the construction elements of SPM heads, resulting in oscillations of a tip in relation to the surface of a test sample. Various protective caps allowing to lower essentially the level of acoustic noise in the area of a working interval of a microscope are applied to protect the SPM against acoustic noise. The most effective protection against acoustic noise is accommodation of the measuring head of a probe microscope in a vacuum chamber.

Stabilization of a thermal drift of a tip position above the surface

One of important problems in the SPM is the problem of stabilization of position of a tip above the surface of a test sample. The main source of instability of position of a tip is the change of environment temperature or warming up of elements of a probe microscope construction during its operation. Temperature change of a solid body results in occurrence of thermoelastic deformations:

$$u_{ik} = \alpha_{ik} \Delta T ,$$

where u_{ik} - deformations tensor, α_{ik} - material thermal expansion coefficients tensor, ΔT - temperature increment. For isotropic materials the thermal expansion coefficient is a scalar value, so

$$\alpha_{ik} = \alpha \cdot \delta_{ik} ,$$

where δ_{ik} - ordinary Kronecker tensor, α - absolute value of the thermal expansion coefficient. Absolute lengthening of microscope construction elements can be estimated proceeding from the following equations:

$$u = \frac{\Delta l}{l_0} = \alpha \cdot \Delta T; \qquad \Delta l = l_0 \alpha \cdot \Delta T .$$

Typical values of materials expansion coefficients make 10^{-5} – 10^{-6} $grad^{-1}$. Thus, at heating a 10 cm long body on 1°C its length increases on ~1 micron. Such deformations influence essentially the operation of probe microscopes. Thermostatting of SPM measuring heads is used or temperature-compensating elements are introduced to the construction of heads to reduce the thermal drift. The idea of temperature-compensation consists in the following. Any SPM construction can be presented as a set of elements with various coefficients of thermal expansion (Fig. 21 (a)).

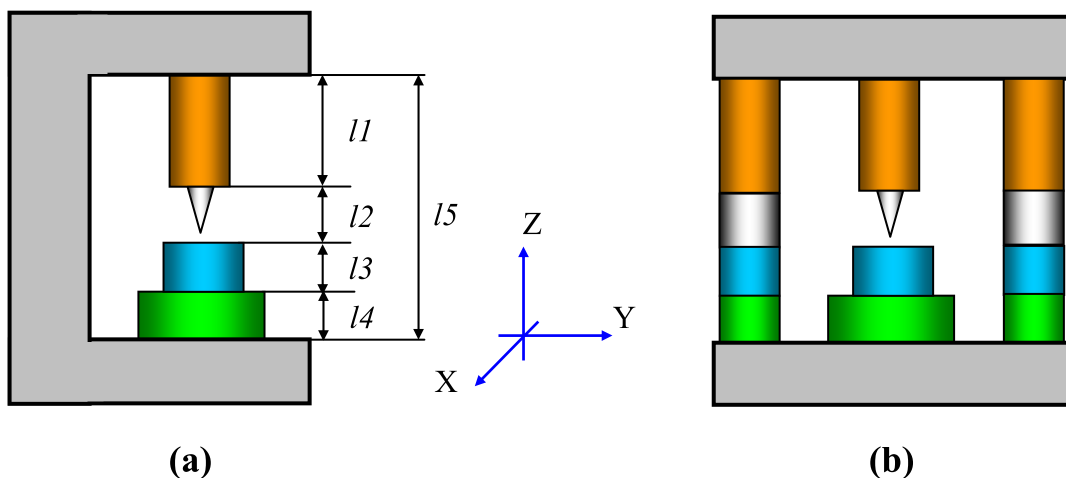

Fig. 21. Compensation of thermal expansions of SPM construction

In order to compensate the thermal drift in the SPM measuring heads construction the compensating elements having various expansion coefficients are introduced, so that the condition of equality to zero of the sum of temperature expansions in various shoulders of a construction is satisfied:

$$\Delta L = \sum_i \Delta l_i = \Delta T \sum_i \alpha_i l_i \Rightarrow 0$$

The simplest way to reduce the thermal drift of the tip position on Z axis is to introduce in the SPM construction compensating elements from the same material and with the same characteristic sizes, as the basic elements of a construction (Fig. 21 (b)). When the temperature of such construction changes, the shift of a tip in Z direction is minimal. The measuring head of microscopes are made as axial-symmetric constructions to stabilize the position of a tip in the X, Y plane.

1.5. Formation and processing of SPM images

Process of scanning of a surface in a scanning probe microscope is similar to movement of an electronic beam on the screen in an electron ray tube of the TV. The tip goes along the line (row) first in forward, and then in the reverse direction (horizontal scanning), then passes to the next line (frame scanning). Movement of a tip is done with the help of the scanner small steps by influence of the sawtooth voltage formed by digital-to-analog converters. Registration of the information on the topography of a surface is made, as a rule, on the forward pass.

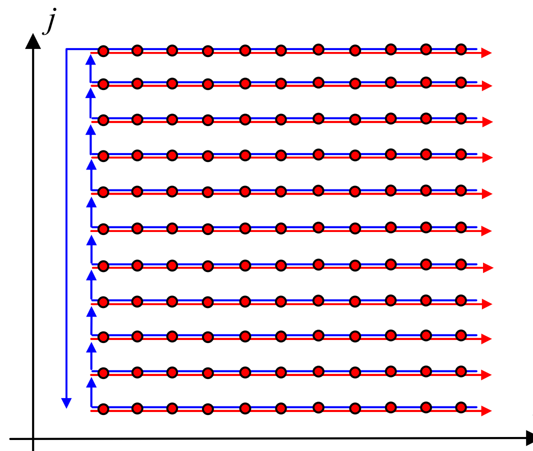

Fig. 22. Schematic image of scanning process.
The direction of a forward motion of the scanner is indicated with red arrows
Reverse motion of the scanner is indicated with dark blue arrows
Registration of the information is made in points on direct pass

The information received with the help of a scanning probe microscope, is stored as an SPM frame - a bidimentional file of a_{ij} integers (matrixes). The physical sense of these numbers is determined by the value, which was digitized during scanning. To each value of *ij* pair of indexes corresponds a certain point of a surface within the scanning area borders. Coordinates of points of a surface are calculated with the help of simple multiplication of a corresponding index on the value of distance between points, where the information was registered:

$$x_i = x_0 \cdot i, \qquad y_j = y_0 \cdot j.$$

Here x_0 and y_0 – distances between the next points along X and Y axes, where the information was recorded. As a rule, The SPM frames represent square matrixes with the 2^n size (mainly, 256x256 and 512x512 elements). Visualization of the SPM frame is done by computer graphics, basically, as three-dimensional (3D) and bidimentional brightness (2D) images. At 3D visualization the image of a surface Z = $f(x,y)$, corresponding SPM to the data, is plotted in an axonometrical prospect with the help of pixels or lines. In addition to this, various ways of pixels brightening corresponding to various height of the topography of a surface are used. The most effective way of 3D images coloring is modeling of conditions of illumination of a surface by a point source located in some point of space above the surface (Fig. 23). Thus it is possible to emphasize small-scale topography inequalities. Same graphical instruments and computer processing are used for scaling and rotation of 3D SPM images. In 2D visualization each point of a surface Z = $f(x,y)$ corresponds to a certain color. Gradient palettes, where coloring of images is made by the tone of a certain color, according to the height of a surface point, are most widely used. As an example, the 2D image of a surface area is presented on Fig. 24.

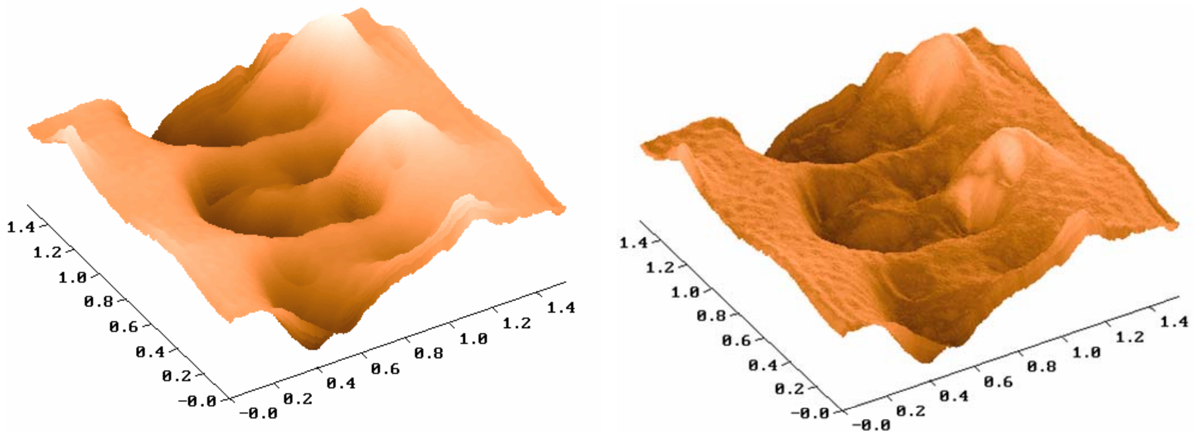

Fig. 23. 3D visualization of a surface topography with illumination on height (a) and with lateral illumination (b)

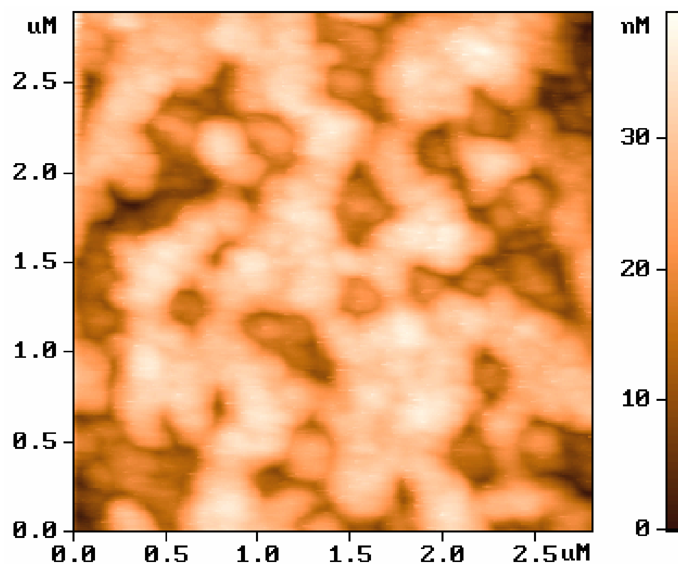

Fig. 24. 2D brightness image of a surface

Local SPM measurements, as a rule, are connected to registration of dependences of the test values on various parameters. For example, these are the dependences of the electric current value flowing through the tip-surface contact on the voltage applied, dependence of various parameters of force interaction of a tip and a surface on the tip-sample distance, etc. This information is stored as vector files or as matrixes of 2×N dimension. A set of standard tools of function diagrams representation is provided in the software of microscopes for visualization of this information.

SPM images, alongside with the helpful information, contain also a lot of secondary information deforming the data on the morphology and surface properties. Possible distortions in SPM images of a surface caused by imperfection of the equipment and external parasitic influences are schematically presented on Fig. 25.

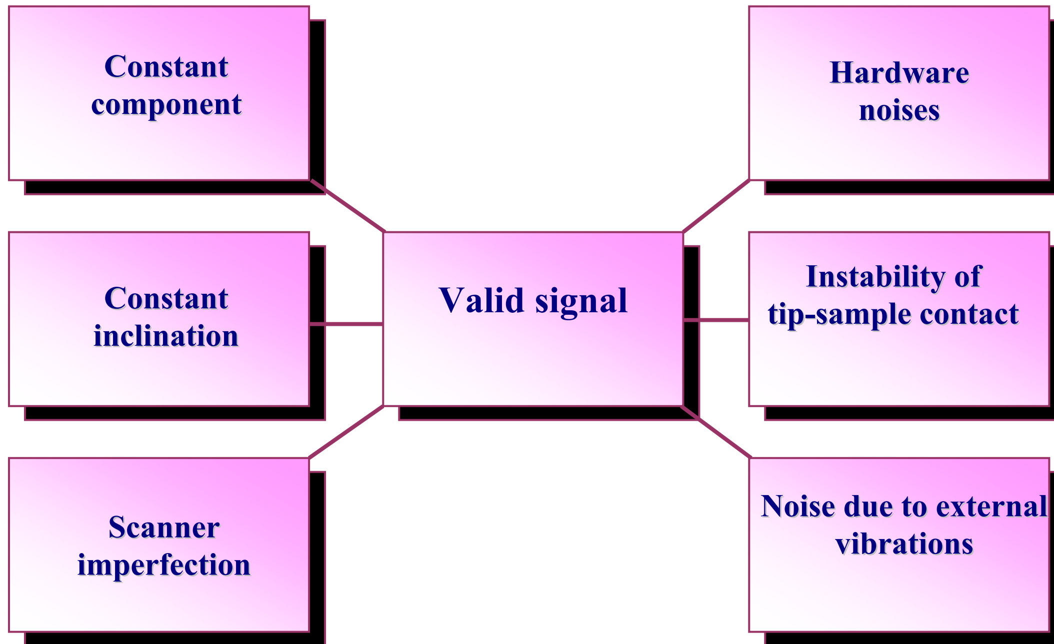

Fig. 25. Possible distortions in the SPM images

Subtraction of a constant component

As a rule, the SPM images contain a constant component, which does not bear useful information about the surface topography, but reflects the accuracy of sample approaching into the center of the dynamic range of scanner movement along the Z axis. The constant component is removed from the SPM frame using software tools so the new values of the topography heights in the frame are equal to

$$Z'_{ij} = Z_{ij} - \overline{Z}, \qquad \text{where } \overline{Z} = \frac{1}{N^2}\sum_{ij} Z_{ij}.$$

Subtraction of a constant inclination

Surface images acquired using probe microscopes, as a rule, have common inclination. It can be caused by the several reasons. First, the inclination may appear as a result of incorrect installation of the sample in regard to the tip or non-flatness of the sample; second, it might be connected with a temperature drift, which results in tip shifting in regard to the sample; third, it might be due to a

non-linearity of the piezo-scanner movement. Inclination imaging takes a large volume of useful space in the SPM frame, so that the small image details become not visible. To eliminate this imperfection, operation of subtraction of the constant inclination is performed. For this purpose at the first stage the method of least squares is used to find an approximating plane $P^{(1)}(x,y)$, which has minimal deviations from the topography of a surface Z = *f(x,y)* (Fig. 26). Then the given plane is subtracted from the SPM image. It is reasonable to subtract in various ways, depending on the inclination nature. If the inclination in the SPM image is caused by an inclination of a sample relatively to the tip axis, it is expedient to turn the plane on an angle corresponding to the angle between the $\vec{n}$ normal to a plane and the Z axis; thus the coordinates of a surface Z = *f(x,y)* will be transformed according to transformations of a spatial turn. However, during such transformation it is possible to obtain the image of a surface as a multiple-valued function $Z = f(x,y)$. If the inclination is caused by a thermal drift, the procedure of inclination subtraction comes to subtraction of Z-coordinates of a plane from Z-coordinates of the SPM image:

$$Z'_{ij} = Z_{ij} - P^{(1)}_{ij}.$$

This allows to keep correct geometrical relations in the X,Y plane between objects in the SPM image.

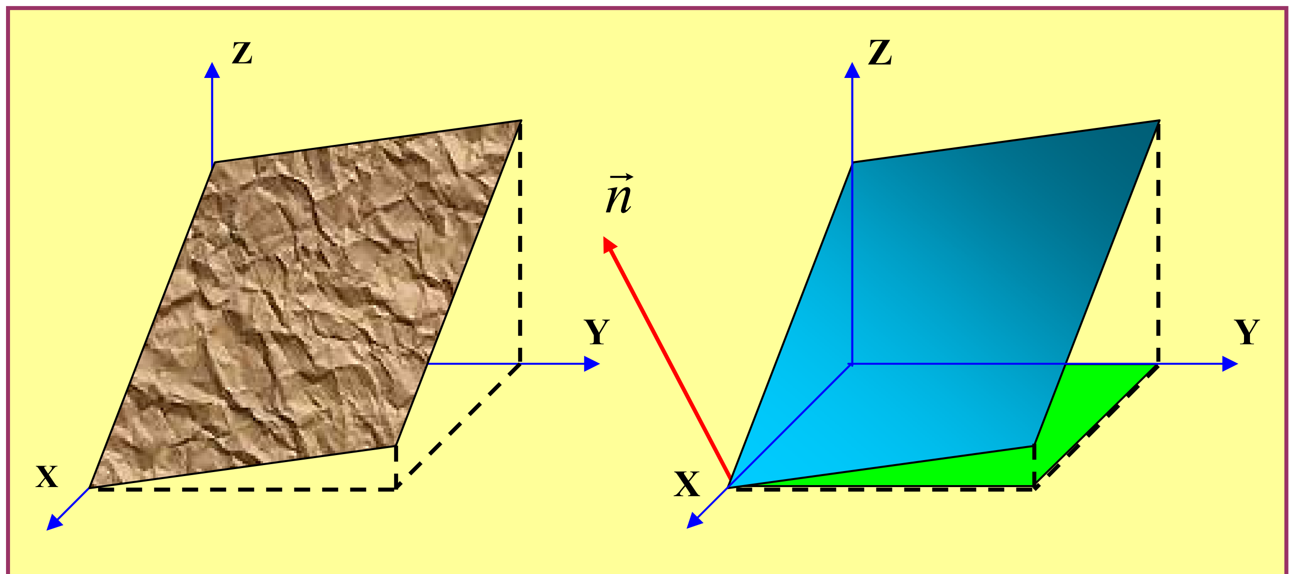

Fig. 26. Subtraction of a constant inclination from SPM images of a surface

Finally, an array with a smaller range of values is obtained, and fine details of the image will be displayed by a big number of colors, becoming more remarkable.

The result of subtraction of a plane from a real AFM image of a surface is presented on Fig. 27.

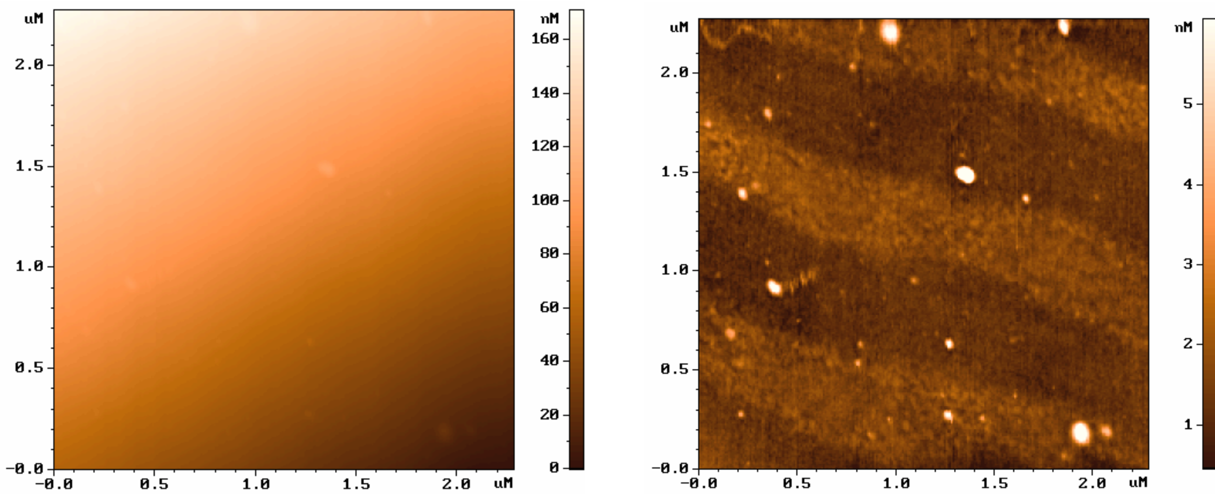

Fig. 27. Subtraction of an inclined plane from AFM image of a surface

Elimination of the distortions due to scanner imperfection

Imperfection of the piezo-scanner properties leads to the situation when the SPM image contains a number of specific artifacts. Partially the scanner imperfections, such as inequity of direct and reverse motions of the scanner (hysteresis), creep and nonlinearity of piezoceramics are compensated by the hardware and selection of optimum modes of scanning. However, despite of it, the SPM images contain distortions, which are difficult to remove on the hardware level. In particular, since the scanner movement in the plane of the sample affects the tip location over the surface (along the z-axis), the SPM images represent a superposition of an actual topography plus some surface of the second (and sometimes of a higher) order (Fig. 28).

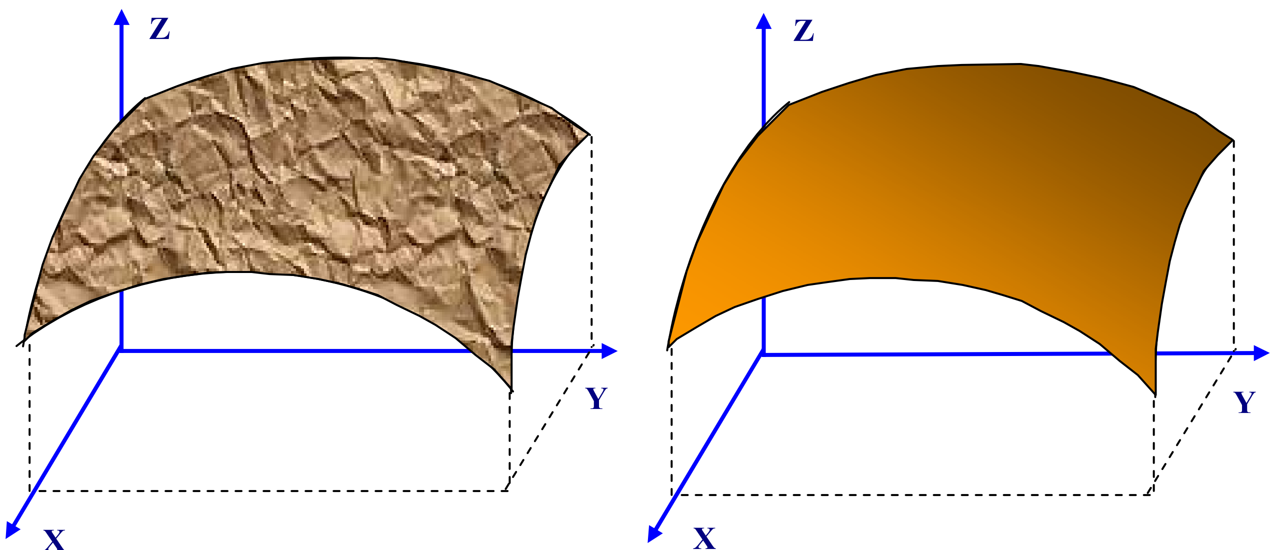

Fig. 28. Subtraction of a surface of the second order from the SPM image of a surface

Approximation plane of the second order $P^{(2)}(x,y)$ is found in order to eliminate the artifacts of such sort using the least-squares method, This plane has minimal deviations from initial function

$Z = f(x,y)$, and then this surface is subtracted from the initial SPM image:

$$Z'_{ij} = Z_{ij} - P^{(2)}_{ij} .$$

The result of subtraction of a surface of the second order from a real AFM image of a surface is presented on Fig. 29.

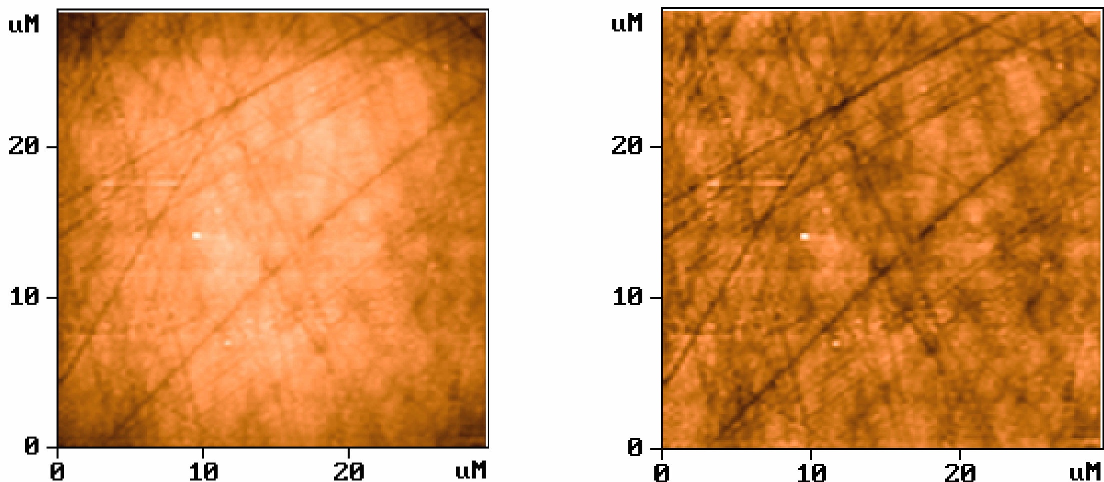

Fig. 29. Subtraction of a surface of the 2nd order from AFM image of a surface

Another type of distortions is connected to nonlinearity and nonorthogonality of movements of the scanner in X, Y planes. This results in distortion of geometrical proportions in various parts of the SPM image of a surface. Procedure of correction of the SPM images with the help of a file of correction coefficients, which is created during scanning by a specific scanner of test structures with a well-known topography, is used to eliminate such distortions.

Filtering of SPM images

Hardware noises, instabilities of the tip-sample contact during scanning, external acoustic noises and vibrations lead to the situation when the SPM images together with useful information contain also a noise component. Partially the SPM image noises can be removed using software tools with help of filters of different types.

Median filtering

Median filtering provides good results during removal of a high-frequency random noise in SPM frames. This is a nonlinear method of image processing, which main point can be explained as follows. The working window of the filter is selected, consisting of $n \times n$ points (for definiteness we shall take a 3×3 window, i.e. containing 9 points (Fig. 30)).

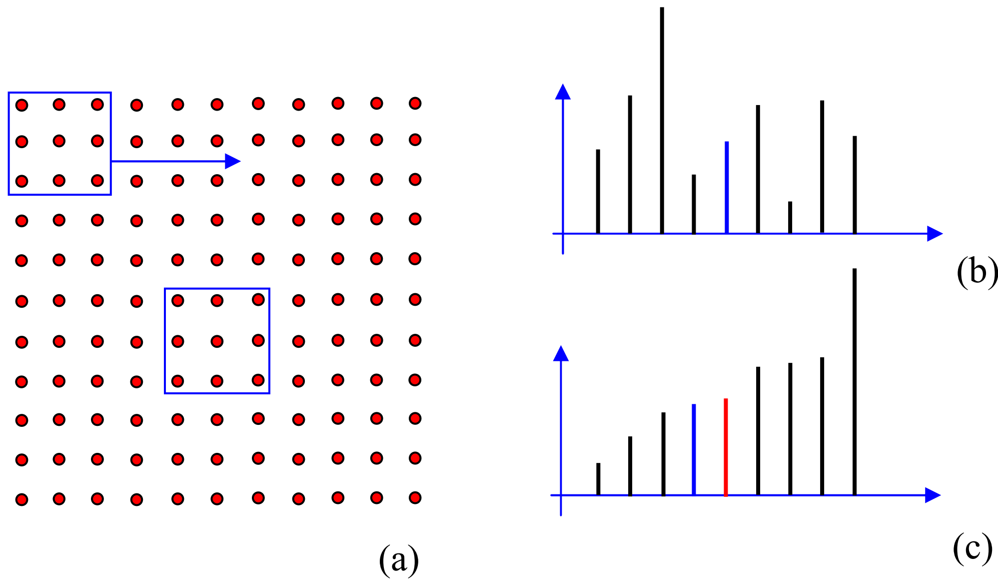

Fig. 30. Principle of work of the median filter with a 3x3 window

(a) – displacement of a window during array filtering;

(b) –arrangement of elements in unsorted array (central element marked in dark blue color);

(c) - arrangement of elements in the sorted array (new central element marked with red color).

During filtering this window moves on the frame from point to point, and the following procedure is performed. Values of the SPM image amplitude in points of this window are lined up in ascending order, and the value in the center of the sorted line is moved to the central point of a window. Then the window is shifted to the next point, and procedure of sorting is repeated. Thus, major random emissions and dip during such sorting always appear at the ends of a sorted file and do not enter the final (filtered) image. We shall notice that during such processing on the edges of the frame there are unfiltered areas which are discarded in the final image. The result of median filtering of a real AFM image of a surface is presented on Fig. 31.

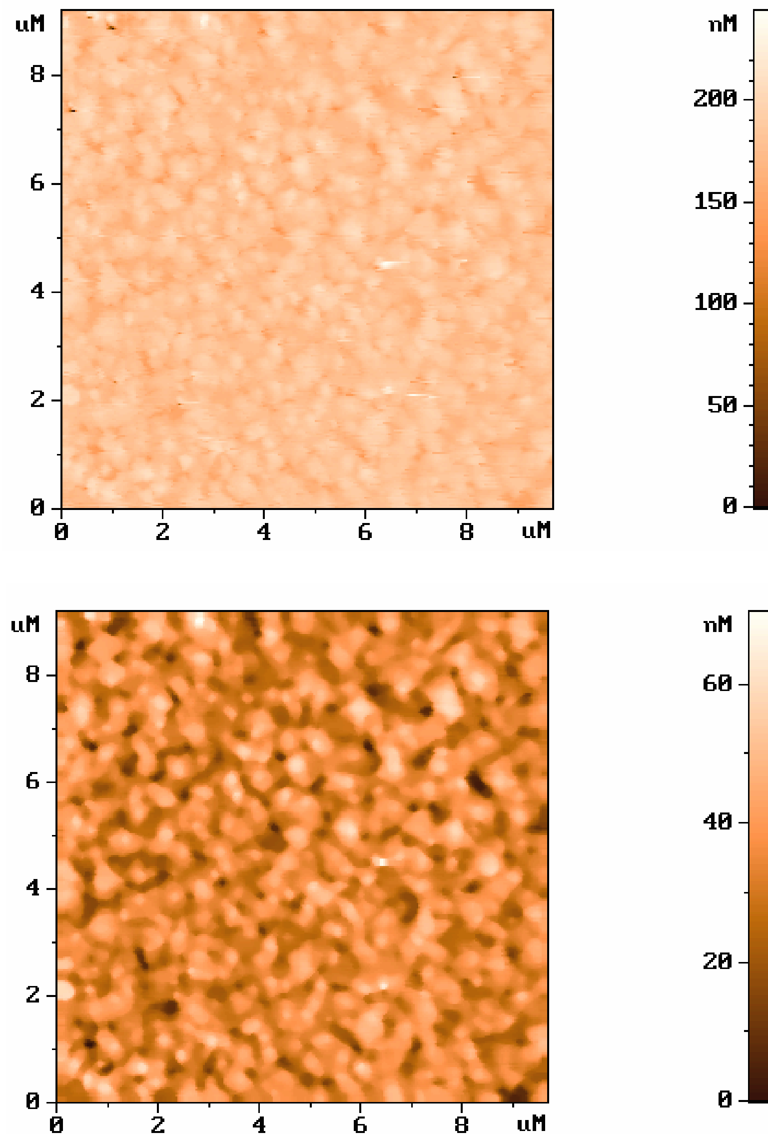

Fig. 31. Results of median filtering with a 5x5 AFM image of a surface window

Averaging over lines

The process of scanning of a surface in a scanning tip microscope occurs in such a manner that the frequency of registration of the information in line strongly (at least, in 100 times) differs from the frequency of registration of lines. It results to that high-frequency noise is contained basically in lines of the SPM image, and low-frequency noises change their position of lines relative to each other. Moreover, the tip-sample distance changes frequently during scanning due to micro movements in the elements of construction of the measuring head of a microscope or due to change of condition of a tip working part (for example, capture by the apex of the tip of a micro particle from a surface, etc.). This leads to the steps appearing parallel to the direction of scanning on the SPM image. These steps are caused by the bias of one part of the SPM frame relative to another (Fig. 32 (a)). It is possible to get rid of such defects of SPM images using the alignment procedure of the frame over the lines. The average topography value is determined in every scanning line:

$$\overline{Z}_j = \frac{1}{N}\sum_i Z_{ij}\,.$$

And then the corresponding average values are subtracted from values in every line of the frame:

$$Z'_{ij} = Z_{ij} - \overline{Z}_j\,,$$

so that in the new frame in every line the average value is equal to zero. This leads to removal from the frame of the steps connected to sharp changes of average value in lines. The result of alignment over the lines of a real AFM image of the surface is presented on Fig. 32.

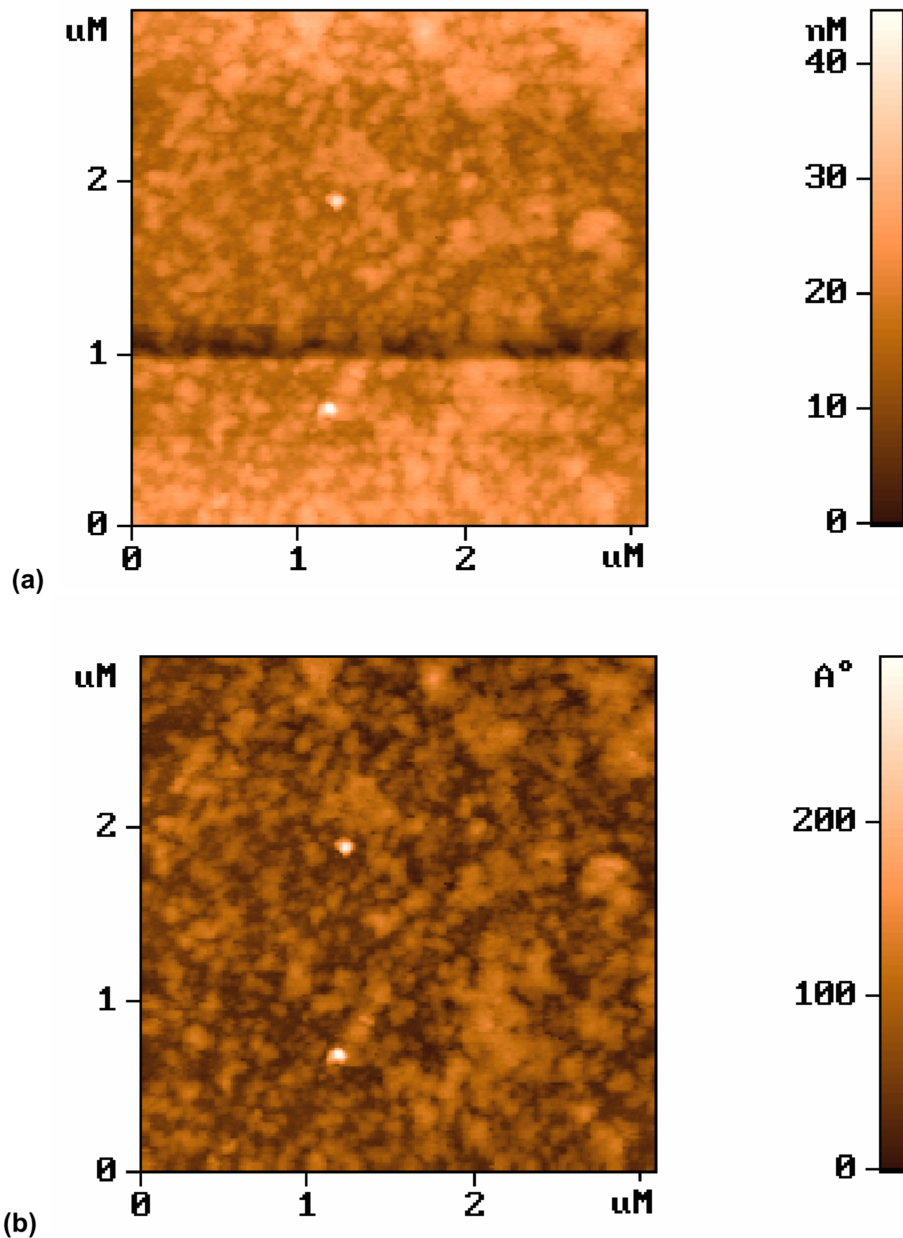

Fig. 32. AFM images of a sample surface
(a) — before averaging over the lines; (b) — after averaging.

Fourier filtration of the SPM images

The spectral filtration based on the Fourier transformations is the one of the powerful methods of the SPM images correction. As is well known, any function can be presented as a Fourier integral. In case of the SPM frame the Fourier transformation is made with discrete values. Fourier image of the surface can be found using the following formulae (the imaginary unit $\sqrt{-1}$ is designated through ν):

$$F_{\alpha\beta} = \frac{1}{N^2} \sum_{ij} Z_{ij}\, exp\left[2\pi\nu(\frac{\alpha \cdot i}{N} + \frac{\beta \cdot j}{N})\right].$$

Accordingly, the reverse Fourier transformation:

$$Z_{ij} = \sum_{\alpha\beta} F_{\alpha\beta}\, exp\left[-2\pi\nu(\frac{\alpha \cdot i}{N} + \frac{\beta \cdot j}{N})\right].$$

During the Fourier-filtration the transformations are made with a spatial spectrum of the surface. The transformed Fourier-image of the surface can be written down as:

$$F'_{\alpha\beta} = F_{\alpha\beta} \cdot H_{\alpha\beta},$$

where $H_{\alpha\beta}$ represents the spectral function of the applied filter. Then the filtered image is obtained as a result of the reverse Fourier transformation for the processed spectrum of the surface:

$$Z'_{ij} = \sum_{\alpha\beta} F_{\alpha\beta} \cdot H_{\alpha\beta}\, exp\left[-2\pi\nu(\frac{\alpha \cdot i}{N} + \frac{\beta \cdot j}{N})\right].$$

The filters of low and high frequencies with circular and square windows are most widespread. For filters of low frequencies the spectral functions of filters are defined as:

$$H^{cir}_{\alpha\beta} = \begin{cases} 1 \; for \; \sqrt{\alpha^2+\beta^2} \le R \\ 0 \; for \; \sqrt{\alpha^2+\beta^2} > R \end{cases}, \qquad H^{sqr}_{\alpha\beta} = \begin{cases} 1 \; for \; |\alpha| \le A; \; |\beta| \le A \\ 0 \; for \; |\alpha| > A; \; |\beta| > A \end{cases},$$

where R and A values represent accordingly the radius of a circular window and the size of a square window of the filter function. By analogy with the filter of high frequencies we have:

$$H^{cir}_{\alpha\beta} = \begin{cases} 0 \; for \; \sqrt{\alpha^2+\beta^2} \le R \\ 1 \; for \; \sqrt{\alpha^2+\beta^2} > R \end{cases}, \qquad H^{sqr}_{\alpha\beta} = \begin{cases} 0 \; for \; |\alpha| \le A; \; |\beta| \le A \\ 1 \; for \; |\alpha| > A; \; |\beta| > A \end{cases}.$$

Results of the Fourier- filtration of one of AFM images of the real surface are shown on Fig. 33.

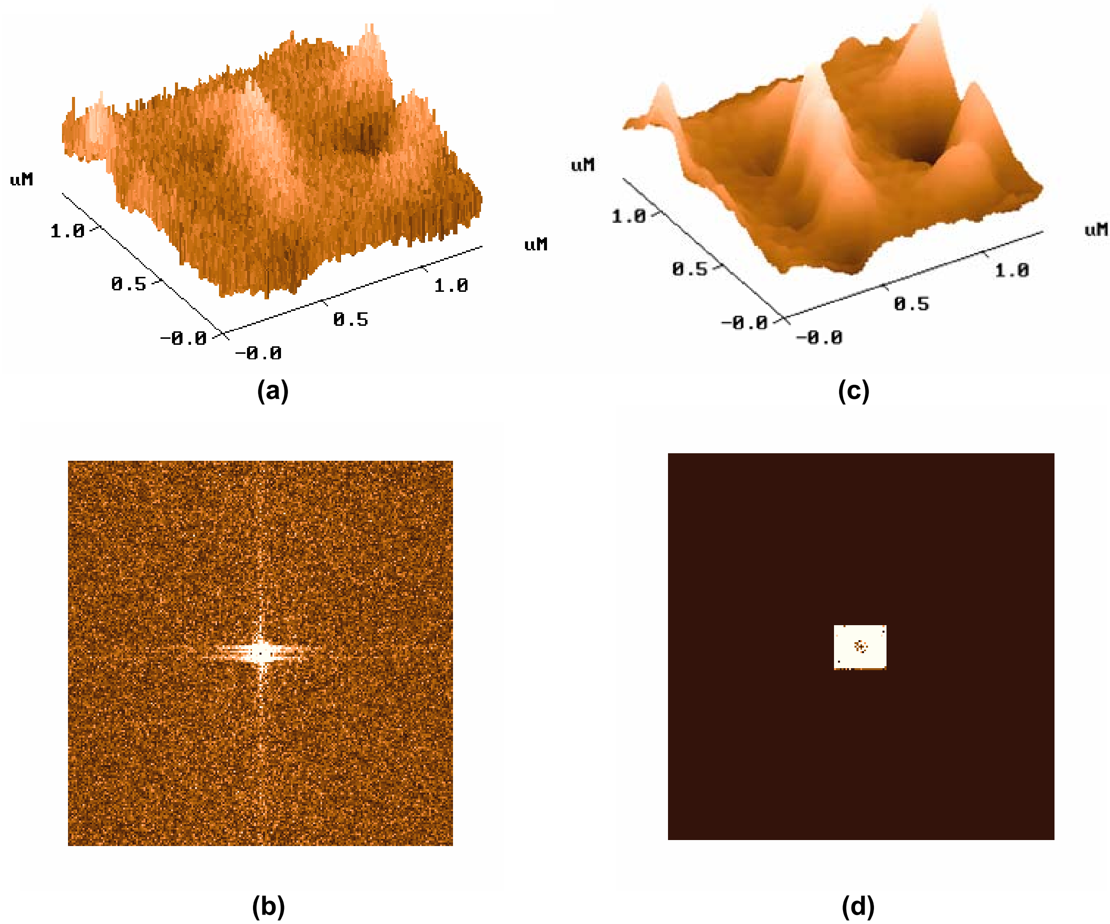

Fig. 33. Example of application of Fourier-filtration to the AFM image of the surface:
(a) – initial AFM image **(b) – spectrum of the initial image**
(c) – filtered image **(d) – processing of spectrum by the low frequencies filter**

Filters with more complex spectral function are applied for elimination of undesirable effects connected to abrupt change of spectral function at the filter edge and on the frame borders. It is possible to calculate on the Fourier-image basis the number of useful characteristics of the surface. In particular, the spectral capacity density is defined as follows:

$$S_{\alpha\beta} = \left|F_{\alpha\beta}\right|^2 = F_{\alpha\beta}F^*_{\alpha\beta}.$$

It is useful also to specify formulae for calculation of an autocorrelation function of the surface:

$$C_{ij} = \sum_{\alpha\beta} F_{\alpha\beta}F^*_{\alpha\beta}\, exp\left[2\pi\nu\left(\frac{\alpha\cdot i}{N} + \frac{\beta\cdot j}{N}\right)\right].$$

Thus, the standard software of probe microscopes includes the wide set of tools for visualization and processing of the SPM data. Moreover, the images that were obtained with a scanning probe microscope can be stored in one of the graphics formats that allow using the additional opportunities given by the modern computer software for processing and correction of images.

Modes of surface restoration using its SPM image

One of the drawbacks inherent to all modes of the scanning probe microscopy is the finite size of the working part of tips used. It leads to essential deterioration of the spatial resolution of microscopes and to significant distortions in SPM images during scanning of surfaces with irregularities of the topography comparable to the typical sizes of a working part of the tip.

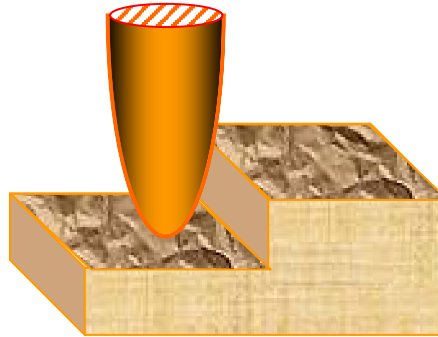

The actually obtained SPM image is a “convolution” of a tip and surface being researched. One-dimensional case of the “convolution” process of the tip form with the surface topography surface is illustrated on Fig. 34.

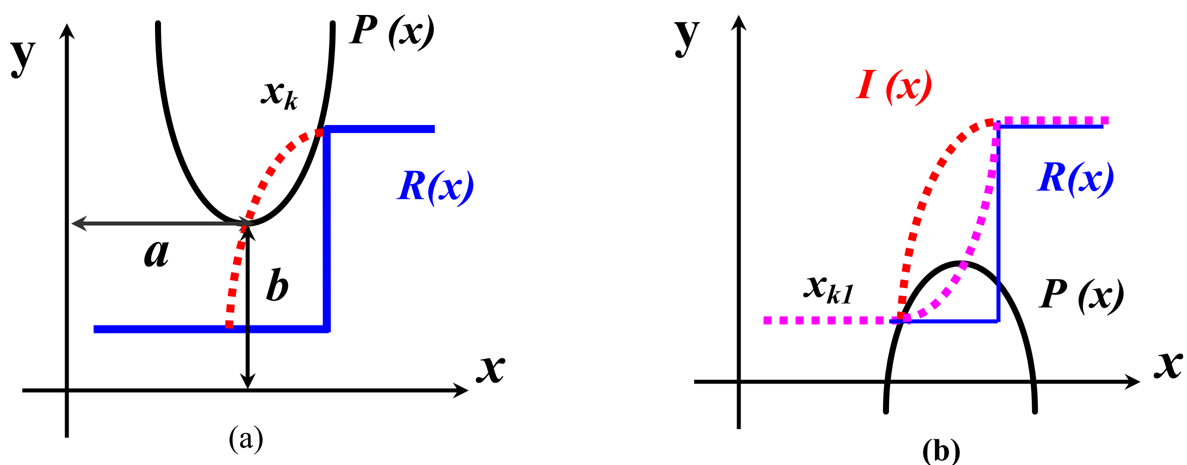

Fig. 34. Schematic drawing of an image acquisition process in the SPM (a) and the process of partial topography restoration with account of finite sizes and the form of a tip (b)

The recently developed modes of restoration of the SPM images based on computer processing of the SPM data accounting the specific form of tips allow solving partially the given problem [Lit. 17, Lit. 18]. The most effective mode of restoration of the surface is the mode of numerical deconvolution [Lit. 18], using the form of a tip, obtained experimentally during scanning test structures (with a well-known topography of the surface). We shall consider the given mode in a one-dimensional case. If the form of a tip is described by the P(x) function, and the form of a true topography of the surface is described by function R(x), then the SPM image of the surface turns out as follows:

$I(a) = R(x_k) - P(x_{k-a})$, under condition that $dR/dx = dP/dx$ in x_k points of contact.

where *a* –tip bias in surface coordinates. Restoration of initial topography of the surface in the given mode is made by a reverse transformation. The main point of this mode is that the SPM image of a

surface is scanned repeatedly (but numerically) by an inverted tip. Then the restored topography image of the surface is as follows:

$R'(x) = I(x_{k1}) - P(x - x_{k1})$, under condition that $dI/dx = dP/dx$ in x_{k1} points of contact.

Here x_{k1} is the abscissa of the point of contact of the SPM image function with the inverted on the y and x axes function of the tip.

It is necessary to note, that the full restoration of the sample surface is possible only when the following two conditions are satisfied: first, during scanning the tip has touched all points of the surface, and, second, at each moment the tip has been touching only one point of the surface. If the tip cannot reach some area of the surface during scanning (for example, if the sample has overhanging parts of topography), then only partial restoration of the topography can be performed. At that, the more points of the surface were touched by the tip during scanning, the more authentically it is possible to reconstruct the surface.

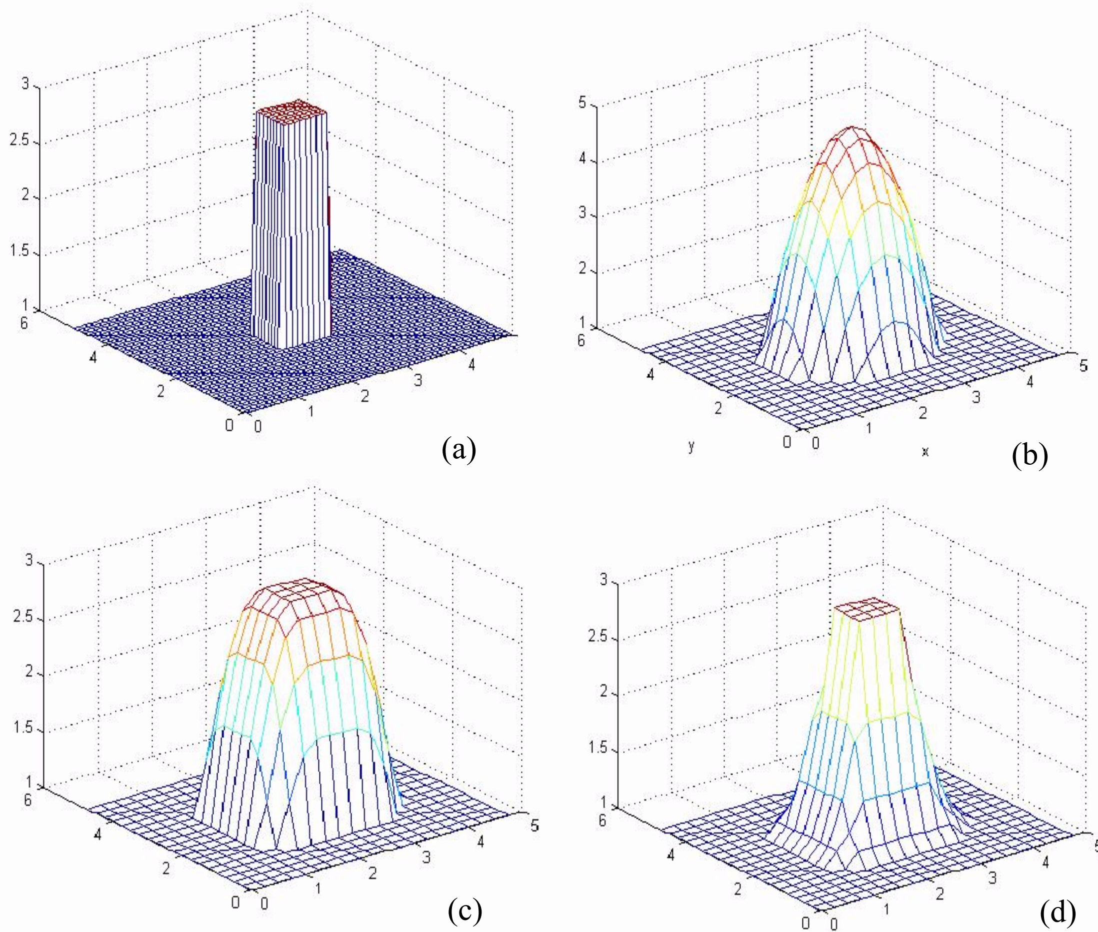

Fig. 35. Modeling of the surface topography restoration process

(a) – initial surface with inclusion in form of rectangular parallelepiped;

(b) – modeling form of the tip as a paraboloid of revolution;

(c) – result of convolution of the tip and initial surface;

(d) – restored image of the surface.

(Dimensions of images on X, Y, Z axes are specified in relative units).

In practice the SPM image and the obtained experimentally form of the tip represent two-dimensional array of discrete values for which the derivative is the ill-defined value. Therefore in practice instead of derivation of discrete functions during numerical deconvolution of the SPM images, the requirement of minimality of the tip-surface distance is used during scanning with a constant average height [Lit. 17]:

$$Min\ \{I(x_{k1}) - P(x-x_{k1})\}\ .$$

In this case it is possible to accept the minimal distance between the tip point and the corresponding point of a surface for the given position of the tip in relation to the surface as the topography height. This requirement in its physical sense is equivalent to the requirement of equality of derivatives; however, it allows to search the points of a tip-surface contact with a more adequate method, which essentially reduces the time of reconstruction of the topography.

Special test structures with known parameters of surface topography are used for calibration and determination of the form of the working part of the tip. Types of the most widespread test structures and their characteristic images that were obtained by an atomic-force microscope are shown on Fig. 36 and Fig. 37.

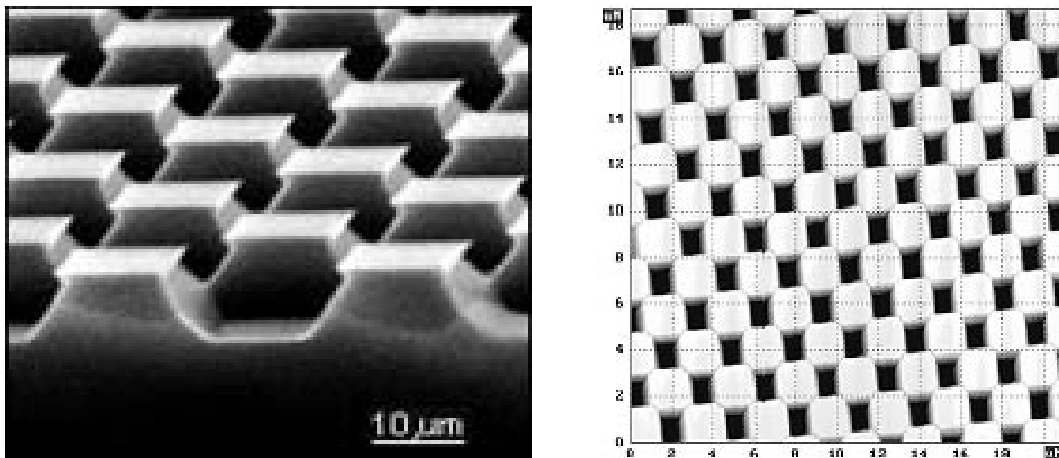

Fig. 36. Rectangular calibration lattice and its AFM image

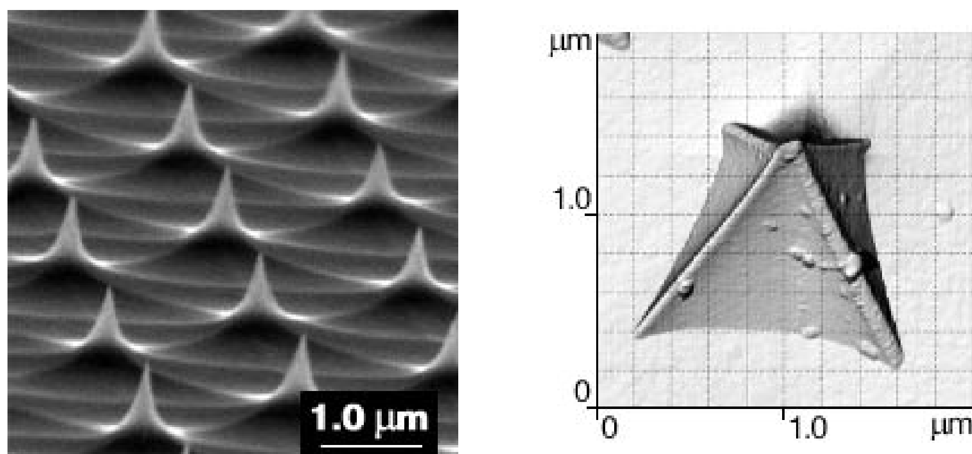

Fig. 37. Calibration lattice in form of sharp pins and its AFM image obtained by a tip of pyramidal form

The calibration lattice in form of sharp pins allows fixing the apex of the tip while the rectangular lattice helps to restore the form of a lateral surface. Combining the results of scanning of these lattices, it is possible to restore completely the form of the working part of tips.

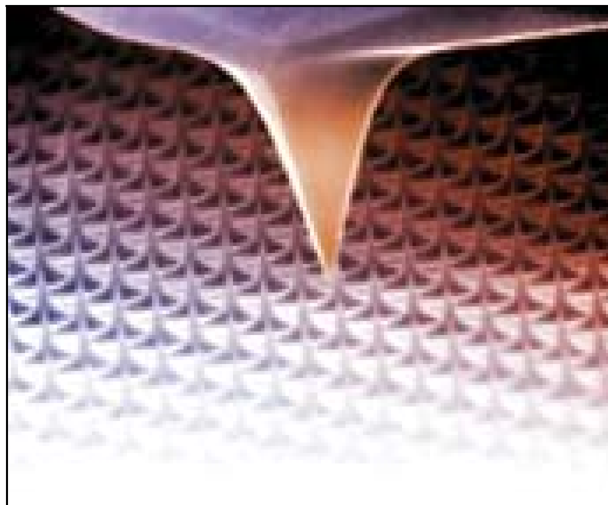

Fig. 38. Electron microscope image of the atomic-force microscope tip during scanning of a test structure

2. Modes of the scanning probe microscopy

2.1. Scanning tunnel microscopy

Historically, the first microscope in the family of probe microscopes is the scanning tunnel microscope. The principle of work of the STM is based on the phenomenon of electrons tunneling through a narrow potential barrier between a metal tip and a conducting sample in an external electric field.

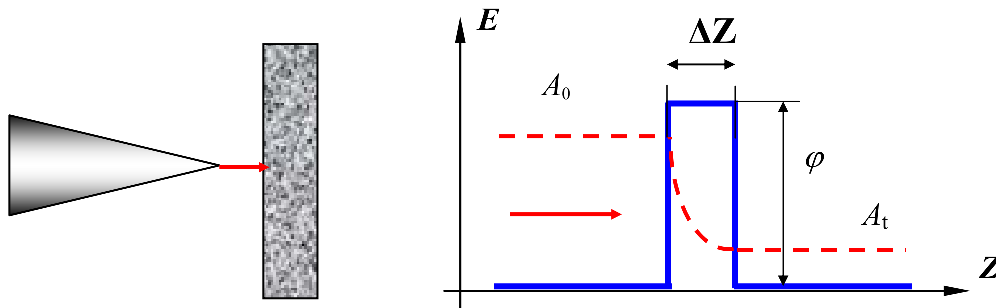

Fig. 39. Scheme of electrons tunneling through a potential barrier in a tunnel microscope

The tip in the STM is approached to the surface of a sample to distances of several Angstrems. This forms a tunnel-transparent barrier, which size is determined mainly by the values of work of electron emission from the material of a tip - φ_P and a sample φ_S. Upon qualitative examination the barrier can be considered rectangular with the effective height equal to the average material emission work:

$$\varphi^* = \frac{1}{2}(\varphi_P + \varphi_S).$$

As it is known from quantum mechanics [Lit. 19, Lit. 20], the probability of electron tunneling (transmission coefficient) through one-dimensional barrier of rectangular form is equal to

$$W = \frac{|A_t|^2}{|A_0|^2} \cong e^{-k\Delta Z},$$

where A_0 - amplitude of electron wave function, moving to a barrier; A_t - amplitude of electron wave function, that passed the barrier; k - attenuation constant of the wave function in the area corresponding to a potential barrier; ΔZ - width of a barrier. For tunnel contact of two metals the attenuation constant can be presented as

$$k = \frac{4\pi\sqrt{2m\varphi^*}}{h},$$

where m - electron weight, φ^* - average electron emission work, h – Planck constant. If the V difference of potentials is applied to the tunnel contact, the tunnel current appears between a tip and a sample.

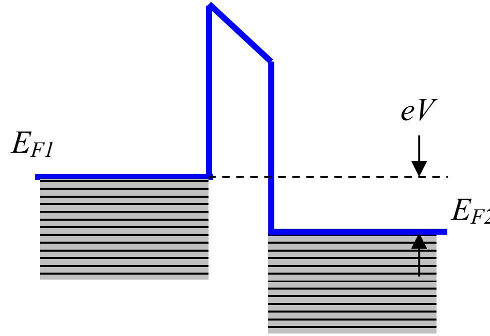

Fig. 40. Energy level diagram of two metals tunnel contact

Basically, electrons with energy near the E_F Fermi level participate in the tunneling process. In case of contact of two metals the expression for the tunnel current density (in one-dimensional approximation) has been derived in works [Lit. 21, Lit. 22]:

$$j_t = j_0\left[\varphi^* exp(-A\sqrt{\varphi^*}\Delta Z) - (\varphi^* + eV)exp(-A\sqrt{\varphi^* + eV}\,\Delta Z)\right], \quad (1)$$

where j_0 and A parameters are set by the following expressions:

$$j_0 = \frac{e}{2\pi\, h\,(\Delta Z)^2}, \qquad A = \frac{4\pi}{h}\sqrt{2m}.$$

Under condition of smallness of the bias voltage ($eV < \varphi$), the expression for a current density can be presented in a more simple kind. Linearizing the second exponent in expression (1) by eV parameter, we get

$$j_t = j_0\, exp(-A\sqrt{\varphi^*}\Delta Z)\cdot\left(\varphi^* - (\varphi^* + eV)\cdot\left(1 - \frac{AeV\Delta Z}{2\sqrt{\varphi^*}}\right)\right).$$

Finally, neglecting the eV tern in comparison with φ^*, the expression for the tunnel current density can be written down as follows:

$$j_t = j_0\frac{A\sqrt{\varphi^*}eV\Delta Z}{2}exp(-A\sqrt{\varphi^*}\Delta Z) = \frac{e^2\sqrt{2m\varphi^*}}{h^2}\cdot\frac{V}{\Delta Z}exp(-\frac{4\pi}{h}\sqrt{2m\varphi^*}\Delta Z).$$

Since the exponential dependence is very strong, the simplified formula is frequently used for estimations and qualitative reasonings:

$$j_t = j_0(V)\, e^{-\frac{4\pi}{h}\sqrt{2m\varphi^*}\,\Delta Z}, \qquad (2)$$

in which the $j_0(V)$ value is considered not dependent on the change of a tip-sample distance. For typical values of emission work ($\varphi \sim 4$ eV) the attenuation constant value $k = 2$ Å^{-1} so, when ΔZ is changed on ~ 1 Å, the value of a current varies in order of magnitude. Real tunnel contact in the STM is not one-dimensional and has more complex geometry; however, the basic features of tunneling, namely the exponential dependence of a current on the tip-sample distance, are the same also in more complex models, which proves to be true experimentally.

For the big values of bias voltage ($eV > \varphi^*$) the well-known Fowler – Nordheim formula for the field emission of electrons into vacuum is derived from expression (1):

$$J = \frac{e^3V^2}{8\pi h\varphi^*(\Delta Z)^2}\, exp\left[-\frac{8\pi\sqrt{2m}(\varphi^*)^{\frac{3}{2}}\Delta Z}{3ehV}\right].$$

The exponential dependence of a tunnel current on distance (2) allows adjusting the distance between a tip and a sample in a tunnel microscope with high accuracy. The STM represents an electromechanical system with a negative feedback. The feedback system keeps the tunnel current value between a tip and a sample at the set level (I_0), selected by the operator. The control of the tunnel current value and consequently, the tip-sample distances is performed by means of moving the tip along the Z axis with the help of a piezoelectric element (Fig. 41).

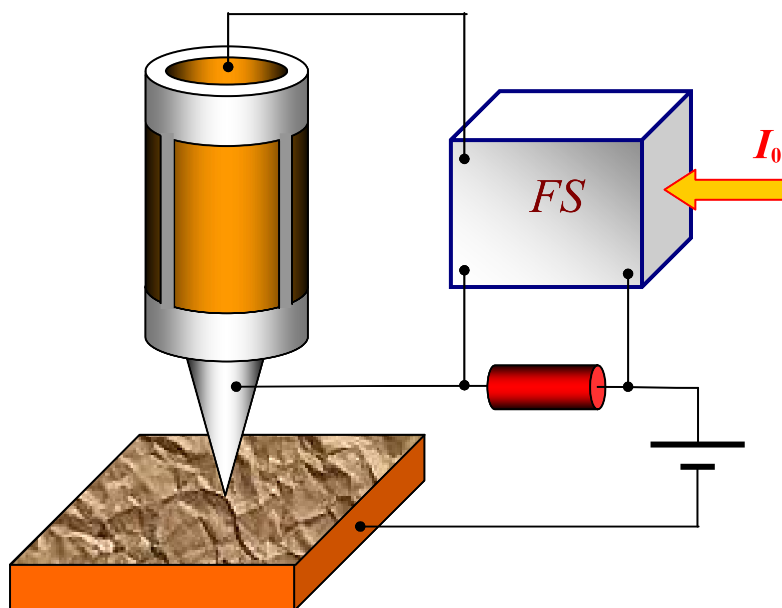

Fig. 41. Simplified scheme of organization of a feedback by the tunnel current

The image of a surface topography in the STM is formed in two ways. In the constant tunnel current mode (Fig. 42 (a)) the tip moves along a surface, performing raster scanning; during this the change of a voltage on the Z-electrode of a piezoelement in a feedback circuit (repeating the surface topography of a sample with high accuracy) is recorded to the memory of a computer as a Z=f(x,y) function, and is later reproduced by computer graphics.

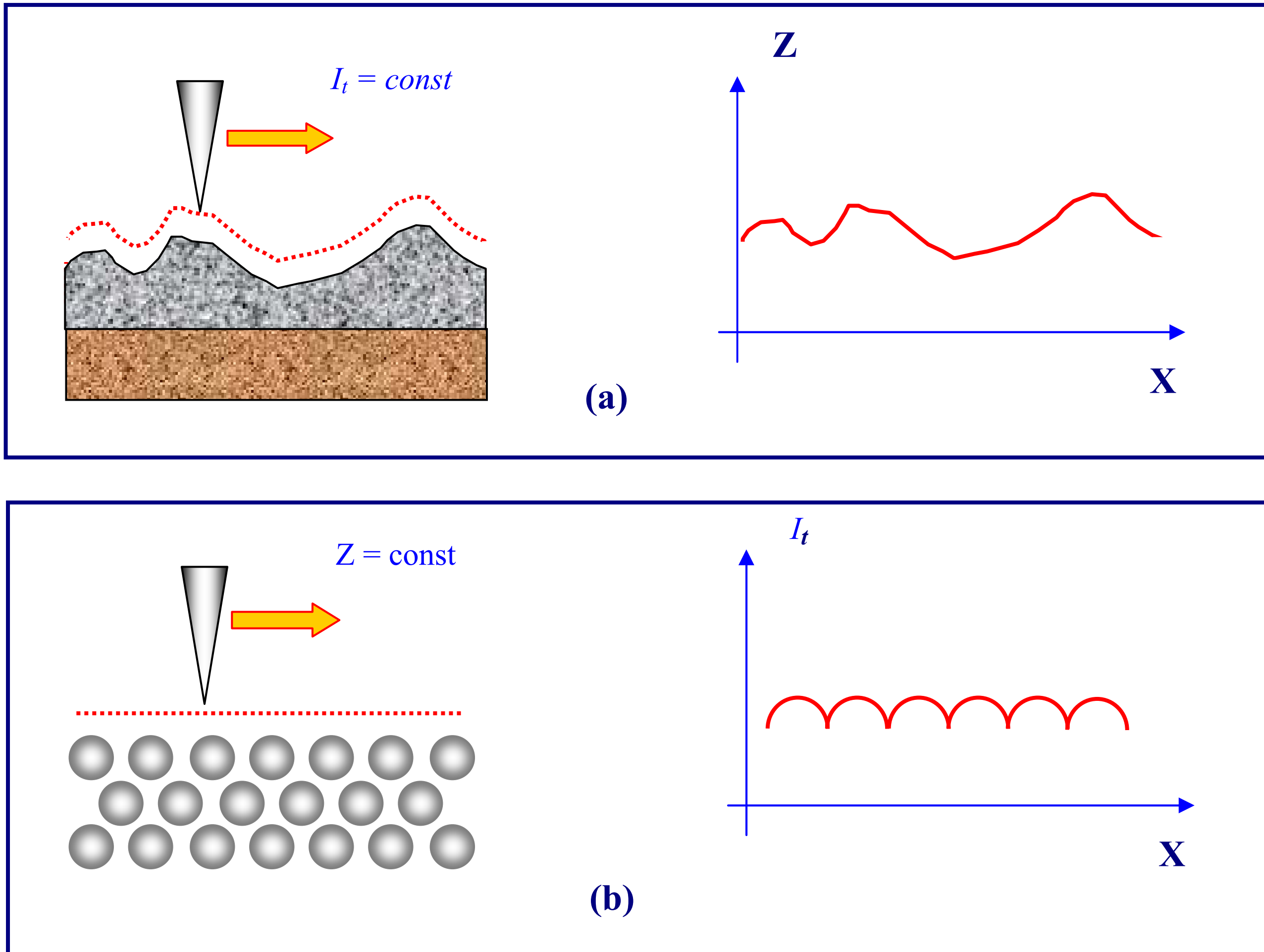

Fig. 42. Formation of STM images of a surface in a constant tunnel current mode (a) and constant average distance mode (b)

During research of atomic-smooth surfaces it is often more effective to acquire the STM image of a surface in the mode of Z = const constant height. In this case the tip moves above the surface on a distance of several Angstrem, thus changes of a tunnel current are registered as the STM image of a surface (Fig. 42 (b)). Scanning is done either with the feedback system switched off, or at a speed exceeding the FS reaction speed so that FS follows to indicate only smooth changes of a surface topography. This way implements very high speeds of scanning and high frequency of STM images acquisition, allowing to observe the changes occurring on a surface practically in real time.

High spatial resolution of the STM is defined by the exponential dependence of a tunnel current on the distance to a surface. The resolution in a direction to the normal to a surface achieves fractions of Angstrem. The lateral resolution depends on the quality of a tip and is determined basically not by the macroscopical radius of curvature of the apex of the tip, but its atomic structure. If the tip was correctly prepared, there is with a high probability either a single projecting atom on its apex, or a small cluster of atoms, which localizes it on the sizes much smaller, than a characteristic radius of the apex curvature. In fact, the tunnel current flows between surface atoms of a sample and atoms of a tip. The atom, projecting above a surface of a tip, is closer to the surface on the distance equal to the size of the crystal lattice spacing. Since the dependence of a tunnel current on the distance is exponential, the current basically flows in this case between the sample surface and the projecting atom on the apex of the tip.

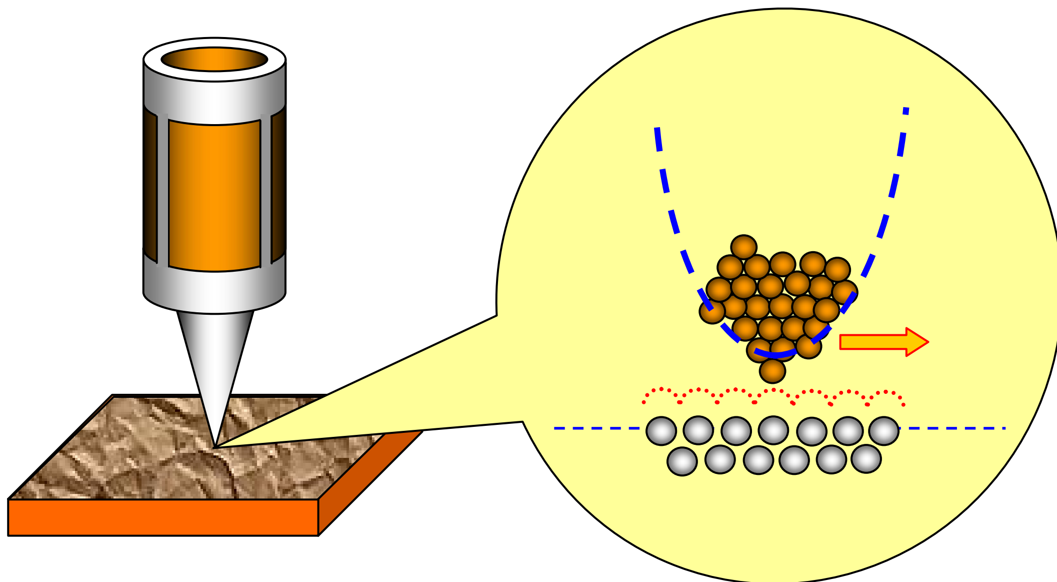

Fig. 43. Realization of the atomic resolution in a scanning tunnel microscope

Using such tips it is possible to acquire the spatial resolution down to atomic, which has been demonstrated by many research groups using samples from various materials.

Tips for tunnel microscopes

Tips of several types are used in scanning tunnel microscopes. In the beginning tips made from a tungsten wire by a method of electrochemical etching were widely used. This technology was well-known and was used for preparation of emitters for autoionic microscopes. The process of preparation of STM tips using this technology is as follows. The tungsten wire workpiece is fixed so that one of its ends passes through a conducting diaphragm (D) and is immersed in a water solution of alkali KOH (Fig. 44). The contact between a diaphragm and a tungsten wire is performed by means of a KOH drop located in the diaphragm opening.

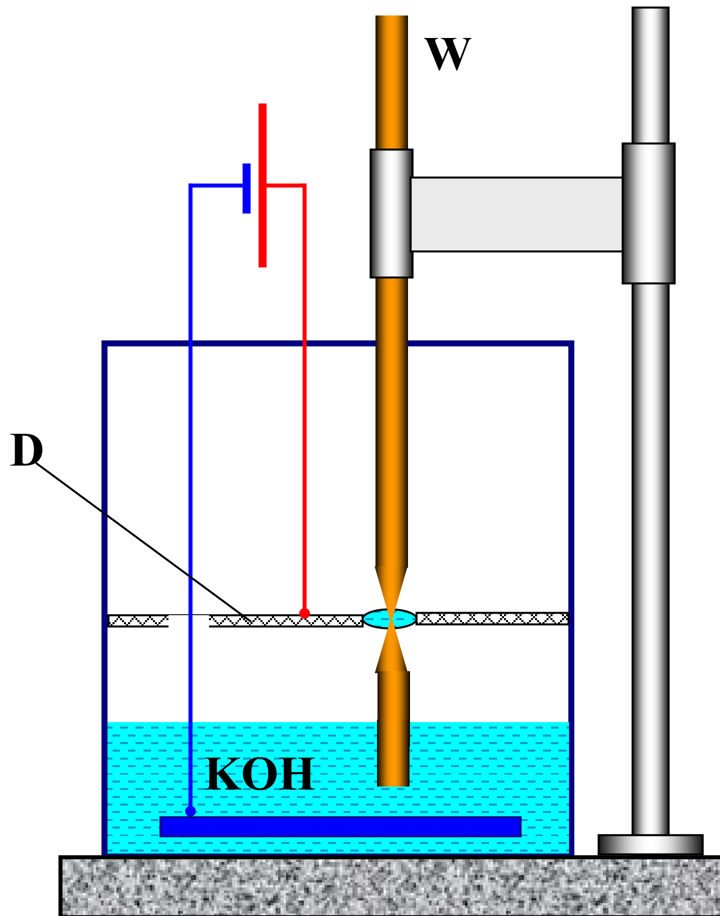

Fig. 44. The STM tips manufacturing scheme from a tungsten wire by electrochemical etching

While passing the electric current between a diaphragm and an electrode located in the KOH solution, excessive etching of a workpiece occurs. As far as etching goes, thickness of the etched area becomes so small, that breakage of the workpiece occurs due to weight of its bottom part. The bottom part falls down, automatically breaking the electric circuit and terminating the process of etching.

Another widely used technique of STM tips preparation is cutting of a thin wire from PtIr alloy using ordinary scissors. The cutting is made at an angle about 45 degrees with simultaneous P tension of a wire to tear it apart (Fig. 45).

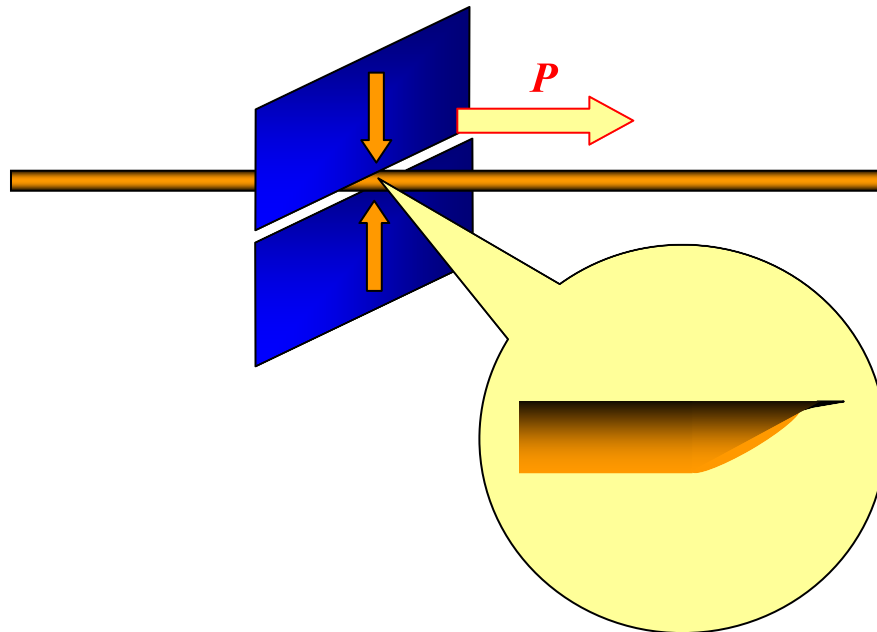

Fig. 45. Schematical image of process of STM apex formation during cutting of a PtIr alloy wire

Process of apex formation in this case is partly similar to the process of manufacturing of an apex of a tip from tungsten. During cutting there is a plastic deformation of a wire in the cutting place and its breakage under action of the P stretching force. As a result, in the place of cutting an extended apex with a ragged (curled) edge is formed with numerous protrusive defects, one of which becomes the working element of the STM tip. This manufacturing technique of STM tips is applied now practically in all laboratories and provides almost always the guaranteed atomic resolution during STM research of a surface.

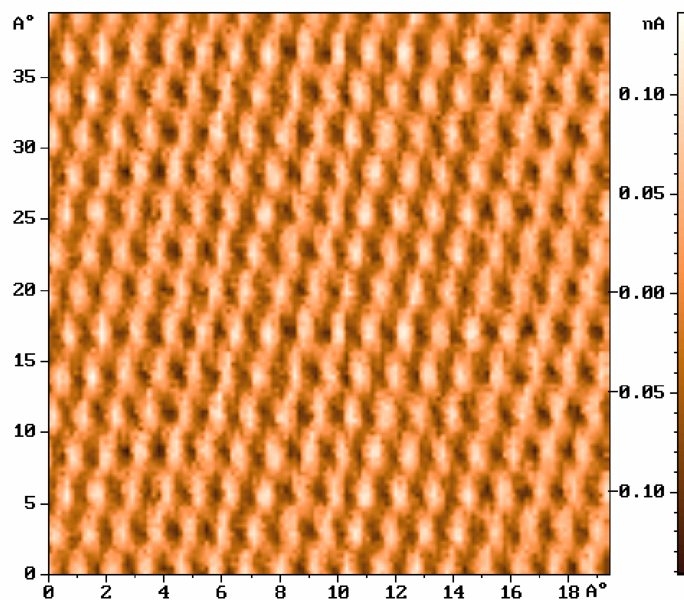

Fig. 46. The STM image of an atomic structure of a surface of pyrolitic graphite

Measurement of the local emission work in the STM

For non-uniform samples the tunnel current is not only a function of tip-sample distance, but also depends on the value of local electrons emission work in the given place of a surface. The method of ΔZ tip-sample distance modulation is applied to obtain the information on distribution of emission work. With this purpose variable voltage from external generator with ω frequency is added during scanning to a control voltage on a Z-electrode of the scanner. Then the voltage on a Z-electrode of the scanner can be presented as

$$U = U_0(t) + U_m Sin(\omega t).$$

It results in that the tip-sample distance appears promodulated on ω frequency:

$$\Delta Z(t) = \Delta Z_0(t) + \Delta Z_m Sin(\omega t),$$

where ΔZ_m and U_m are connected to each other through the electromechanical connection coefficient of the K piezo-scanner:

$$K = \frac{\Delta Z_m}{U_m}.$$

Frequency ω is selected bigger than the frequency of a passband of a feedback loop so that the feedback system could not follow to indicate the given oscillations of a tip. The amplitude of U_m variable voltage is selected small enough so that disturbance of a tunnel interval was also small.

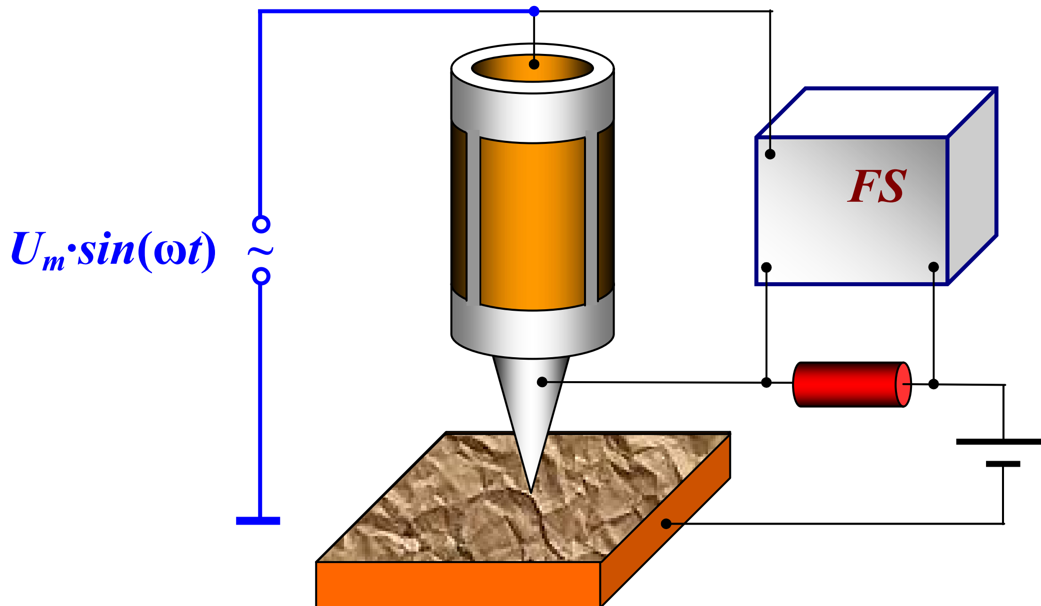

Fig. 47. Local emission work registration scheme

In turn, oscillations of the tip-sample distance result in that there is a variable current component with ω frequency:

$$I_t \cong I_0(V)\, e^{-\alpha\sqrt{\varphi^*}\,(\Delta Z_0 + \Delta Z_m\, Sin(\omega t))}$$, where $\alpha = \frac{2}{\hbar}\sqrt{2m}$.

Since the amplitude of a modulation signal and accordingly the amplitude of oscillations of a tunnel interval are small, the tunnel current can be presented as

$$I_t \cong I_o(V)\, e^{-\alpha\sqrt{\varphi}\,\Delta Z_0}(1-\alpha\sqrt{\varphi}\,\Delta Z_m Sin(\omega t)).$$

Thus, the amplitude of small oscillations of a tunnel current with ω frequency appears proportional to a root square of the local electrons emission from a sample surface work value:

$$I_\omega = I_0 \frac{2KU_m}{\hbar}\left[2m\varphi^*(x,y)\right]^{\frac{1}{2}}.$$

Detecting the amplitude of oscillations of a tunnel current in each point of the frame, it is possible to build the distribution of local emission work φ (x, y) simultaneously with the Z = f (x, y) topography on a test area of a surface.

Measurement of tunnel contact volt-ampere characteristics

Using STM it is possible to measure tunnel contact volt-ampere characteristics (VAC) in various points of a surface that allows to judge local conductivity of a sample and to study features of local density of states in a power spectrum of electrons. The following procedure is applied to register volt-ampere characteristics of a tunnel contact in the STM. The area of a sample, where measurements will be conducted, is selected on the STM image of a surface. The STM tip is moved by the scanner to a corresponding point of the surface. To acquire the contact VAC the feedback is broken for a short time, and the linearly increasing voltage is applied to the tunnel interval. During this the current flowing through the tunnel contact is registered synchronously with the voltage change. During VAC measurement the potential equal to the potential right before the feedback breakage is applied to the scanner electrode for the period of feedback breakage.

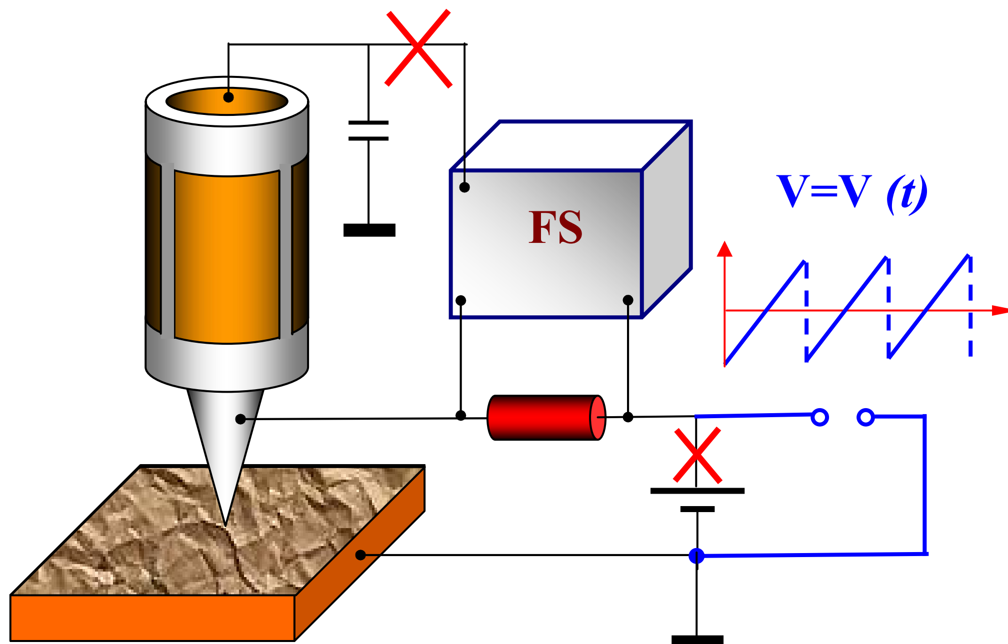

Fig. 48. VAC registration scheme of the STM tunnel interval

Several VACs are measured in every point. Final volt-ampere characteristic is obtained by averaging the VAC set, measured in one point. Averaging allows to minimize essentially the influence of noise on the tunnel interval.

STM control system

The simplified STM control system scheme is presented on Fig. 49. The STM control system consists of a digital part realized on the basis of a personal computer, and an analog part, executed usually as a standalone block. The digital part consists of a DAC and ADC set and is indicated on the scheme with red dotted border. The analog part is shown on the circuit by a dark blue dashed line. The *U* voltage on a tunnel interval is set by the operator using DAC, and the current *I*, supported by the feedback system, is set using DAC. Two-channel digital-to-analog converters DAC - X and DAC – Y serve to form horizontal and vertical scanning. The feedback loop consists of the preliminary PU amplifier structurally located in the STM measurement head, the differential RU amplifier, the low-frequency filter, amplifiers U4 and U5, the piezo-converter, controlling the tunnel interval value.

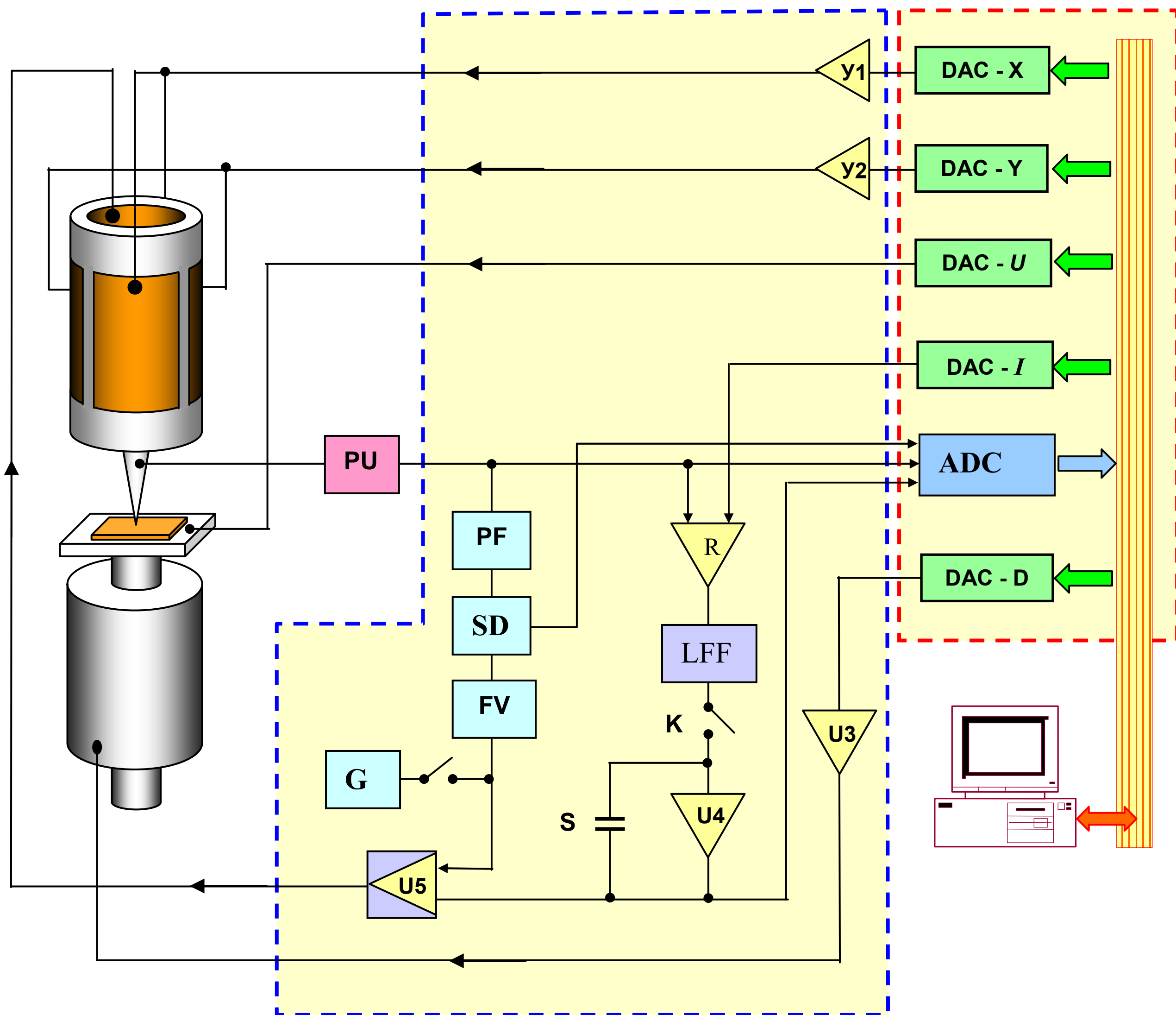

Fig. 49. The scanning tunnel microscope control system scheme

Prior to the start of work the operator establishes working parameters of a tunnel current and voltage and switches on the system of tip-sample approach. During this the control voltage is submitted to the motor from DAC–D. In the initial state there is no current in a feedback loop, and the scanner is extended as much as possible in a direction to a sample. When the tunnel current appears, the feedback retracts the scanner, and the system changes over to the mode of exact installation of a sample. In this mode there is a mutual movement of a sample and retraction (by the feedback system) of the tip until the scanner sets in the middle of the dynamic range. The value of a tunnel current set by the operator is supported constant in a feedback loop during this.

Scanning of a sample is performed when the sawtooth form voltage is submitted to external electrodes of the tubular scanner with the help two-channel DAC–X and DAC–Y and two-channel high-voltage amplifiers U1 and U2. During scanning the feedback system keeps the tunnel current constant. It is done in the following way. The real instantaneous value of a tunnel current I_t is compared on the differential amplifier to the I_0 value, set by the operator. The differential signal $(I_t - I_0)$ is amplified (by U4 and U5 amplifiers) and submitted to the internal Z-electrode of the scanner. Thus, the voltage on the Z-electrode of the scanner appears during scanning proportional to the surface topography. The signal from U4 amplifier output is recorded by ADC as the information on a surface topography.

To acquire the information on distribution of local emission work the G generator signal is mixed up on U5 amplifier to the Z-electrode voltage. The corresponding component of a tunnel current with ω frequency is extracted by the strip filter PF and is detected with the help of synchronous detector SD, to which the base voltage from the driving generator is also applied. The phase of signals is synchronized with the help of phase shifter FV. The current amplitude with ω frequency is recorded in memory of a computer by ADC as a signal proportional to the local emission work.

Registration of a tunnel contact VAC in a set point of a sample is performed as follows. The feedback is broken off for a short time using K electronic key. The voltage on an internal electrode of the piezo-tube is kept constant by the C condenser so that the tip hangs above the surface for a short time. After that the sawtooth form *U (t)* voltage is applied to a tunnel interval from DAC - *U*, and synchronously with it the information on a tunnel current from the preliminary amplifier PU output is recorded in ADC. After that the key K is closed, and the feedback system restores the tunnel contact state corresponding to the $I_t = const$ condition. If necessary, the procedure of VAC measurement is repeated *N* times to create average dependences of a tunnel current from voltage.

Constructions of scanning tunnel microscopes

Today hundreds of various scanning probe microscope constructions are described in the literature. On the one hand, such number of developed SPMs is caused by practical necessity, since certain SPM configuration is frequently needed for solution of specific tasks. On the other hand, relative simplicity of the SPM mechanical part stimulates manufacturing of measurement heads, adapted as much as possible to conditions of a specific experiment directly in scientific laboratories.

Construction of the STM measuring head should satisfy to a lot of requirements for its effective work. The most important of them is the requirement of high noise immunity. It is caused by the big sensitivity of a tunnel interval to external vibrations, temperature drops, electric and acoustic interference. Wide experience is obtained for today in this direction; ways of STM protection from influence of various external factors are developed effectively enough. Finally, the choice of a vibration isolation and thermal compensation system is dictated, basically, by the expediency and

convenience of use. Another not less important group of requirements to the STM construction is connected to conditions of application of a developed microscope and determined by the tasks of a specific experiment.

As an example, the STM measuring head construction with thermal drift compensation of a tip position is schematically shown on Fig. 50.

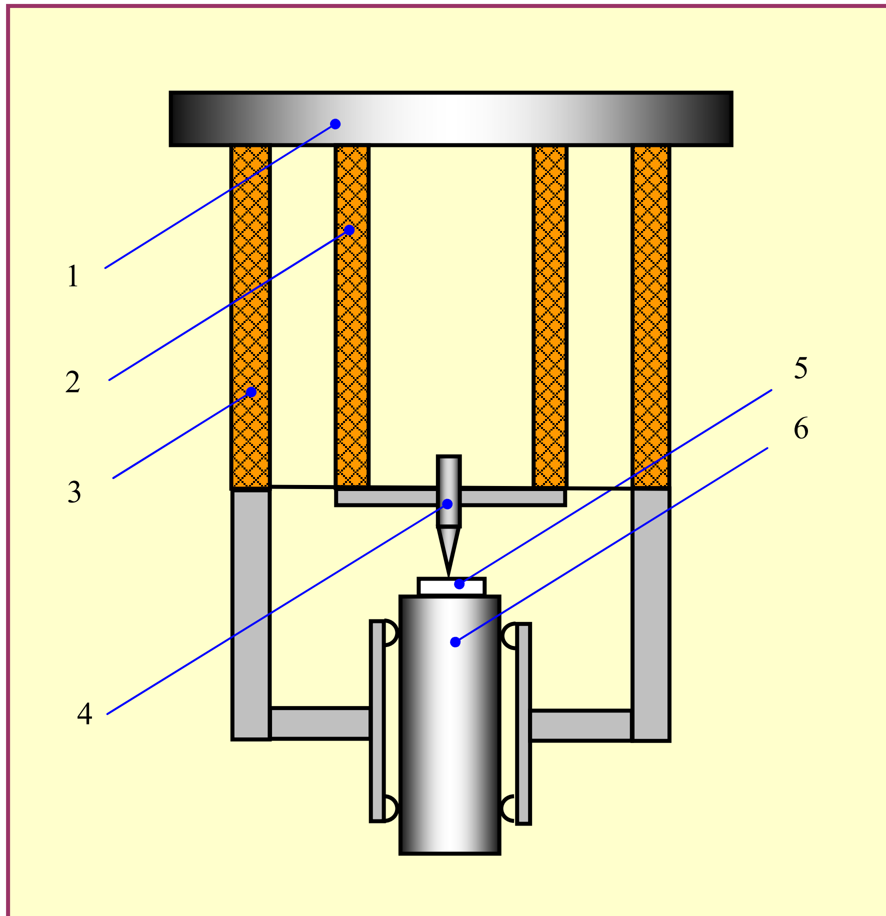

Fig. 50. STM measuring head construction
1 - base; 2 – tubular three-coordinate piezo-scanner;
3 – temperature-compensating piezo-tube, serving as a working element of a step-by-step piezo-motor; 4 – metal tip; 5 – sample;
6 - cylindrical holder of a sample

The basis of a construction are the two coaxial piezoceramic tubes of various diameter fixed on the common base (1). The internal tube (2) plays the role of a three-coordinate piezo-scanner. The external tube (3) is a multipurpose part of a construction. First, the external tube plays the role of the internal tube thermal deformations equalizer, stabilizing the position of a tip in a direction of a normal to a researched surface. Second, it is a working element of a step-by-step piezo-motor, serving to approach the tip to a sample. The whole STM construction has axial symmetry that reduces tip position thermal drift in the plane of a researched sample surface.

Tunnel spectroscopy

The scanning tunnel microscope allows to receive volt-ampere characteristics (VAC) of tunnel tip-surface contact in any point of a surface and to investigate local electric properties of a sample. For characteristic voltages on the tunnel contact of about 0.1–1 V and tunnel currents at a level of 0.1–1 μA the R_t tunnel contact resistance under the order of magnitude makes $10^8 \div 10^{10}$ Ohm. As a rule, the R_S resistance of samples researched in STM is much less than R_t and the VAC character is defined, basically, by the properties of a small sample area near the tunnel contact.

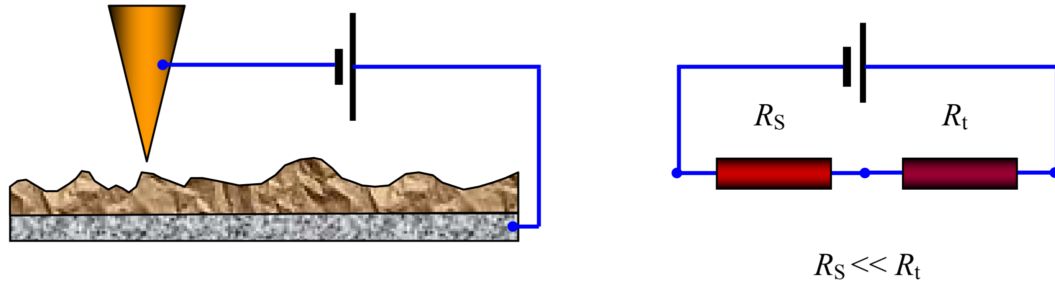

Fig. 51. Equivalent scheme of a direct current tunnel contact

The character of a tunnel VAC essentially depends on the electrons power spectrum in a sample. Fig. 52 shows the power diagram of a tunnel contact of two metals.

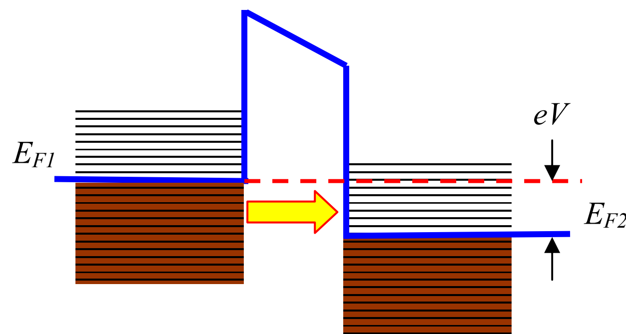

Fig. 52. Power diagram of a tunnel contact of two metals

Mainly electrons with energies near to Fermi level participate in a tunnel current. During direct bias (Fig. 52) the electrons are tunneling from the filled states of a conductivity area of the tip to the free states of a conductivity area of a sample. During reverse bias the electrons are tunneling from a sample to the tip. The value of a tunnel current is defined by the bias voltage, the barrier transparency coefficient and the density of states near Fermi level. The expression for a tunnel current in case of a discrete electronic spectrum has been received in works [Lit. 23-Lit. 25]. In approximation of near-continuous spectrum of electrons the expression for a tunnel current can be written down in the following way [Lit. 22, Lit. 26]:

$$dI = A \cdot D(E)\rho_P(E)f_P(E)\rho_S(E)(1 - f_S(E))dE,$$

where A – some constant; $D(E)$ - barrier transparency; $\rho_P(E)$, $\rho_S(E)$ - density of states in a material of the tip and a researched sample accordingly; $f(E)$ - Fermi distribution function. In the simplest case of a rectangular barrier at low temperatures and on the assumption, that the density of

states near Fermi level in the tip metal is practically constant, the expression for a current can be written down as

$$I(V) = B\int_0^{eV} \rho_S(E)dE$$

In this case the dependence of a tunnel current on a voltage is determined, basically, by the density of states in a power spectrum of a sample. In practice the $\rho_S(E)$ value is estimated by the value of a tunnel current derivative with respect to voltage:

$$\rho_S(eV) \sim \frac{\partial I}{\partial V} \ .$$

Researches of local tunnel spectra of various materials is performed, as a rule, in conditions of high vacuum (since the tunnel current is very sensitive to the state of a surface of researched samples) and at low temperatures (since the thermal excitation dither strongly the features in electronic spectra).

Metal - metal contact VAC

Electron tunneling through a barrier between two metals was examined in many works long before the STM occurrence [Lit. 27, Lit. 28]. As it has been shown above, for small bias voltages the dependence of a tunnel current on a voltage is linear, and the conductivity of a tunnel contact is defined, basically, by parameters of a barrier:

$$j_t = j_0(V)\, e^{-\frac{4\pi}{h}\sqrt{2m\varphi^*}\,\Delta Z} \ .$$

At very high voltages the form of a barrier will strongly change, and the current will be described by the Fowler-Nordheim formula. A typical VAC, observed for the metal-metal tunnel contact, is represented schematically on Fig. 53.

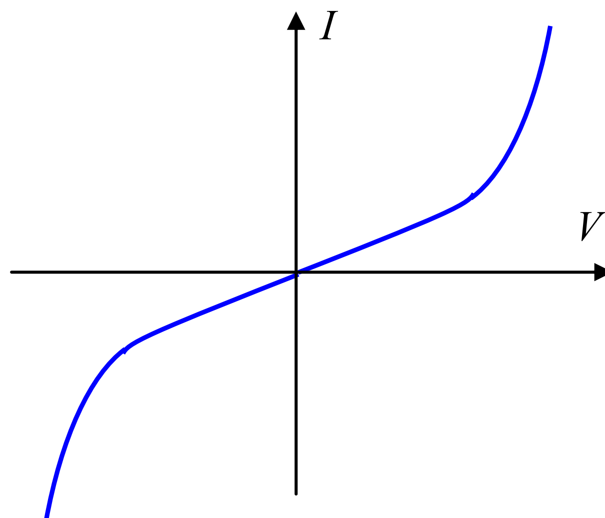

Fig. 53. Generic metal-metal tunnel contact VAC

As it can be seen from the figure, the volt-ampere characteristic of the metal-metal tunnel contact is nonlinear and, as a rule, is practically symmetric.

Metal–semiconductor contact VAC

Semi-conductor samples have more complex structure of the electron power spectrum.

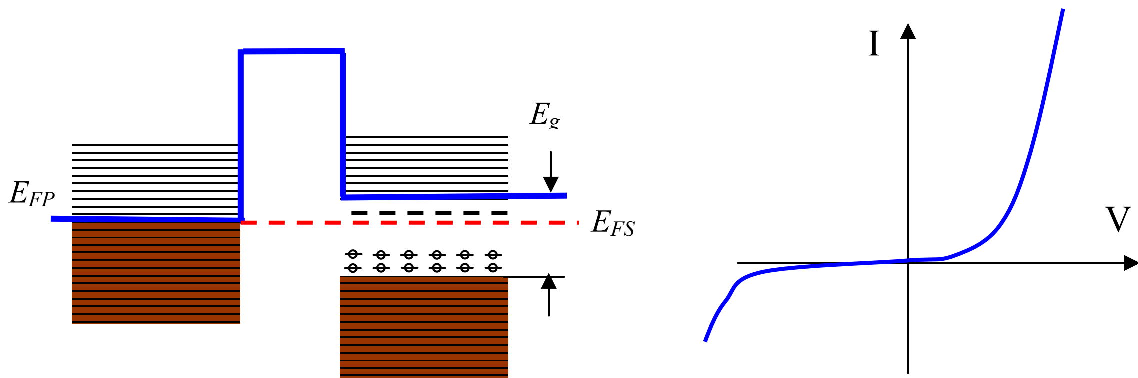

Fig. 54. Power diagram and generic VAC of a metal-semiconductor tunnel contact

Presence of an energy gap band and impurity levels in a spectrum of semi-conductor materials makes the VAC of a metal-semiconductor tunnel contact strongly nonlinear. Essential contribution to the tunnel current is made also by the surface states and the levels of energy connected to foreign atoms adsorbed on a surface. Therefore researches of local tunnel spectra of semi-conductor materials are conducted in conditions of high vacuum. Uncontrollable presence on a surface of adsorbed atoms strongly complicates the interpretation of tunnel spectra obtained in experiment. Besides that, thermal excitations result in significant widening of discrete energy levels corresponding to localized states, and also strongly dither the position of a conductivity zone and a valence energy band edges. As an example, the tunnel spectrum of a GaAs sample acquired in work [Lit. 29] is presented on Fig. 55.

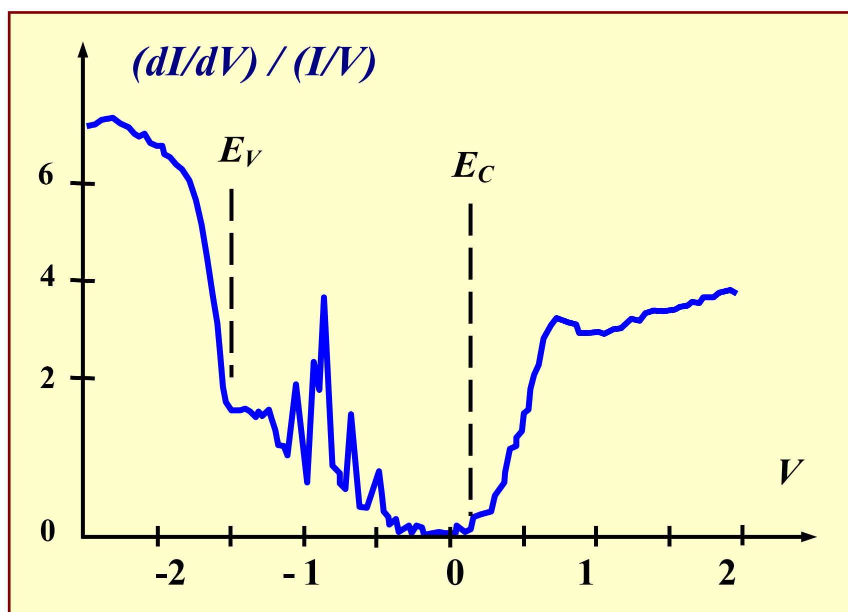

Fig. 55. STM spectrum of a n-GaAs crystal surface

Tunnel spectra allow to determine positions of edges of a conductivity zone and a valence energy band in regard to the Fermi level, and also to identify the spectral peaks due to impurity states inside the energy gap band of semiconductors.

Metal-superconductor contact VAC

There is a phase transition in superconducting materials at temperatures below critical accompanying with reorganization of the electron power spectrum. At low temperatures electrons form the superconducting pairs and are condensed at a level, distant on the Δ value from the conductivity zone. The power diagram of a metal–superconductor contact is presented on Fig. 56 [Lit. 30].

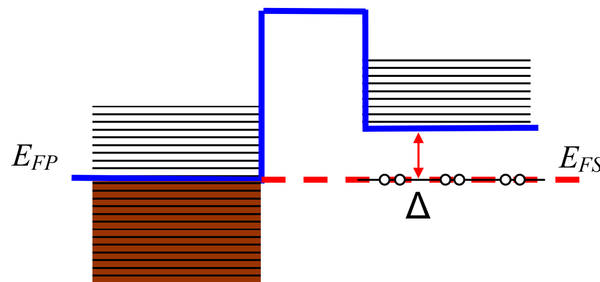

Fig. 56. Power diagram of a metal–superconductor contact

During direct bias the tunnel current through the contact occurs only at eV>Δ voltage. For simplicity we count the barrier thin, so the potential is not falling on it. In this case the electrons from a tip are tunneling to the free states of a superconducting sample (Fig. 57 (a)).

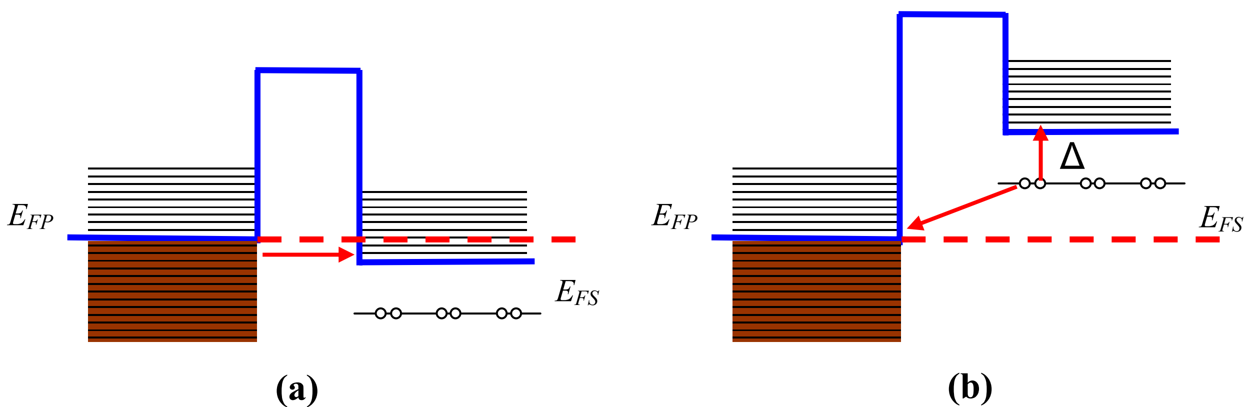

Fig. 57. Power diagram of a metal– superconductor contact during direct and reverse biases

During reverse bias the picture of tunneling is little bit more complex. Since during tunneling the energy of the system is conserved, the tunneling process in this case occurs as follows. The superconducting pair is split; thus one electron leaves with a loss of energy to the free state near the Fermi level of metal, and the second electron, receiving the Δ energy, jumps to the excited state in a superconductor spectrum. Thus, the volt-ampere characteristic of a metal-superconductor tunnel

contact at T = 0 temperature contains two branches at $|eV| > \Delta$ (Fig. 58 (a)). The corresponding density of states in a superconductor spectrum is presented on Fig. 58 (b).

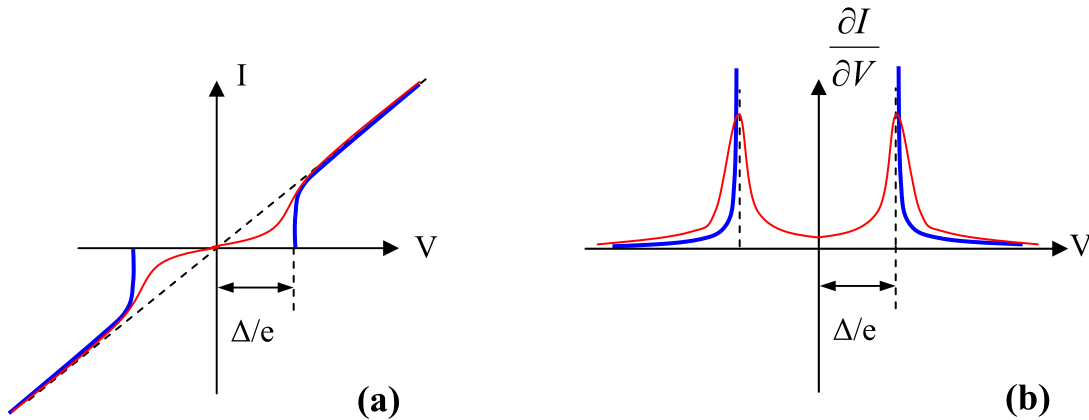

Fig. 58. Volt-ampere characteristic of a metal-superconductor contact (a) and density of states of a superconductor (b) at T = 0 (shown in dark blue color). (Red color shows the VAC and the density of states at T ≠ 0)

At non-zero temperatures the power spectrum of a superconductor is partly dithered, so spectral features of superconductors are expressed less precisely in real volt-ampere characteristics.

One of the scanning tunnel microscopy and spectroscopy applications is the research of heterogeneity of electric properties of complex structure samples. In this case the simultaneous analysis of morphology of a surface and the volt-ampere characteristics which, have been measured in various points of a surface, allows to judge on the distribution of various phases on surfaces of composite structures, to investigate correlations between technological parameters of their acquisition and electronic properties. In particular, measuring a VAC in various points of a surface, it is possible to investigate the distribution of a superconducting phase in samples of non-uniform structure. With this purpose VAC is measured during scanning simultaneously with registration of a surface topography in every point. The value of Δ parameter, which is recorded in a separate file, is calculated using local VAC. $\Delta = f(x, y)$ distribution is built henceforth, characterizing the structure of a superconducting state of a sample.

2.2. Atomic force microscopy

Atomic force microscope (AFM) was invented in 1986 by Gerd Binnig, Calvin Calvin F. Quate and Christopher Herber [Lit. 31]. In a basis of AFM work lies the force interaction between a tip and a surface for registration of which special probes are used, representing an elastic console with a sharp tip on the end (Fig. 59). The force affecting the tip from the surface, results in a console bend. Registering the size of a bend, it is possible to control the interaction force of the tip with the surface.

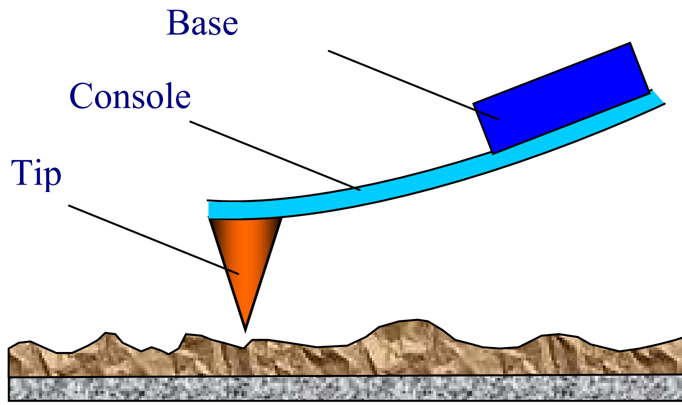

Fig. 59. AFM probe schematic image

Work of the AFM can be qualitatively explained by the example of van der Waals forces [Lit. 32]. Most frequently the van der Waals interactions energy of two atoms, located on the r distance from each other, is approximated by the exponential function - Lennard-Jones potential:

$$U_{LD}(r) = U_0 \left\{ -2\left(\frac{r_0}{r}\right)^6 + \left(\frac{r_0}{r}\right)^{12} \right\}.$$

The first term of sum in the given expression describes the long-distance attraction caused, basically, by a dipole-dipole interaction of atoms. The second term takes into account the atoms repulsion on small distances. The ro parameter is the equilibrium distance between atoms, U_0 - energy value in the minimum.

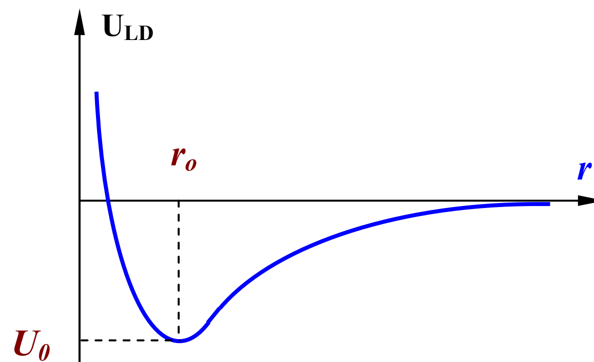

Fig. 60. Lennard-Jones potential qualitative form

Lennard-Jones potential allows to estimate the interaction force of a tip with a sample [Lit. 33]. The common energy of the system can be derived, summarizing elementary interactions for each of the atoms of a tip and a sample.

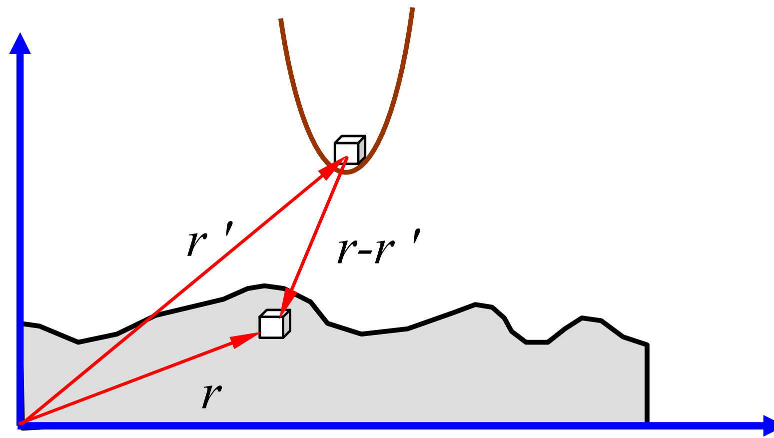

Fig. 61. To calculation of interaction energy of a tip and a sample

Then for the interaction energy we get:

$$W_{PS} = \iint_{V_P V_S} U_{LD}(r - r')\, n_P(r')\, n_S(r) dV dV' ,$$

where $n_S(r)$ and $n_P(r')$ - densities of atoms in a material of a sample and a tip. Accordingly, the force affecting the tip from a surface can be calculated as follows:

$$\vec{F}_{PS} = -grad(W_{PS}).$$

Generally this force has both a normal to a surface component as well as a lateral one (laying in the plane of a sample surface). Real interaction of a tip with a sample has more complex character; however, the basic features of the given interaction are the same – the AFM tip experiences attraction from the sample on big distances and repulsion on small ones.

Acquisition of the AFM images of a surface topography is connected to the registration of small bends of the probe elastic console. For this purpose optical methods (Fig. 62) are widely used in atomic force microscopy.

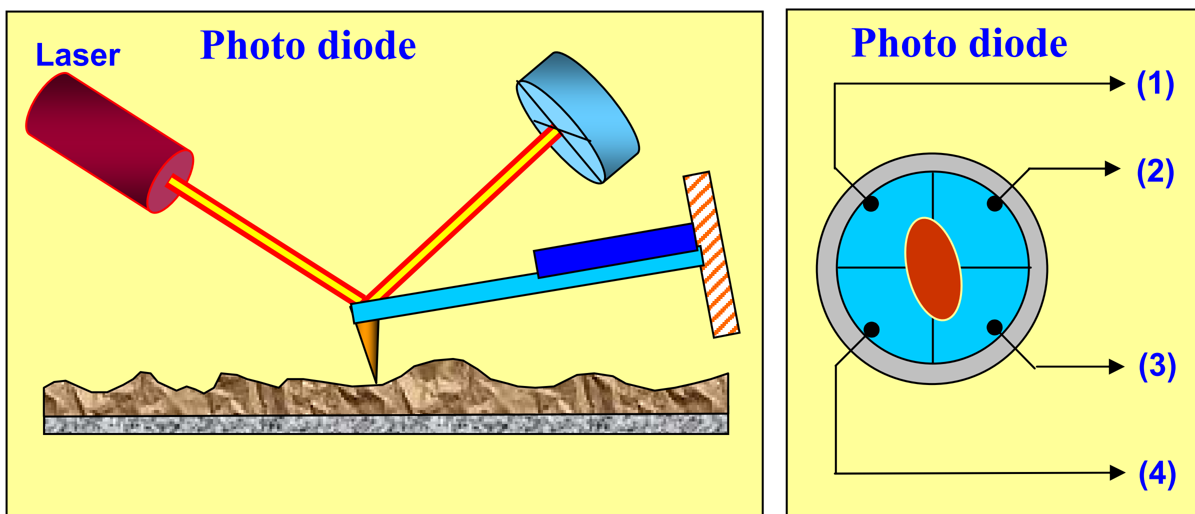

Fig. 62. Optical registration of a bend of the AFM probe console scheme

The optical AFM system is aligned so that radiation of the semi-conductor laser is focused on the probe console, and the reflected beam hits the center of a photosensitive area of a photodetector. Four-section semi-conductor photodiodes are applied as position-sensitive photodetectors.

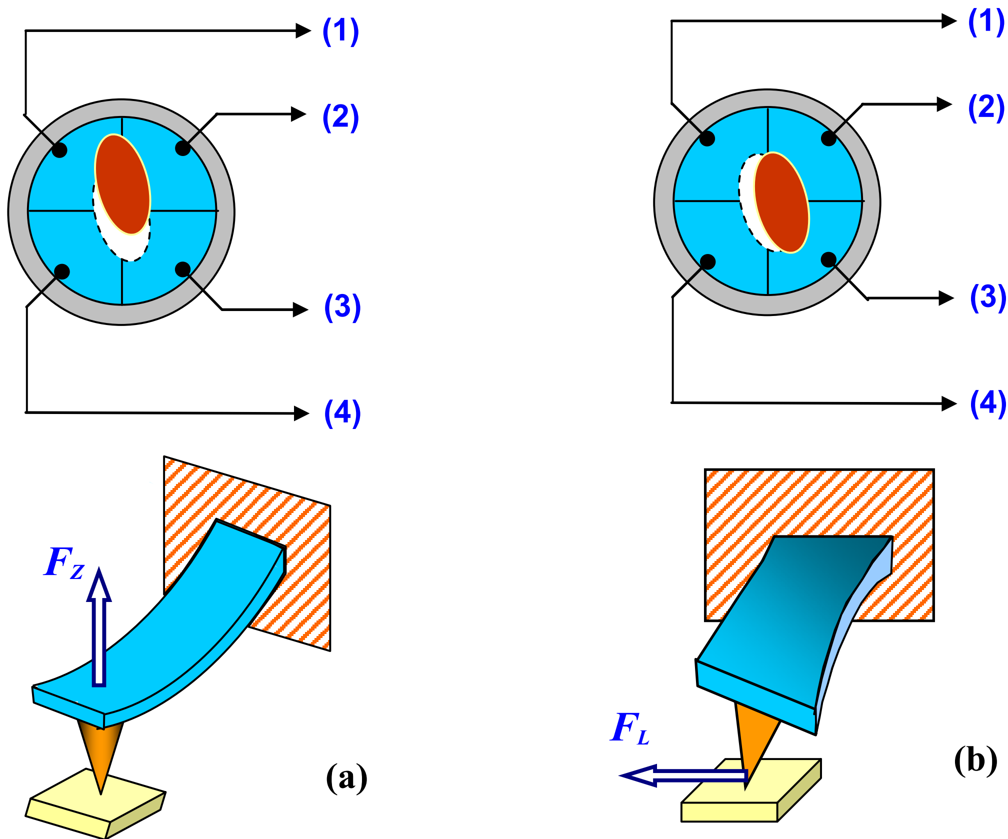

Fig. 63. Conformity between the types of bending deformations of the probe console and the change of exposure spot position on the photodiode

The basic parameters registered by the optical system are the bending deformations of the console under influence of Z-components of attraction or repulsion forces (F_Z) and deformations of console torsion under influence of lateral components of (F_L) interaction forces of a tip with a surface. If reference values of a photocurrent in the photodiode sections are designated as I_{01}, I_{02}, I_{03}, I_{04}, and I_1, I_2, I_3, I_4 are the values of currents after change of the console position, then differential currents from various sections of the photodiode $\Delta I_i = I_i - I_{0i}$ will identically characterize the value and direction of a bend of the AFM probe console. In fact, the difference of currents of the following kind

$$\Delta I_z = (\Delta I_1 + \Delta I_2) - (\Delta I_3 + \Delta I_4)$$

is proportional to the console bend under influence of the force acting normally to a sample surface (Fig. 63 (a)), and the combination of differential currents of the following kind

$$\Delta I_L = (\Delta I_1 + \Delta I_4) - (\Delta I_2 + \Delta I_3)$$

characterizes the console bend under influence of lateral forces (Fig. 63 (b)).

The ΔI_Z value is used as an input parameter in a feedback loop of the atomic force microscope (Fig. 64). The feedback system (FS) provides $\Delta I_Z = const$ with the help of a piezoelectric actuating element, which supports the console bend ΔZ equal to the ΔZ_0 value set by the operator.

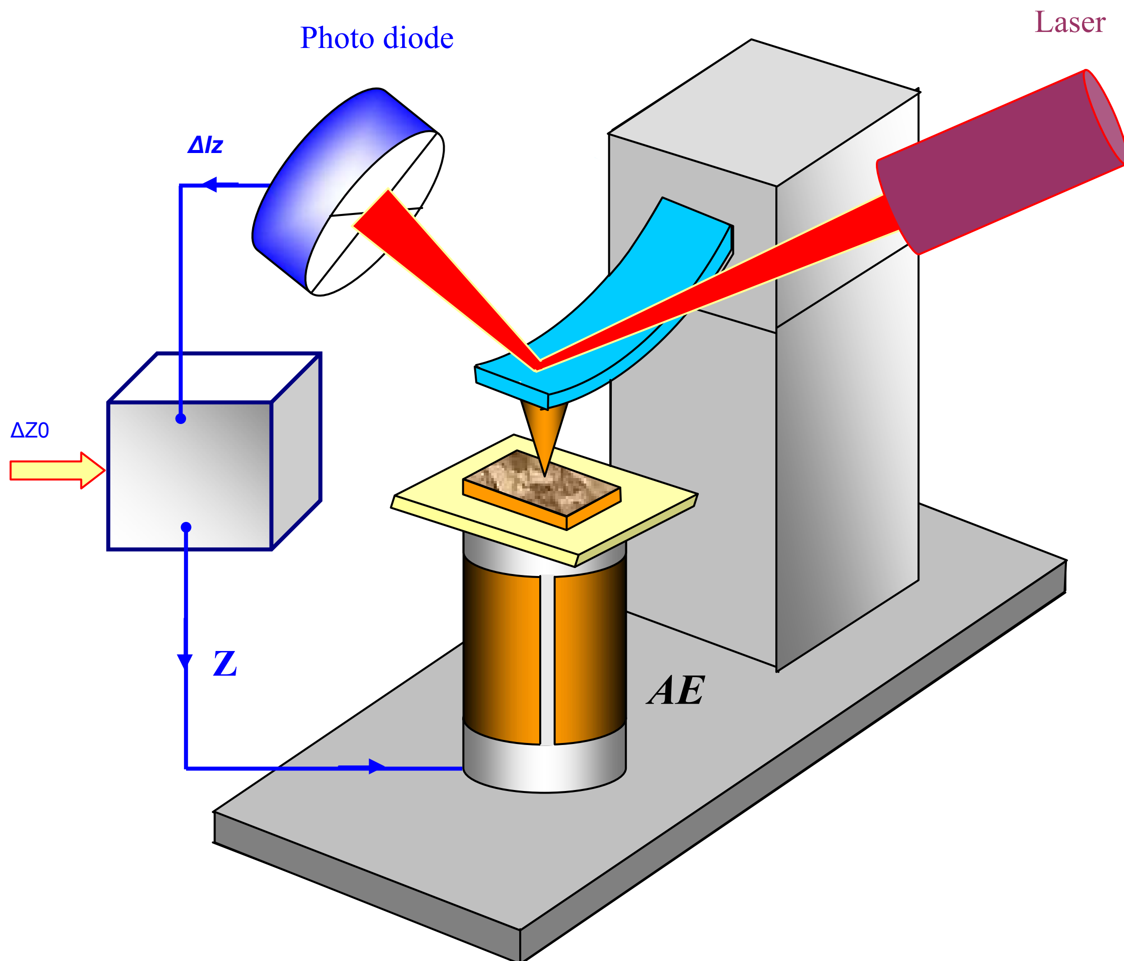

Fig. 64. Simplified scheme of feedback organization in the atomic force microscope

When scanning a sample in a $\Delta Z = const$ mode the tip moves along the surface, thus the voltage on a Z-electrode of the scanner is recorded in a computer memory as a surface topography Z = f (x, y). The AFM spatial resolution is defined by the rounded radius of a tip and sensitivity of the system recording the deviations of the console. Currently the AFM constructions are realized to allow obtaining the atomic resolution during the research of sample surfaces.

Atomic force microscopes probes

Surface sensing in the atomic force microscope is performed using special probes representing an elastic console – cantilever with a sharp tip on the end (Fig. 65). Gauges are made by photolithography and etching of silicon plates methods. Elastic consoles are formed, basically, from thin layers of alloyed silicon, SiO_2 or Si_3N_4.

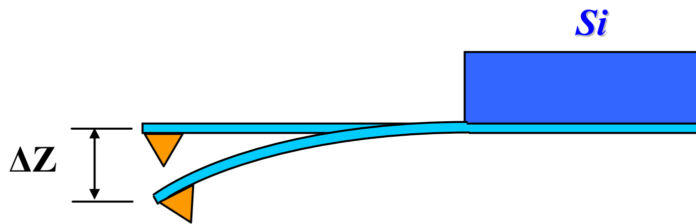

Fig. 65. Schematical image of the AFM probe

One end of the cantilever is firmly fixed on the silicon base - the holder. On the other end of the console the tip (as a sharp needle) is actually located. The rounded radius of modern AFM tips makes 1 ÷ 50 nanometers depending on the type of a tip and technologies of manufacturing. The angle at top of a tip is 10 ÷ 20º. The interaction force F of a tip with the surface can be estimated as follows:

$$F = k \cdot \Delta Z ,$$

where k – rigidity of the cantilever; ΔZ – the value describing its bend. The k coefficients of cantilevers rigidity vary in a range of 10^{-3} ÷ 10 N/m depending on materials used for their manufacturing and their geometrical sizes. The resonant properties of cantilevers are important during the AFM probes operation in oscillatory modes. Own frequencies of bending oscillations of the rectangular section console are determined by the following formula (see, for example, [Lit. 34]):

$$\omega_{ri} = \frac{\lambda_i}{l^2}\sqrt{\frac{EJ}{\rho S}} , \qquad (3)$$

where l – length of the console; E – Young's modulus; J – the inertia moment of the console section; ρ – material density; S - the cross section area; λ_i - numerical coefficient (in a 1÷100 range), dependent on a bending oscillations mode.

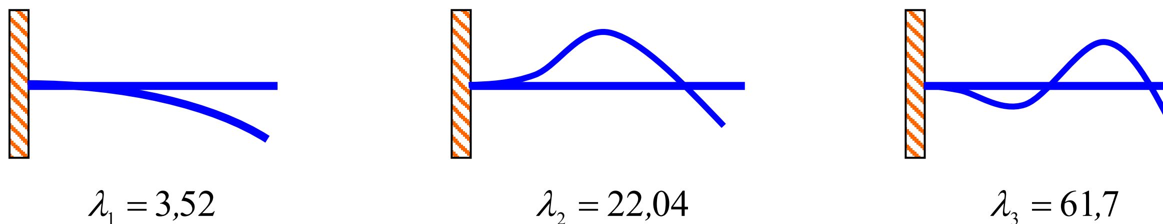

$\lambda_1 = 3{,}52$ $\lambda_2 = 22{,}04$ $\lambda_3 = 61{,}7$

Fig. 66. Main console bending oscillations modes

As it can bee seen from expression (3), the resonant frequency of the cantilever is defined by its geometrical sizes and properties of a material. Frequencies of the main modes reside in a 10÷1000 kHz range. Good quality of cantilevers mainly depends on the media in which they operate. Typical values of quality factors during operation in vacuum make 10^3 – 10^4. In the air the quality factor is reduced down to 300 – 500, and in a liquid it decreases down to 10 – 100.

Basically, probes of two types are applied in the atomic force microscopy – with a cantilever as a beam of rectangular section and with a triangular cantilever, formed by two beams. The general view of a probe with a cantilever as a beam of rectangular section is presented on Fig. 67.

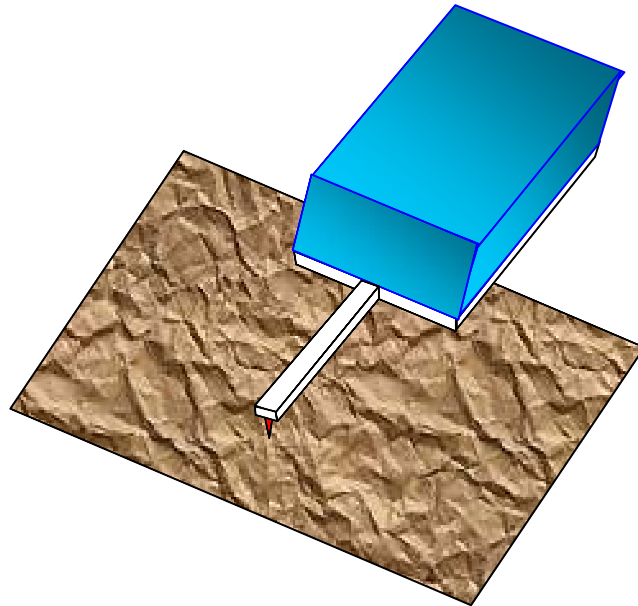

Fig. 67. General view of the AFM probe with a single console of rectangular section

Electron microscope images of serially produced (by **"NT-MDT"** company) NSG - 11 probes with the rectangular sections console are shown on Fig. 68.

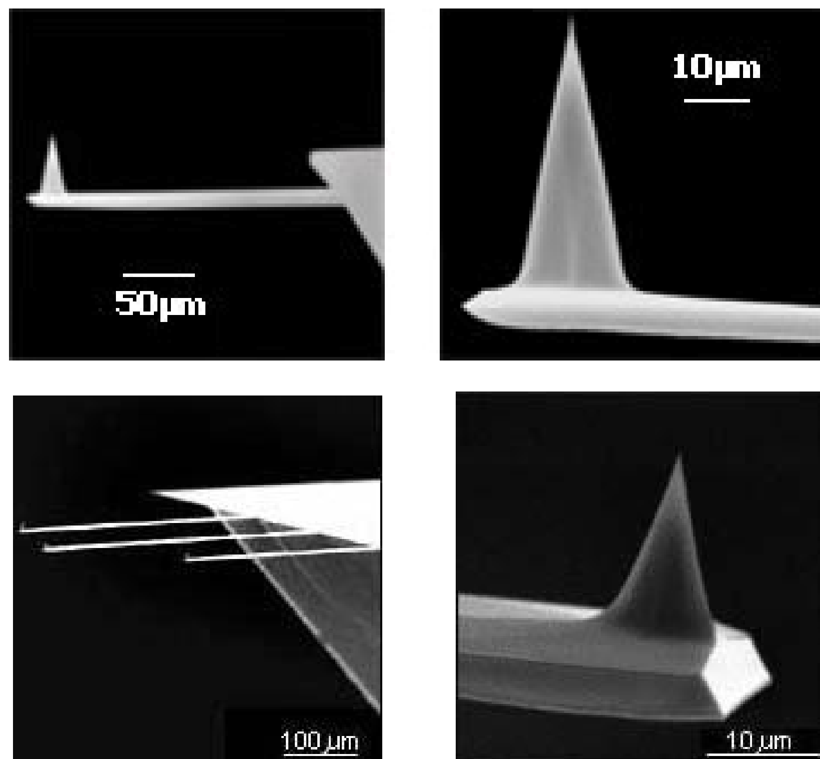

Fig. 68. Electron microscope image of the AFM tip, located on a rectangular console [Lit. 12]

Sometimes the AFM probes have few cantilevers of various length (hence, of various stiffness as well) on one base. In this case selection of a working console is done by corresponding alignment of the AFM optical system.

Probes with triangular cantilever have the higher stiffness at the same sizes and, hence, higher resonant frequencies. They are usually applied in oscillatory AFM techniques. The general view and dimensions of the probes with triangular consoles are presented on Fig. 69 and Fig. 70.

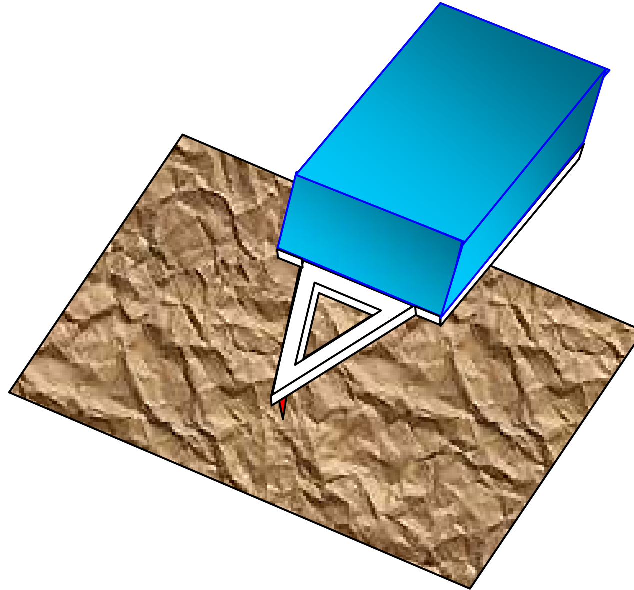

Fig. 69. General view of the probe with a triangular cantilever

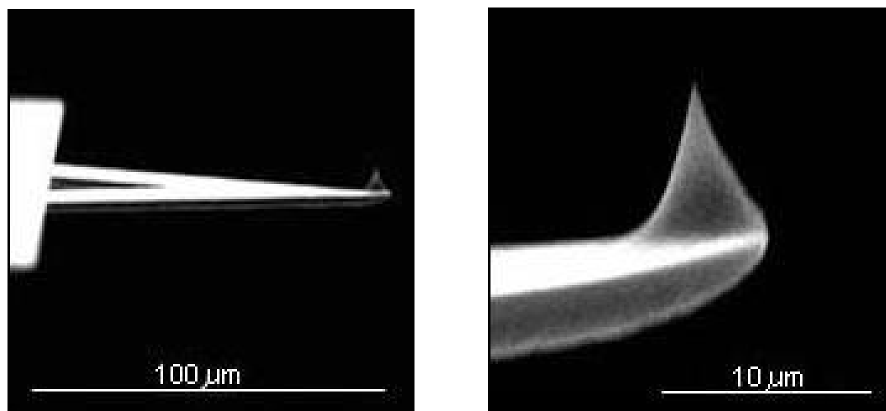

Fig. 70. Electron microscope image of the AFM tip, located on a triangular cantilever [Lit. 12].

Manufacturing of probes for the AFM represents a complex enough technological process including photolithography, ionic implantation, chemical and plasma etching operations. The basic stages of one of possible probe manufacturing techniques are submitted on Fig. 71.

The AFM probe manufacturing techniques

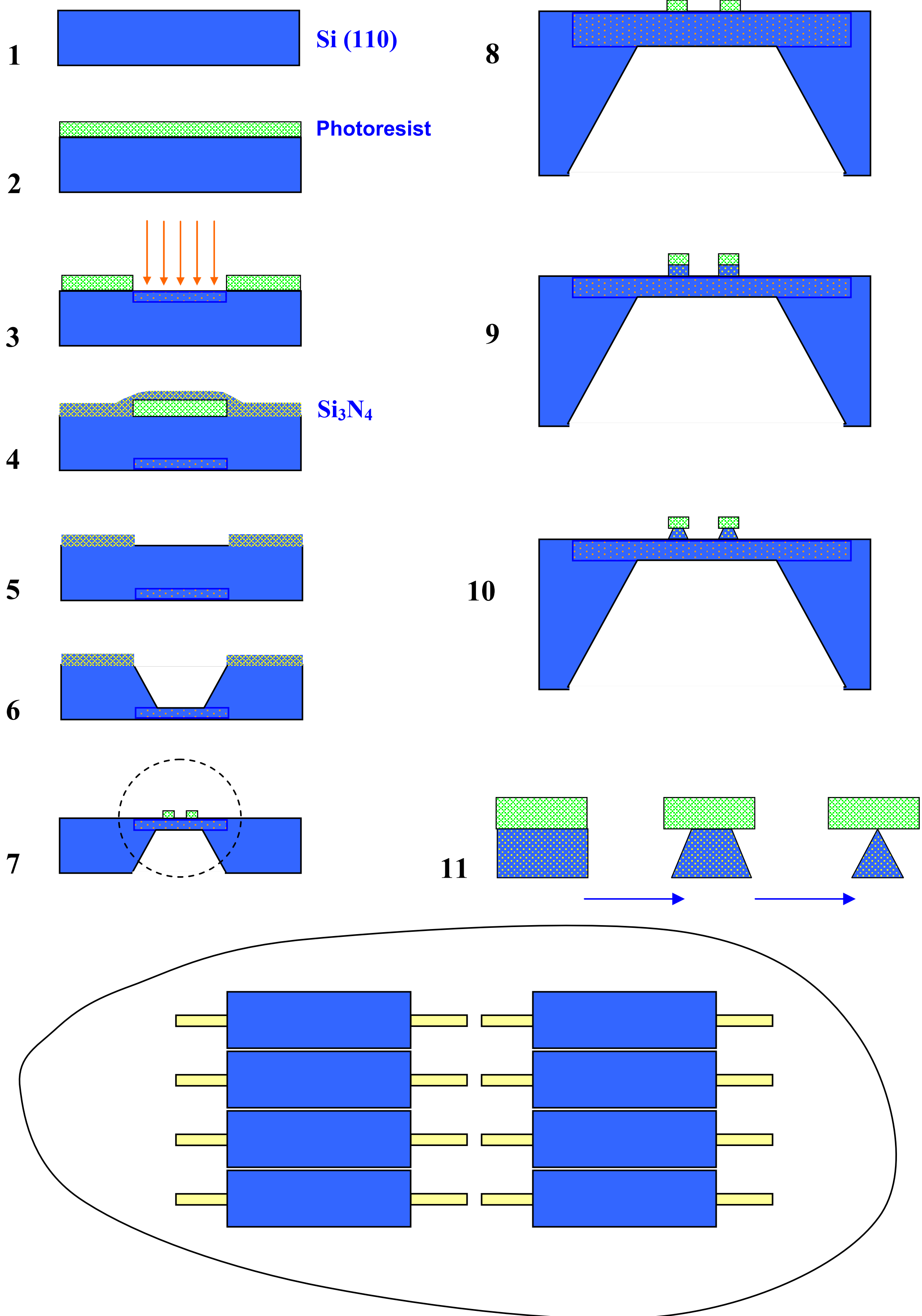

Fig. 71. Basic stages of the probe manufacturing process

Plates of crystal orientation silicon (110) are used for probe manufacturing. A thin photoresist layer (Fig. 71, stage 2) is precipitated on a surface of a plate. Then photoresist is exposed through a photo mask, and a part of photoresist is removed by means of chemical etching. After that ions of boron are implanted, so that ions penetrate to the depth of about 10 microns into the silicon area, unprotected by photoresist (stage 3). The photoresist is further washed off in a special etching agent, and then the plates are thermally annealed, resulting in atoms of boron building in the crystal lattice of silicon. The silicon alloyed by boron, forms a so-called stop-layer which stops the process of etching for some selective etching agents. Then on the reverse side of a plate the photolithography is done again, as a result of which the photoresist layer is formed exactly above the area implanted by boron. After that the plate becomes covered by a thin Si_3N_4 layer (stage 4). Then the photoresist is selectively etched, and during dissolution photoresist bloats and strips off the thin Si_3N_4 film located directly above it (stage 5). The silicon plate is etched through to the stop-layer by the selective etching agent, which reacts with silicon and does not react with alloyed silicon and Si_3N_4 layer, (stage 6). After that Si_3N_4 is washed off, and photoresist islands are formed on the reverse side of a plate in the alloyed area by a photolithography method (stages 7,8). Then the silicon is etched, resulting in formation of columns of silicon under photoresist islands (stage 9). After that needles are formed with the help of plasma etching from silicon columns (stages 10,11). Cantilevers from the reverse side (in relation to the apex) are covered with a thin layer of metal (Al, Au) by a vacuum sedimentation method to improve the reflective properties. As a result of these technological operations the whole set of probes is made on one silicon plate. For electric measurements the conducting coatings from various materials (Au, Pt, Cr, W, Mo, Ti, W_2C, etc.) are applied on a tip. Tips in magnetic AFM probes are covered with thin layers of ferromagnetic materials, such as Co, Fe, CoCr, FeCr, CoPt, etc.

Contact atomic force microscopy

Nominally the information acquisition methods on a topography and properties of a surface using AFM can be split in two big groups – contact quasi-static and contactless oscillatory methods. In contact quasi-static techniques the apex of a tip is in direct contact with a surface, and the attraction and repulsion forces, acting from a sample side, are counterbalanced by the elasticity force of the console. Cantilevers are used during AFM operation in such modes with relatively small stiffness coefficients, allowing to provide high sensitivity and to avoid undesirable excessive influence of a tip on a sample.

The image of a researched surface topography is formed in AFM quasi-static mode either at a constant interaction force of a tip with a surface (attraction or repulsion force), or at a constant average distance between the probe base and the surface of a sample. During scanning of a sample in the F_z = const mode the feedback system supports the constant value of a cantilever bend, and consequently, the interaction force of a tip with a sample as well (Fig. 72). Thus the control voltage in a feedback loop, applied on a Z-electrode of the scanner, will be proportional to the sample surface topography.

The mode of scanning at a constant average distance between the probe base and the surface (Z = *const*) is frequently applied during research of samples with small (about several Angstrem) differences of topography heights. In this case the probe moves on some average height Z_{av} above the sample (Fig. 73); during this the console bend ΔZ, proportional to the force influencing the tip from the surface is registered in every point. The AFM image in this case characterizes the spatial distribution of interaction force of a tip with a surface.

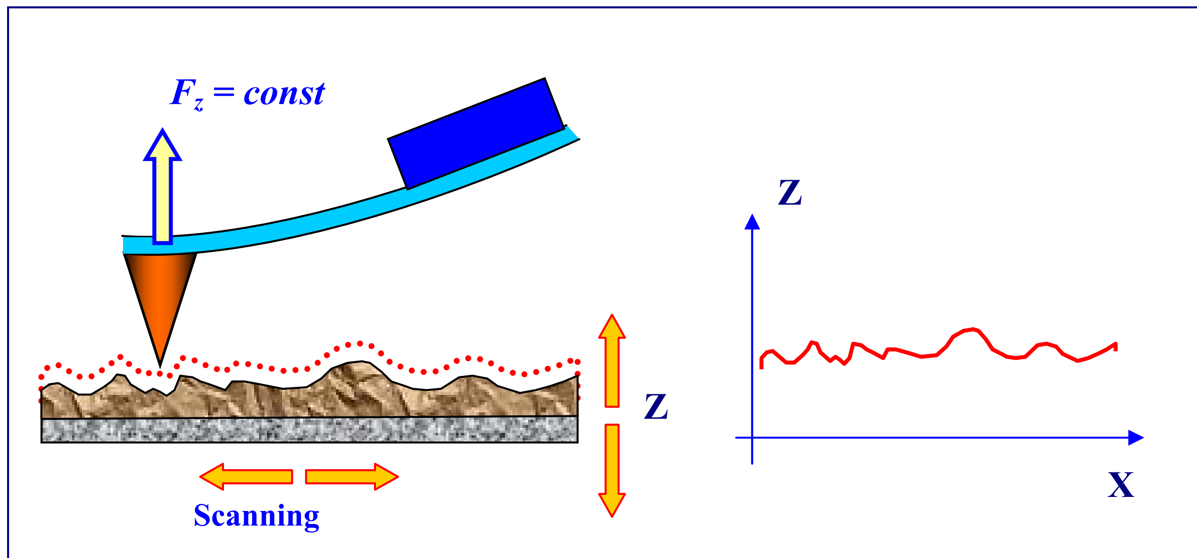

Fig. 72. Formation of the AFM image at a constant interaction force of a tip with a sample

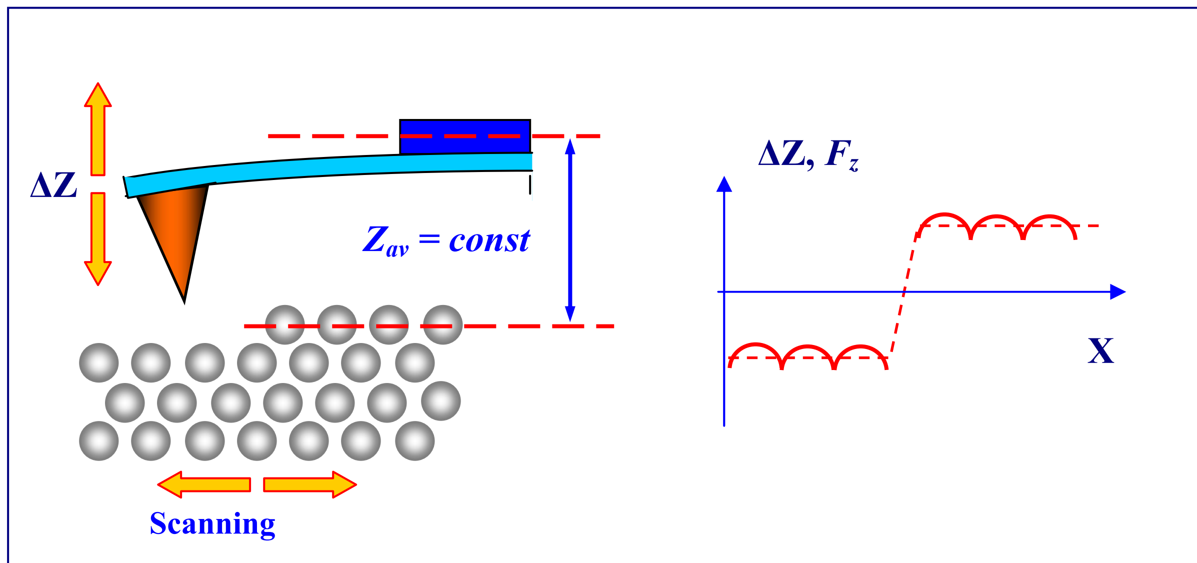

Fig. 73. Formation of the AFM image at a constant distance between a probe and a sample

A drawback of contact AFM techniques is the direct mechanical interaction of a tip with a surface. It frequently results in breakage of tips and destruction of a surface of samples during scanning. Besides that, contact techniques are practically not suitable for research of the samples having small mechanical stiffness, such as structures on the basis of organic materials and biological objects.

Dependence of the force on the probe-sample distance

With the help of the atomic force microscope it is possible to study features of local force interaction of a tip with a surface and to judge on the properties of a surface of various samples on the basis of results of these researches. With this purpose the so-called curves of a tip approach to a surface and curves of retraction are measured. Actually these are the dependences of a cantilever bend value ΔZ (and consequently, interaction forces of a tip with a surface) from coordinate z during probe approach to a sample. Similar measurements are performed during tip retraction from a surface. The typical $\Delta Z = f(z)$ dependence is represented on Fig. 74.

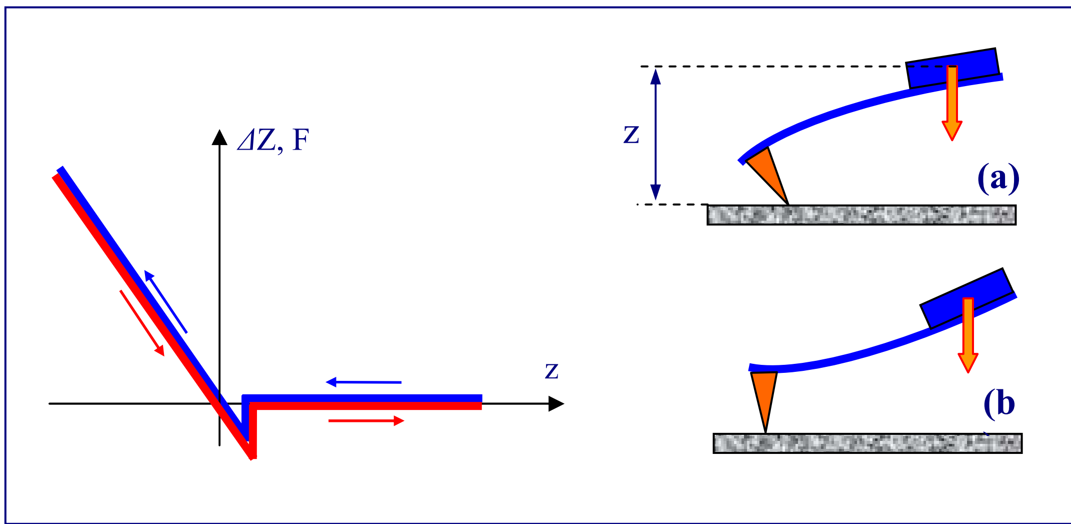

Fig. 74. Schematic image of a cantilever bend dependence (interaction forces of a tip with a surface) on the z probe-sample distance. Direct and reverse motions are shown in different colors

During approach to a surface of a sample the tip gets in the reach of attraction forces. This causes a cantilever bend in a direction to a surface (Fig. 74, insert (a)). The jump of a tip to a surface phenomenon can be observed in this area, caused by the presence of a big gradient of attraction forces near the sample surface. For a Lennard-Jones type potential the area of big gradients of an attraction force makes Z* ~ 1 nanometer. Dependences of the Lennard-Jones force and its derivative with respect to the tip-surface distance are schematically shown on Fig. 75.

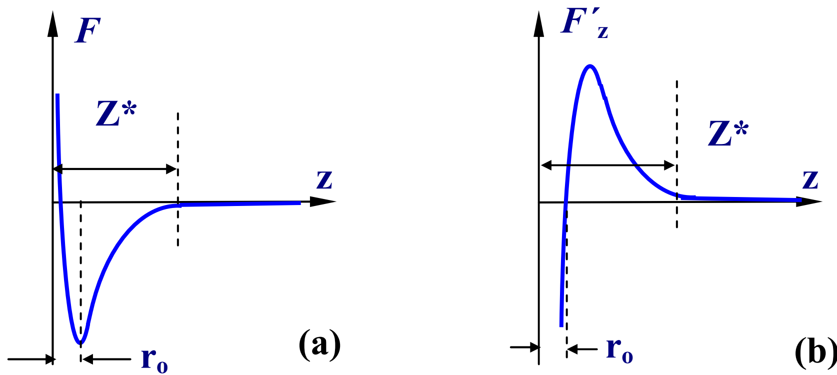

Fig. 75. Schematic image of the dependence of a force (a) and its derivative (b) on the z coordinate with respect to the tip-surface distance.

For observation of the jump effect of a tip to a surface it is necessary, that the stiffness of a selected cantilever was less than a derivative force maximum on the z coordinate. Let us explain this effect by an example of the small oscillations of a console model. In fact, the equation of an elastic cantilever movement near a surface is as follows:

$$m\ddot{z}_1 = -kz_1 + F(d + z_1),$$

where z_1 – cantilever bias from the equilibrium condition, k – cantilever stiffness, m - its weight, F - interaction force of a tip with a surface, d – distance between the equilibrium position of a cantilever and a surface. Linearizing the given equation, we receive:

$$F = F(d) + F_z'(d) \cdot z_1$$

$$m\ddot{z}_1 + (k - F_z'(d))z_1 = F(d).$$

After transition to new variables, $z_2 = z_1 - \frac{F(d)}{k - F_z'(d)}$, the movement equation looks in the following form:

$$\ddot{z}_2 + \omega_0^2 z_2 = 0, \qquad \omega_0^2 = \frac{k - F_z'(d)}{m}.$$

This is the equation of an oscillator with the frequency dependent on the d distance between a cantilever and a sample. If the force gradient surpasses on any distance the stiffness value of a cantilever, then $\omega_0^2 < 0$. This condition corresponds to an unstable pendulum (pendulum in the top position). Any small disturbance results in loss of stability, and the cantilever moves to the surface.

During further approach of a probe to a sample the tip starts to experience repulsion from surface, and the cantilever is bent to another side (Fig. 74, insert (b)). The $\Delta Z = f(z)$ curve inclination on this area is determined by elastic properties of a sample and cantilever. If interaction of a tip with a sample is absolutely elastic, the dependence of a cantilever bend on the AFM probe-surface distance, registered during reverse motion, coincides with the dependence obtained during direct motion (Fig. 74). For soft (plastic) samples, such as film of organic materials, biological structures, etc., and also for samples on the surface of which there are adsorbed layers of various materials, the $\Delta Z = f(z)$ curves have a more complex character. In this case the kind of dependence is essentially influenced by the capillary and plasticity effects. As an example, approach-retraction curves for a sample containing a layer of a liquid on its surface are shown on Fig. 76. The hysteresis due to capillary effect is observed on these dependences. During probe approach to the sample the tip is wetted by the liquid contained on the surface of a sample. During this a meniscus is formed on the border of a tip contact with a liquid. The tip, submerged in a liquid, is affected by an additional force of surface tension. This leads to a situation when the separation of a cantilever from a sample surface is shifted to the area of big Z values during removal of the probe.

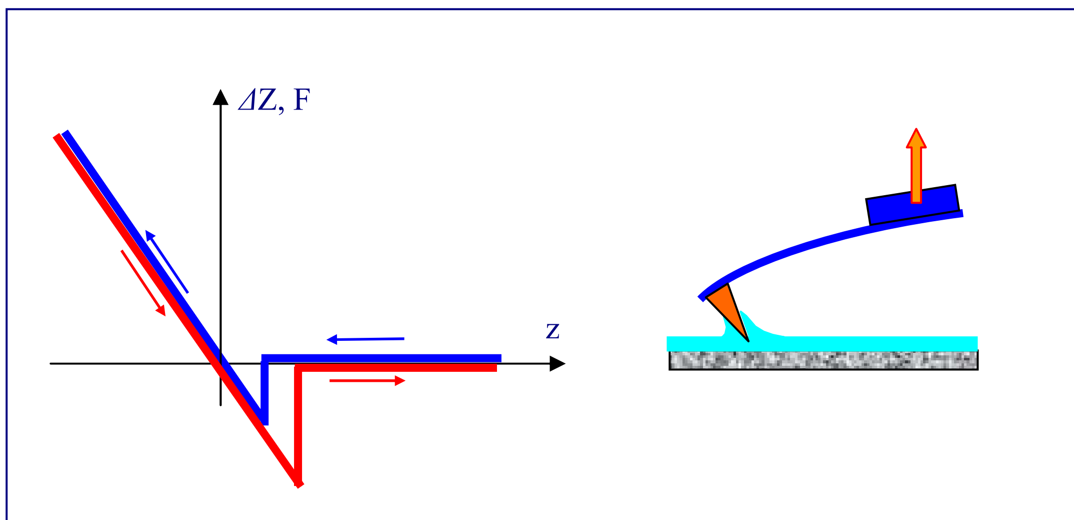

Fig. 76. Schematic image of dependence of a cantilever bend on the z distance between a probe and a sample with an adsorbed layer of a liquid on its surface.

Thus, by the type of the $\Delta Z = f(z)$ dependence it is possible to judge on the character of a tip-surface interaction, to research the local stiffness in various points of a sample, to study distribution of forces of adhesion on sample surfaces.

AFM control system during cantilever operation in a contact mode

The simplified circuit of the AFM control system during cantilever operation in a contact mode is presented on Fig. 77. The control system consists of a digital part realized on the basis of a personal computer, and an analog part, executed usually as a standalone block. The digital part contains, basically, digital-to-analog (DAC) and analog-digital (ADC) converters. Two-channel digital-to-analog converters DAC-X and DAC-Y serve to form horizontal and vertical scanning. The feedback loop consists of the preliminary PU amplifier structurally located in the AFM measurement head, the circuit of comparison (CC), high-voltage amplifier U2 and piezo-converter, regulating the bend value of a cantilever, and consequently, the interaction force of a tip with a surface. In the initial state the K1 electronic key is closed, and K2 is open.

Before the beginning of work the operator aligns the optical circuit of system of cantilever bias registration so that the current from various sectors of the photodiode is constant, and its value is maximal. Then, the voltage proportional to the working value of a cantilever bias ΔZ , which will be kept constant by the feedback system is established by means of the DAC-Set. After that the system of tip approach to a sample is switched on. Thus the control voltage from DAC-SM is supplied to the step-by-step motor (SM). In the initial state the voltage in a feedback loop (proportional to the difference of currents between vertical sectors of the photodiode) is less, than the value established by the operator by the DAC-Set, and the scanner is extended as much as possible in the direction of a tip. During approach of a sample to a tip the cantilever is bent, the differential current appears from the photodiode, and the system of approach passes to the procedure of exact installation of a sample. There is a further movement of a sample to a tip in this mode with the help of the motor and simultaneous retracting of it with the help of the scanner (the FS keeps the cantilever bend constant) until the sample surface plane sets in the position corresponding to the middle of a dynamic range of scanner movements. After that the microscope is ready for operation.

Scanning of a sample is performed during sawtooth form voltage supply on external electrodes of the tubular scanner with the help of two-channel DAC-X and DAC-Y converters and two-channel high-voltage U4, U5 amplifiers. During this the value of a photodiode differential current selected by the operator in a feedback loop, corresponding to a certain value of a cantilever bend is kept constant. During sample scanning in the F_z = const mode the voltage on a Z-electrode of the scanner is proportional to the surface topography. This happens as follows. The real instant value of U voltage, proportional to the differential PD current, is compared in the circuit of comparison (CC) with the U_0 value, set by the operator. The differential signal (U-U_0) is amplified (amplifier U2) and supplied to the internal Z-electrode of the scanner. The scanner executes this signal until the (U-U_0) difference becomes equal to zero. Thus, during scanning the voltage on a Z-electrode of the scanner appears proportional to the surface topography. The output signal of the comparison circuit is recorded by ADC as the information on a surface topography.

It is possible to measure in the selected point of a sample the dependence of a cantilever from bend value on the probe-surface distance: $\Delta Z = f(z)$. For this purpose the feedback is broken with the help of K1 electronic key, and the sawtooth form voltage is applied on a Z-electrode of the scanner from the DAC-Z. Synchronously with the change of voltage the ADC registers the output voltage of the preliminary amplifier PU, which is proportional to the cantilever bias and consequently, to the interaction force of a tip with a surface. The acquired data are transformed to the $\Delta Z = f(z)$ dependence, which is thereupon plotted by means of computer graphics.

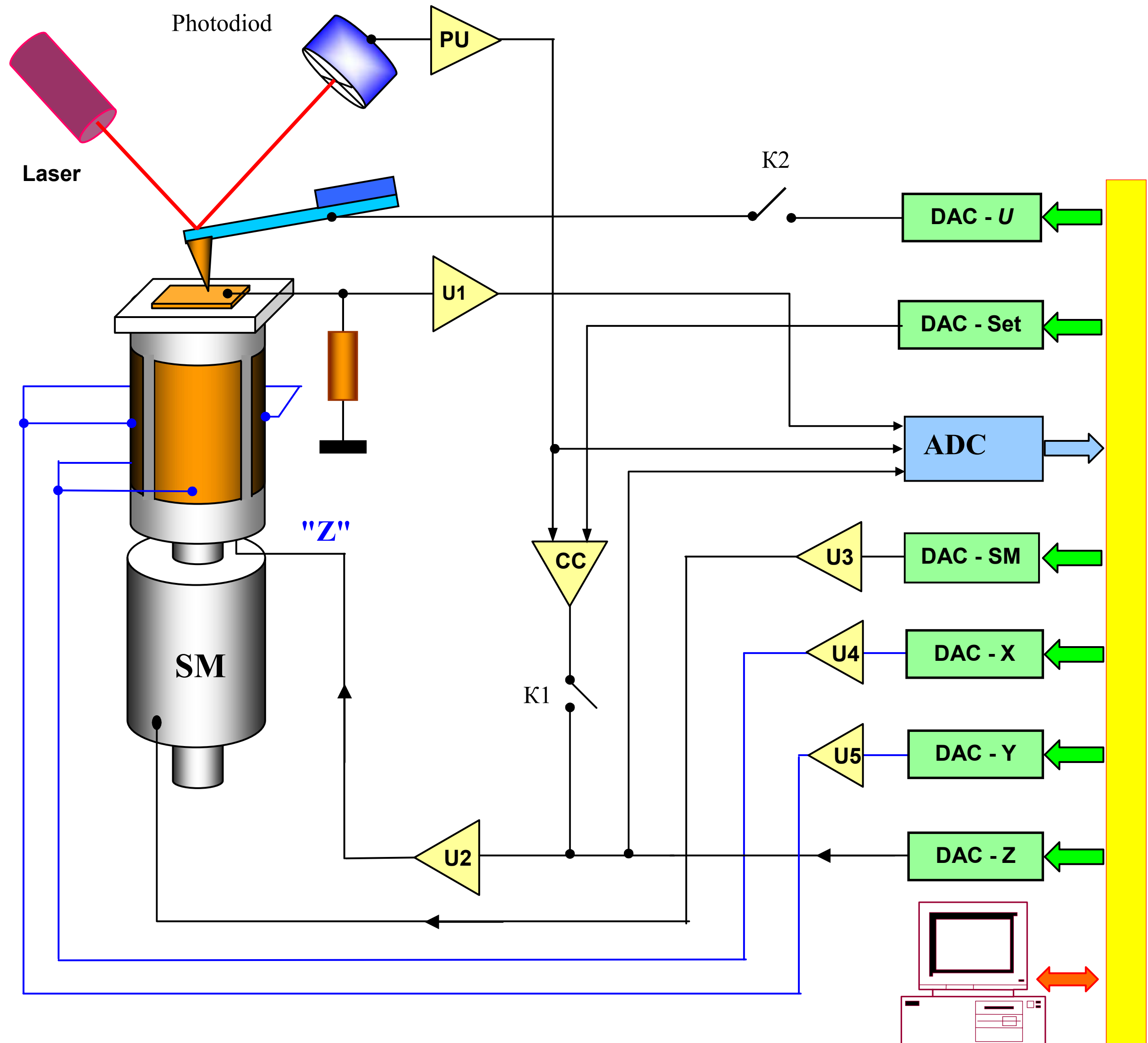

Fig. 77. Simplified circuit of the atomic force microscope control system during cantilever operation in a contact mode

Acquisition of the AFM image with constant average distance Z_{cp}*=const* between the probe and the sample is done in the following way. In the beginning the $\Delta Z = f(z)$ dependence is measured and the exact position of a tip above a surface is determined. Then the feedback is broken, and with the DAC-Z help the value of a tip-sample distance selected by the operator is set. After that the sample is scanned, and the output voltage from the preliminary amplifier, proportional to the cantilever bias, is recorded as a file of $F(x, y)$ force distribution along the sample surface.

Registration of volt-ampere characteristics of a tip-sample contact in a selected point of a surface is possible with the use of cantilevers with a conducting coating. The K2 key is closed to obtain the VAC, and the sawtooth form voltage is applied from the *DAC-U* on the cantilever. Synchronously with this, the voltage, proportional to the current through a contact, is amplified (amplifier U1), recorded by the ADC in a computer memory and visualized by means of computer graphics.

Oscillatory AFM techniques

As it was specified above, the drawback of AFM contact techniques is the direct mechanical interaction of a tip with a surface. It frequently results in breakage of tips and destruction of a surface of samples. Besides that, contact techniques are practically not suitable for the research of samples having small mechanical stiffness (structures on the basis of a number of organic materials and many biological objects). Oscillatory AFM techniques, based on registration of parameters of interaction of an oscillating cantilever with a surface, are applied for research of such samples. These techniques allow to reduce essentially the mechanical influence of a tip on a surface during scanning. Besides that, development of oscillatory techniques has essentially expanded the scope of AFM opportunities on the measurement of various properties of a sample surface.

Forced oscillations of a cantilever

The exact description of cantilever oscillations of the AFM probe represents a complex mathematical task. However, the basic features of the processes occurring during interaction of an oscillating cantilever with a surface can be understood on the basis of elementary models, in particular, with the help of the localized mass model [Lit. 1]. Let us present a cantilever as an elastic console (with the *k* stiffness) with the *m* localized mass on one end. The other end of the console is fixed on the PV piezo-vibrator (Fig. 78).

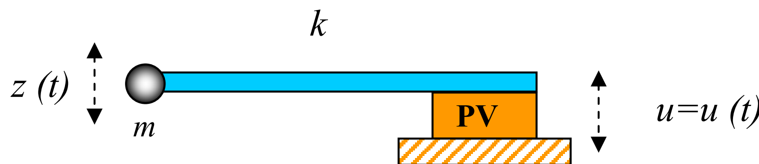

Fig. 78. Probe model as an elastic console with a mass on one end

Let the piezo-vibrator harmonically oscillate with the ω frequency:

$$u = u_o Cos(\omega t).$$

Then the movement equation of such oscillatory system will be written down as

$$m\ddot{z} = -k(z-u) - \gamma\dot{z} + F_0,$$

where the term, proportional to the first $\gamma\dot{z}$ derivative, takes into account the forces of viscous friction from the air, and by means of F_0 the gravity and other possible constant forces is designated. As is known, the constant force only displaces the equilibrium position of the system

and does not influence the frequency, the amplitude and the oscillation phase. Replacing the variables (i.e. examining the oscillations relatively to a new equilibrium condition):

$$z = z + F_0 / k ,$$

it is possible to bring the equation of cantilever movement to the following form:

$$m\ddot{z} + \gamma\dot{z} + kz = ku_0 Cos(\omega t) .$$

Having divided the equation by *m* and having introduced the parameter of good quality of the system $Q = \frac{\omega_0 m}{\gamma}$, we receive:

$$\ddot{z} + \frac{\omega_0}{Q}\dot{z} + \omega_0^2 z = \omega_0^2 u_0 Cos(\omega\ t) .$$

The simplest solution of the given equation is found on a plane of complex numbers. For the η complex value we have:

$$\ddot{\eta} + \frac{\omega_0}{Q}\dot{\eta} + \omega_0^2\eta = \omega_0^2 u_0 e^{-i\omega\ t} . \quad (4)$$

The general solution of the given equation represents the superposition of fading oscillations with $\delta=\omega_0 / 2Q$ decrement and persistent forced oscillations with ω frequency. Let us find the steady-state oscillations in such system. We search for the solution in a form of

$$\eta = a \cdot e^{-i\omega\ t} . \quad (5)$$

Substituting (5) in the equation (4), we receive for the complex amplitude *a*:

$$a = \frac{\omega_0^2 u_0}{\omega_0^2 - \omega^2 - i\frac{\omega\omega_0}{Q}} .$$

The module of this expression is equal to the forced oscillations amplitude $A(\omega)$:

$$A(\omega) = \frac{u_0\omega_0^2}{\sqrt{(\omega_0^2 - \omega^2)^2 + \frac{\omega^2\omega_0^2}{Q^2}}} . \quad (6)$$

The a complex amplitude phase coincides with the phase of our system $\varphi(\omega)$ oscillations:

$$\varphi(\omega) = arctg\left[\frac{\omega\omega_0}{Q(\omega_0^2 - \omega^2)}\right]. \quad (7)$$

From expression (6) it follows, that the amplitude of oscillations of a tip with ω_0 frequency is determined by the good quality of a system and is equal to $Q\,u_0$. Besides that, presence of a dissipation in the system results in the resonant frequency bias of cantilever oscillations. Indeed, differentiating the radicand with respect to ω^2 in expression (6) and equating the derivative to zero, we receive for the resonant frequency of a dissipative system ω_{rd} the following:

$$\omega_{rd}^2 = \omega_0^2\left(1 - \frac{1}{2Q^2}\right).$$

Then the dissipative system resonant frequency bias becomes equal to

$$\Delta\omega = \omega_0 - \omega_{rd} = \omega_0\left(1 - \sqrt{1 - \frac{1}{2Q^2}}\right).$$

This ends in that the amplitude-frequency characteristic of a system is biased to the area of low frequencies (Fig. 79).

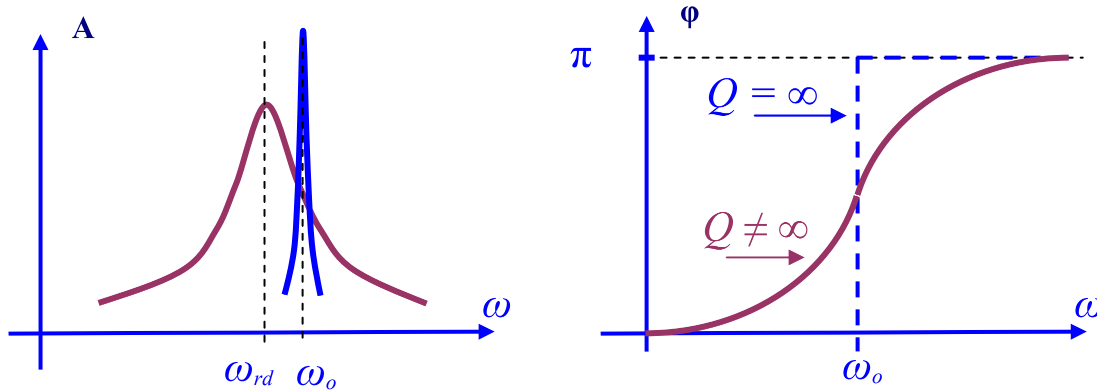

Fig. 79. Change of the amplitude-frequency characteristic and the phase response in a system with dissipation. Dark blue color shows characteristics of a dissipativeless system.

However, as the estimations show, for typical values of good quality of cantilevers in the air the bias value of a resonant frequency due to dissipation is small. Influence of the dissipation amounts, basically, to essential reduction of the oscillations amplitude and extension of the amplitude - frequency characteristic and phase response of a system (Fig. 79).

Contactless mode of AFM cantilever oscillations

In a contactless mode the cantilever makes forced oscillations with a small amplitude about 1 nanometer. During approach of a tip to a surface the cantilever is affected by an additional F_{PS} force acting from the sample. At van der Waals interaction this corresponds to the area of tip-sample distances, where the force of attraction exercises. If the AFM tip is located on z_0 distance from a surface, then it is possible to write down for small oscillations the following equation:

$$F_{PS} = F_{PS0} + \frac{\partial F}{\partial z}(z_0) \cdot z(t).$$

It results to that in the right part of the equation describing oscillations in such system, additional terms appear:

$$m\ddot{z} = -k(z-u) - \gamma\dot{z} + F_0 + F_{PS0} + F_z' z .$$

Introducing new variables: $z = z + (F_0 + F_{PS0})/k$, we come to the following equation:

$$m\ddot{z} + \gamma\dot{z} + (k - F_z') \cdot z = ku_0 Cos(\omega t).$$

I.e. presence of a force gradients results in a change of effective stiffness of the system:

$$k_{eff} = k - F_z' .$$

After standard reexpressions the equation is written down in the following form:

$$\ddot{z} + \frac{\omega_0}{Q}\dot{z} + \left(\omega_0^2 - \frac{F_z'}{m}\right) \cdot z = \omega_0^2 u_0 Cos(\omega t).$$

Making calculations similar to calculations, carried out for a free cantilever, we receive the amplitude-frequency characteristic of a system:

$$A(\omega) = \frac{u_0\omega_0^2}{\sqrt{(\omega_0^2 - \omega^2 - \frac{F_z'}{m})^2 + \frac{\omega^2\omega_0^2}{Q^2}}} . \qquad (8)$$

And, accordingly, the phase response:

$$\varphi(\omega) = arctg\left[\frac{\omega\omega_0}{Q\left(\omega_0^2 - \omega^2 - \frac{F_z'}{m}\right)}\right] . \qquad (9)$$

Thus, presence of a gradient of interaction force of a tip with a surface of a sample results in additional bias of the amplitude-frequency characteristic and the phase response of a system. The resonant frequency at presence of ωrf external force can be presented as

$$\omega_{rf}^2 = \omega_0^2\left(1 - \frac{1}{2Q^2} - \frac{F_z'}{k}\right) = \omega_{rd}^2 - \frac{E_z'}{m}.$$

Hence, additional bias of the amplitude-frequency characteristic is equal to

$$\Delta\omega = \omega_{rd} - \omega_{rf} = \omega_{rd}\left(1 - \sqrt{1 - \frac{F'_z}{m\omega_{rd}}}\right).$$

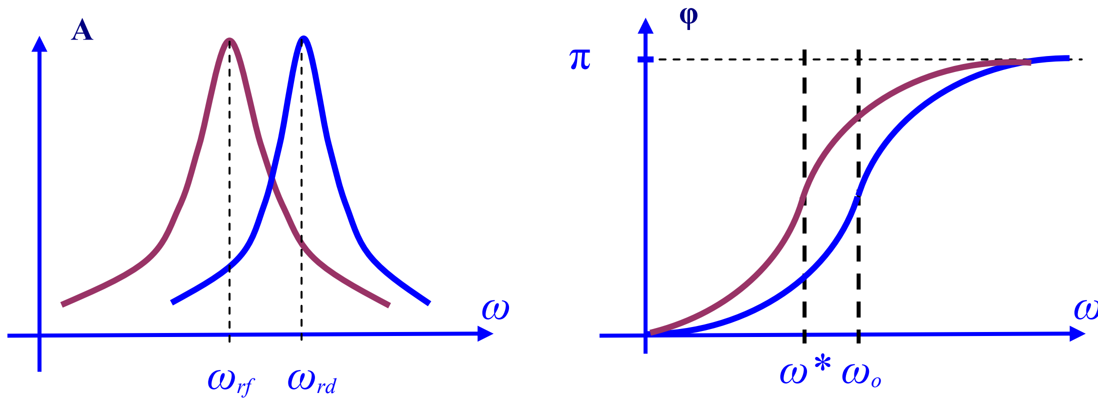

Fig. 80. Change of the amplitude-frequency characteristic and the phase response of a cantilever under influence of a force gradient.

From expression (9) it also follows, that the presence of a force gradient results in phase response bias so that the point of its inflection ω^* is located on the following frequency:

$$\omega^* = \omega_0\sqrt{1 - \frac{F_z'}{k}} \qquad \text{And } \Delta\omega = \omega_0 - \omega^* = \omega_0\left(1 - \sqrt{1 - \frac{F_z'}{k}}\right).$$

Let the cantilever perform forced oscillations with ω_0 frequency far from a surface, then the bias of the phase of its oscillations makes π/2. During approach to a surface the phase of oscillations (let us consider $F_z' < k$) is equal to

$$\varphi(\omega_0) = arctg\left[\frac{k}{QF_z'}\right] \approx \frac{\pi}{2} - \frac{QF_z'}{k}.$$

Hence, the additional phase bias at presence of a force gradient will be equal to [Lit. 35]:

$$\Delta\varphi = \frac{\pi}{2} - \varphi(\omega_0) \cong \frac{QF_z'}{k} \ .$$

It is defined by a *z*-component derivative of a force with respect to the *z* coordinate. This fact is used obtain the phase contrast in the AFM researches of a surface.

"Semi-contact" mode of the AFM cantilever oscillations

Registration of amplitude and phase of cantilever oscillations change in a contactless mode requires high sensitivity and stability of a feedback. In practice the so-called "semi-contact" mode of cantilever oscillations (sometimes it is referred to as “intermittent-contact” or "tapping" modes) is used more frequently. During work in this mode the forced cantilever oscillations are excited near to a resonance with an amplitude about 10–100 nanometers. The cantilever is approached to the surface so that in the lower semioscillation there is a contact with the surface of a sample (this corresponds to the area of repulsion on the diagram of dependence of the force on the distance (Fig. 81)).

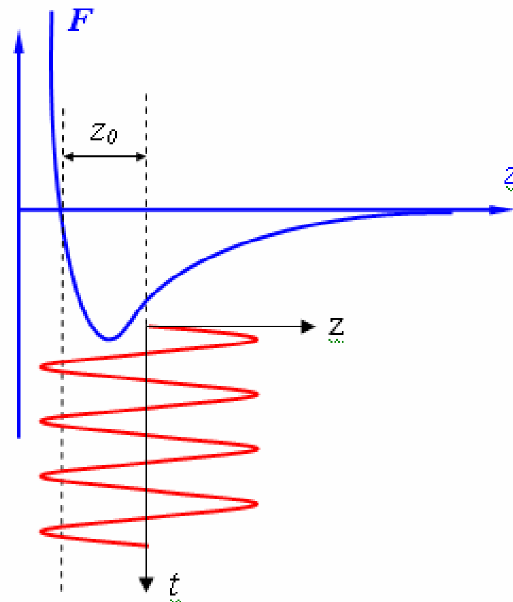

Fig. 81. Selection of a working point during "semi-contact" mode of cantilever oscillations

During scanning of a sample the change of amplitude and phase of cantilever oscillations is registered. Cantilever interaction with a surface in a "semi-contact" mode consists in van der Waals interactions to which the elastic force influencing the cantilever from the surface is added at the moment of a contact. If z_0 is the distance between equilibrium position of an oscillating cantilever and a surface, and $F_{PS}(z(t))$ is the combined force, then the equation of cantilever movement can be written down in the following form:

$$\ddot{z} + \frac{\omega_0}{Q}\dot{z} + \omega_0^2(z(t) - z_0 - u_0 Cos(\omega t)) = \frac{\omega_0^2}{k}F_{PS}(z(t)),$$

where the z coordinate is reckoned from a surface. We shall notice, that the "semi-contact" mode is realized only when the z_0 distance is less than the amplitude of cantilever oscillations:

$$z_0 < Q u_0 .$$

The theory of a "semi-contact" mode is much more complex than the theory of a contactless mode, since in this case the equation describing cantilever movement is essentially non-linear. The $F_{PS}(z(t))$ force now cannot be expanded into a series of small z values. However the characteristic features of this mode are similar to the features of a contactless mode - the amplitude and the phase of cantilever oscillations depend on a degree of interaction of a surface with a tip in the bottom point of cantilever oscillations. Since in the bottom point of oscillations the tip interacts mechanically with a surface, then in this mode the local stiffness of a surface of samples has essential influence on the change of amplitude and phase of cantilever oscillations.

The phase lag between oscillations of the excitation piezoelectric vibrator and the established cantilever oscillations can be estimated if the energy dissipation process during interaction of a tip with a sample is examined [Lit. 36-Lit. 38]. During established oscillations the energy coming to a system, is exactly equal to the energy, dissipated by the system. The energy coming to the system from a piezo-vibrator during one period of oscillations is equal to:

$$E_{EX} = \int_t^{t+\frac{2\pi}{\omega}} k\, u_0 Cos(\omega t)\cdot\frac{dz}{dt}dt .$$

This energy is spent compensate the losses during interaction of cantilever with an atmosphere and a sample. The E_{PA} energy, dissipated in an atmosphere during one period, can be calculated as follows:

$$E_{PA} = \int_t^{t+\frac{2\pi}{\omega}} \frac{m\omega_0}{Q}\left(\frac{dz}{dt}\right)^2 dt .$$

The E_{PS} energy spent to compensate the losses during dissipative interaction of a tip with a sample, is equal to:

$$E_{PS} = \int_t^{t+\frac{2\pi}{\omega}} F_{PS}(z)\frac{dz}{dt}dt .$$

From the equilibrium condition it follows that:

$$E_{EX} = E_{PA} + E_{PS} \ .$$

Assuming that the established oscillations of a cantilever look like $z = A \cdot Cos(\omega t + \varphi)$, we receive:

$$E_{PS} = \frac{\pi \ k \ u_0 A}{Q} Sin(\varphi) - \frac{\pi \ k\omega \ A^2}{\omega_0 Q} \ .$$

Therefore, the following expression is derived for a phase shift:

$$Sin\varphi = \frac{\omega \ A}{\omega_0 u_0} + \frac{QE_{PS}}{\pi \ ku_0 A} \ .$$

Thus, the phase shift of cantilever oscillations in a "semi-contact" a mode is determined by the energy of a dissipative interaction of a tip with a surface of a sample.

Formation of the AFM image of a surface in a mode of cantilever oscillations is done as follows. With the help of piezo-vibrator the cantilever oscillations with the ω frequency (close to the resonant frequency of a cantilever) are excited with the A_ω amplitude. During scanning the AFM feedback system keeps the amplitude of cantilever oscillations constant at the A_0 level, set by the operator ($A_0 < A_\omega$). The voltage in a feedback loop (on the z-electrode of the scanner) is recorded in a computer memory as the AFM image of a surface topography. Simultaneously with scanning of a sample the change of a phase of cantilever oscillations in every point is registered and recorded as a phase contrast distribution. As an example, the AFM images of a polythene film area, obtained in a "semi-contact" mode (peak and phase contrast) [Lit. 12] are presented on Fig. 82.

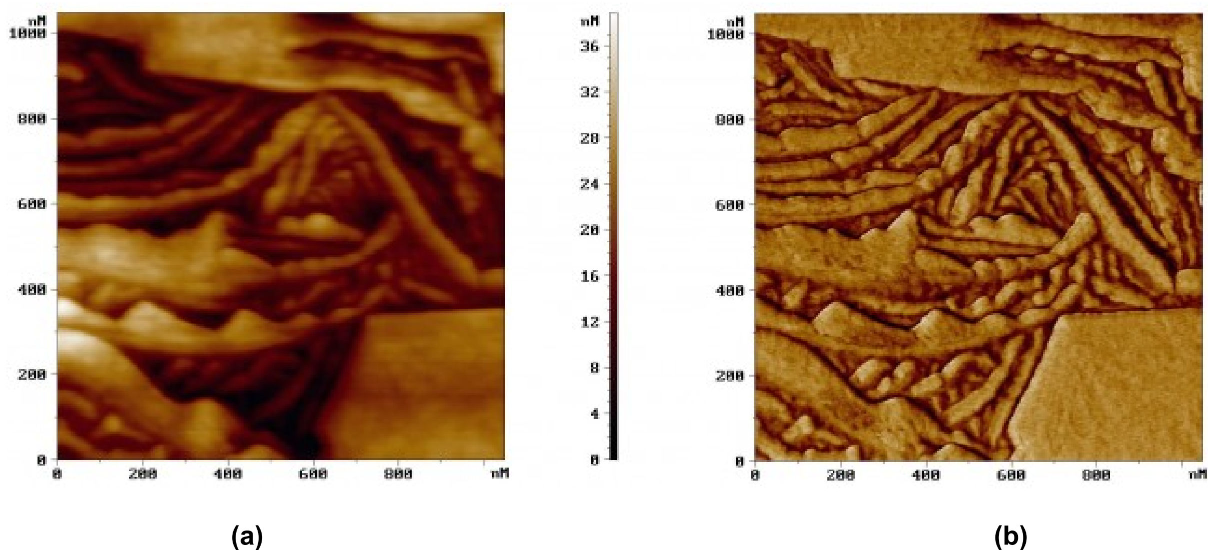

(a) **(b)**

Fig. 82. AFM images of a polythene film area surface, obtained in a "semi-contact" ("tapping") mode

(a) - surface topography obtained in a constant amplitude mode;

(b) - corresponding distribution of a phase contrast

2.3. Electric force microscopy

For acquisition of the information on properties of a surface the electric interaction between a tip and a sample is used in the electric force microscopy. Let us consider a system consisting from a probe with a tip with conducting coating, and a sample representing a thin layer of a material on a well conducting substrate.

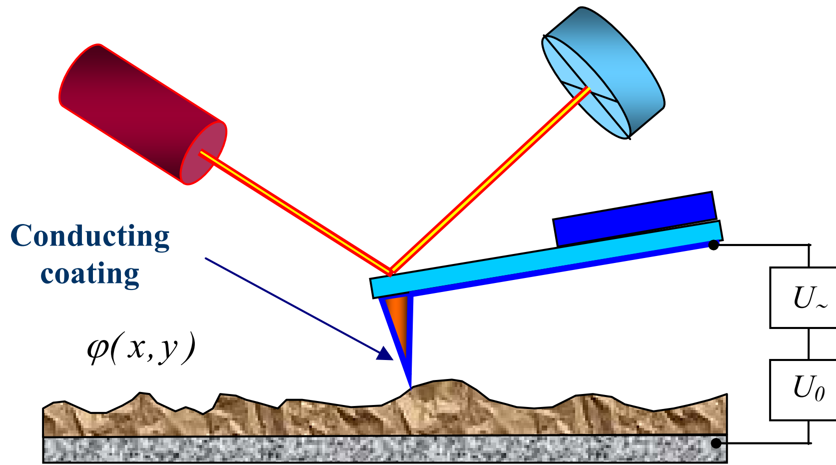

Fig. 83. Measurement circuit of the electric tip-sample interaction

Let the U0 constant and U~ = U1 ·Sin (ωt) variable voltages be applied between a tip and a sample. If the thin layer on a substrate represents a semiconductor or a dielectric, then it can contain a surface charge so that there is a distribution of the φ (x, y) potential on a sample surface. The voltage between a tip and a sample surface can be presented as

$$U = U_0 + U_1 Sin(\omega t) - \varphi(x,y).$$

The tip-sample system has some electric capacity C so that the energy of such system can be presented in the following form:

$$E = \frac{CU^2}{2}.$$

Then electric force of tip-sample interaction is equal to

$$\vec{F} = -grad(E).$$

And its Z-component can be presented as

$$F_z = -\frac{\partial E}{\partial z} = -\frac{1}{2}U^2\frac{\partial C}{\partial z}.$$

Thus, the Z-component of the electric force influencing the tip from the sample is equal to

$$F_z = -\left\{\frac{1}{2}\left((U_0 - \varphi(x,y))^2 + \frac{1}{2}U_1^2\right) + \left[U_0 - \varphi(x,y)\right]\cdot U_1 Sin(\omega t) - \frac{1}{4}U_1^2 Cos(2\omega t)\right\} \times \frac{\partial C}{\partial z}.$$

From the last expression it follows, that the interaction force has three components:

$$F_{z(\omega=0)} = -\left\{\frac{1}{2}\left((U_0 - \varphi(x,y))^2 + \frac{1}{2}U_1^2\right)\right\} \times \frac{\partial C}{\partial z}$$ constant component;

$$F_{z(\omega)} = -\left[\left(U_0 - \varphi(x,y)\right)\cdot U_1 Sin(\omega t)\right] \times \frac{\partial C}{\partial z}$$ component with ω frequency;

$$F_{z(2\omega)} = \left\{\frac{1}{4}U_1^2 Cos(2\omega t)\right\} \times \frac{\partial C}{\partial z}$$ component with 2ω frequency.

Detecting of the cantilever oscillation amplitude with 2ω frequency allows to investigate the distribution along a surface of the $C_z^{'}(x,y)$ size - a capacity derivative with respect to the z-coordinate (the so-called capacitance microscopy [Lit. 39]). With the help of this mode it is possible to study local dielectric properties of subsurface layers of samples. It is necessary that the electric force in a tip-sample system was determined, basically, by the interaction between a tip and a surface to obtain the high resolution in the given technique. The interaction force of a tip with a surface on the basis of a simple flat condenser model can be presented as

$$F_{PS} = -\frac{1}{2}U^2\frac{\partial C}{\partial z} \cong -\frac{1}{2}\alpha U^2\frac{\pi R^2}{h^2} ,$$

where α is a constant, R – characteristic radius of the apex of the tip rounding, h - tip-surface distance (or thickness of a dielectric film on a conducting substrate). On the other hand the force influencing the cantilever from a sample is:

$$F_{CS} = -\frac{1}{2}U^2\frac{\partial C}{\partial z} \cong -\frac{1}{2}\alpha U^2\frac{LW}{H^2} ,$$

where α is a constant, L - cantilever length, W - cantilever width, H - distance to a surface (defined by the sizes of a tip). From the $F_{PS} > F_{CS}$ condition it follows that

$$h < \sqrt{\frac{\pi R^2 H^2}{LW}} .$$

From here for typical values of probe parameters (L ~ 100 microns, W ~ 30 microns, H ~ 30 microns, R ~ 10 nanometers) it is possible to obtain the following estimation:

h <10 nanometers.

Since the $\frac{\partial C}{\partial z}$ value depends on the tip-sample distance, the two-pass technique is applied for research of dielectric properties of samples. The following procedure is performed in every scanning line. During the first pass cantilever oscillations are excited by the piezo-vibrator with a frequency close to the resonant frequency ω_0, and the AMF image of a topography in a «semi-

contact» mode is registered. Then the probe is retracted from a surface to the z_o distance, a variable voltage (with $\omega = \omega_0$ frequency) is applied between a tip and a sample, and scanning is repeated (Fig. 84). During the second pass the probe moves above a surface with a trajectory repeating the topography of a sample. Since during scanning the local distance between the probe and a surface is constant in every point, changes of cantilever oscillation amplitude with the 2ω frequency will be connected to the change of a tip-sample system capacity due to the change of dielectric properties of a sample.

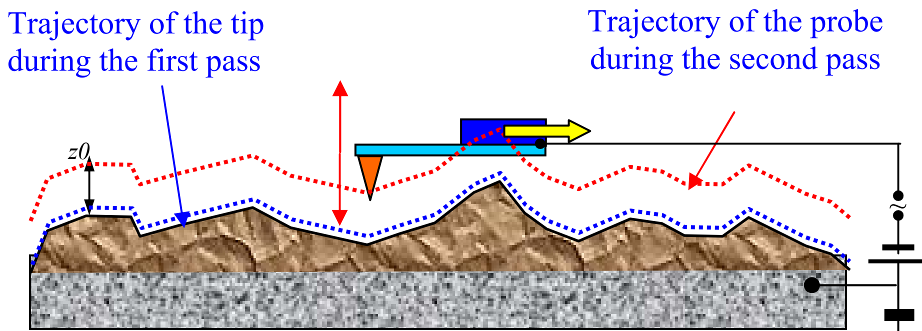

Fig. 84. EFM two-pass technique

Thus, the final EFM frame represents the bidimentional function $C_z'(x,y)$ describing local dielectric properties of a sample.

The signal detection with the ω frequency allows to study the distribution of a surface potential $\varphi(x,y)$ (the so-called Calvin method [Lit. 40]). The following procedure is performed for this purpose during sample scanning in the second pass in every point. With the help of a readjusted source the constant U_0 voltage value is selected so that the cantilever oscillation amplitude with the ω frequency becomes equal to zero. It occurs if $U_0 = \varphi(x,y)$ in the given point of a surface. The AMF image of a surface topography and the distribution of a surface potential for a composite film containing azobenzene [Lit. 41] are presented as an example on Fig. 85. Molecules of azobenzene with a strong dipole moment are showing up on the image of superficial potential.

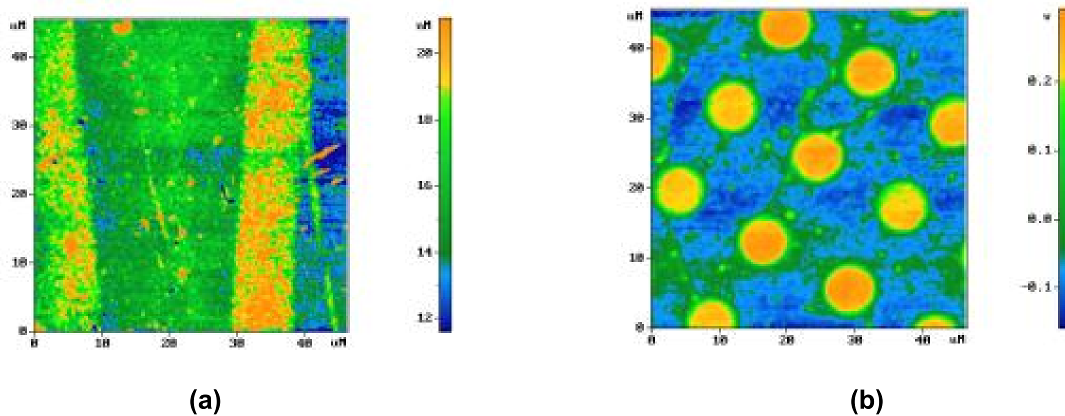

(a) (b)

Fig. 85. Surface topography (a) and distribution of superficial potential (b) of a azobenzene film

2.4. Magnetic force microscopy

Magnetic force microscope (MFM) [Lit. 42, Lit. 43] has been invented by I. Martin and K. Vikramasinghe in 1987 for research of local magnetic properties of samples. This device represents an atomic force microscope, the tip of which is covered with a layer of a ferromagnetic material with specific $\vec{M}(\vec{r})$ magnetization.

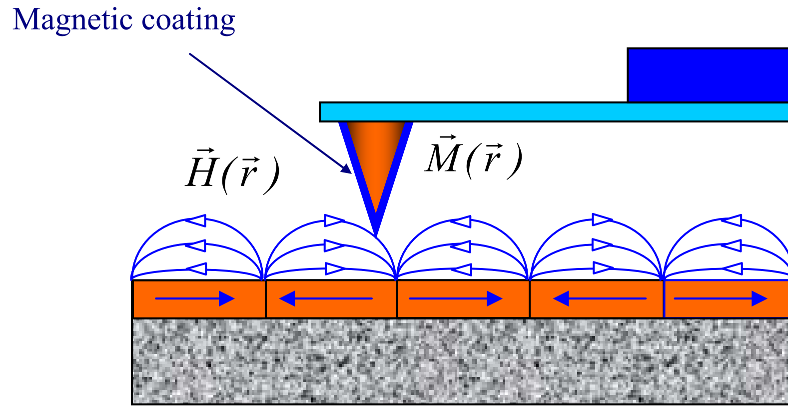

Fig. 86. The MFM tip in a magnetic field of a sample

Generally the description of interaction of the MFM tip with a field of a sample $\vec{H}(\vec{r})$ represents a considerably complex problem. We shall consider the MFM tip as a single magnetic dipole described by the $\vec{m}$ magnetic moment [Lit. 44] as the simplest model. Potential energy of such system is equal to

$$w = -(\vec{m}\vec{H}).$$

The magnetic dipole is influenced in the $\vec{H}$ field by the following force:

$$\vec{f} = -grad(w) = \vec{\nabla}(\vec{m}\vec{H})$$

and the moment of forces is equal to

$$\vec{N} = [\vec{m}\vec{H}].$$

In a homogeneous magnetic field the force $\vec{f}$ = 0 so the dipole is affected only by the moment of forces which turns the $\vec{m}$ magnetic moment along the field. In a non-uniform field the dipole is retracted in the area with greater $\vec{H}$ intensity.

Generally the magnetic moment of the MFM tip can be presented as a superposition of dipoles of the following from:

$$\vec{M}(\vec{r})dV,$$

where $\vec{M}$ - specific magnetization of a magnetic covering, dV - elementary volume.

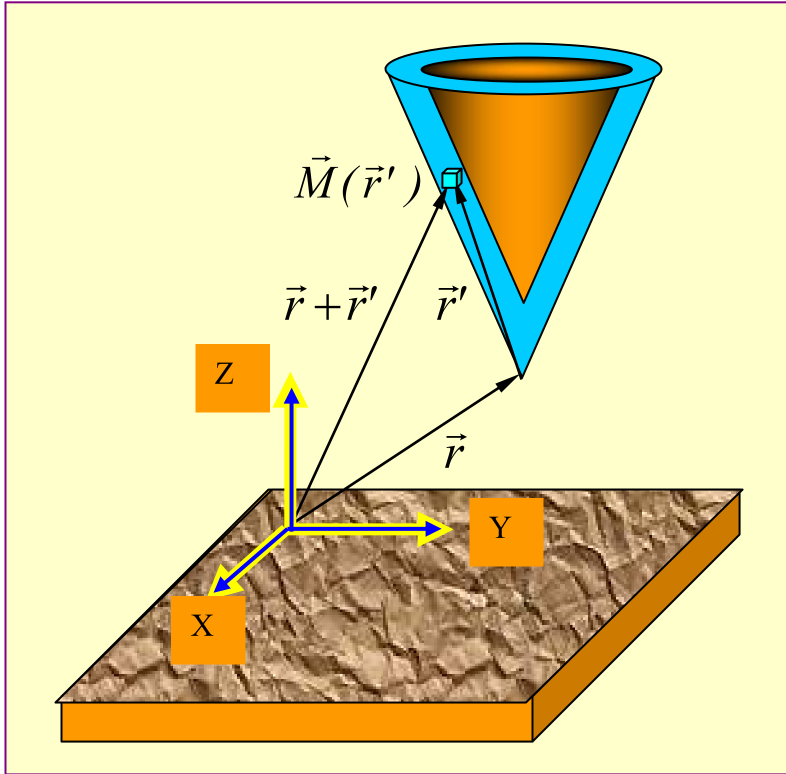

Fig. 87. Interaction of a MFM tip with a magnetic field of a sample

Then full energy of magnetic interaction of a tip and a sample can be presented (see Fig. 87) in the following form:

$$W_{маг} = -\int_{V_p} \vec{M}(\vec{r}') \cdot \vec{H}(\vec{r} + \vec{r}')dV'$$

(integration is performed by a magnetic layer of a tip). From here the interaction force of a tip with a field of a sample is equal to

$$\vec{F} = -grad\,(W_{маг}) = \int_{V_P} \vec{\nabla}(\vec{M}\vec{H})dV'.$$

Accordingly, the Z-component of a force is as follows:

$$F_z = -\frac{\partial W_{маг}}{\partial z} = \int_{V_P} \left(M_x \frac{\partial H_x}{\partial z} + M_y \frac{\partial H_y}{\partial z} + M_z \frac{\partial H_z}{\partial z} \right) dV'.$$

Quasy-static and oscillatory techniques are applied to acquire the MFM images of samples.

Quasy-static MFM techniques

The MFM image of a surface of samples having underdeveloped topography of a surface is obtained as follows. During scanning the tip moves above the sample on some $h=const$ distance. Thus the value of a cantilever bend, registered by the optical system, is recorded as the MFM image $F(x, y)$, representing the distribution of magnetic interaction force of a tip with a sample.

The two-pass technique is applied for MFM researches of magnetic samples with a considerable topography of a surface. In each scanning line the following procedure is performed. On the first pass the AMF image of a topography in a contact or "semi-contact" mode is obtained. Then the tip is retracted from a surface to a z_o distance, and the scanning is repeated (Fig. 88). The z_o distance is selected so that the van der Waals force is less than the magnetic interaction force.

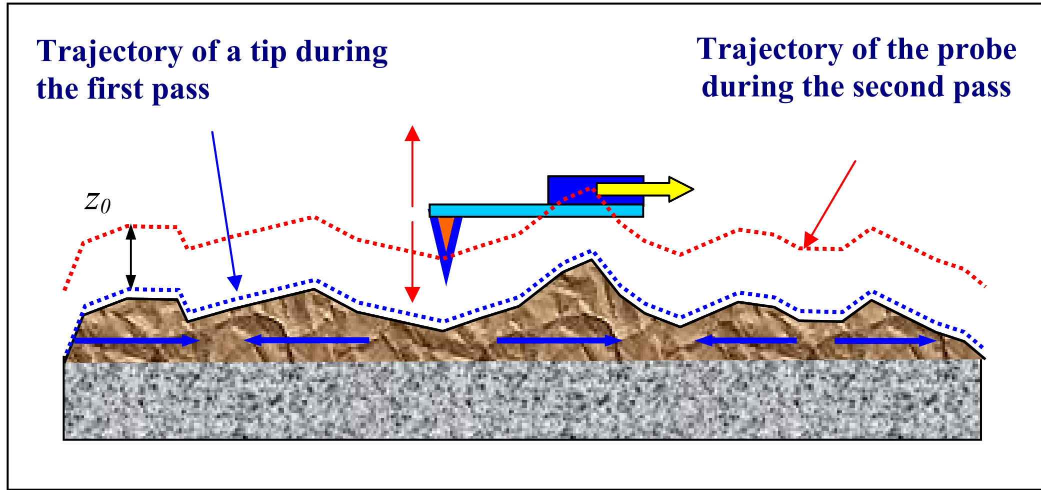

Fig. 88. Two-pass technique of the MFM acquisition

During the second pass the probe moves above a surface with a trajectory repeating the topography of a sample. Since the local distance between the tip and a surface in every point is constant in this case, changes of a cantilever bend during scanning are connected to the heterogeneity of the magnetic forces affecting the tip from a sample. Thus, the final MFM frame represents a bidimentional function F (x, y), describing the distribution of magnetic interaction force of a tip with a sample.

Oscillatory MFM techniques

Application of oscillatory techniques in the magnetic force microscopy allows to implement big (in comparison with quasy-static techniques) sensitivity and to receive better MFM images of samples. As it has been shown in the section devoted to the contactless AFM technique, presence of a force gradient results in the resonant frequency change, and consequently, in the AFC and phase response shift in a tip-sample system. These changes of resonant properties of a system are used to obtain information on non-uniform distribution of magnetization on surfaces of samples. In case of magnetic interaction of a tip with a surface the resonant frequency shift of an oscillating cantilever is determined by a F_z value derivative with respect to the z coordinate:

$$F'_z = \frac{\partial F_z}{\partial z} = \int_{V_P} \vec{M}(\vec{r}\,')\,\frac{\partial^2}{\partial z^2}\,\vec{H}(\vec{r}+\vec{r}\,')\,dV' \; .$$

Or in a componentwise form:

$$F'_z = \frac{\partial F_z}{\partial z} = \int_{V_P} \left(M_x \frac{\partial^2 H_x}{\partial` z^2} + M_y \frac{\partial^2 H_y}{\partial z^2} + M_z \frac{\partial^2 H_z}{\partial z^2} \right) dV \; .$$

The two-pass technique is used to acquire the MFM image of a surface. With the help of a piezo-vibrator cantilever oscillations are excited with the ω frequency in vicinity of resonance. During the first pass in a "semi-contact" mode the topography of a surface is recorded. On the second pass the tip goes above a sample with a trajectory corresponding to the topography so that the distance between the tip and a surface is equal in every point to the $z_0 = const$ value, defined by the operator. The MFM image is formed by means of registration of changes in the amplitude or the phase of cantilever oscillations.

The amplitude and phase of cantilever oscillations can be presented (provided that $F_z^{'}$ variations along the surface are insignificant) as follows:

$$A(F_z^{'}) = A(F_{z0}^{'}) + A_{F_z^{'}}^{'}(F_z^{'})\Big|_{F_{z0}^{'}} \Delta F_z^{'} \ ,$$

$$\varphi(F_z^{'}) = \varphi(F_{z0}^{'}) + \varphi_{F_z^{'}}^{'}(F_z^{'})\Big|_{F_{z0}^{'}} \Delta F_z^{'} \ .$$

Then the changes of oscillation amplitude and phase shift, connected with variations of a force gradient, will be equal to

$$\Delta A = A(F_z^{'}) - A(F_{z0}^{'}) = A_{F_z^{'}}^{'}(F_z^{'})\Big|_{F_{z0}^{'}} \Delta F_z^{'} \ ,$$

$$\Delta\varphi = \varphi(F_z^{'}) - \varphi(F_z^{'}) = \varphi_{F_z^{'}}^{'}(F_z^{'})\Big|_{F_{z0}^{'}} \Delta F_z^{'} \ .$$

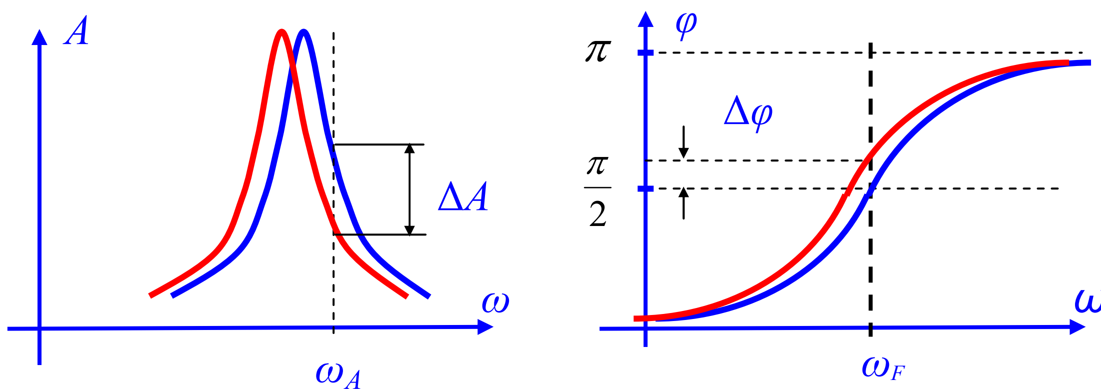

Fig. 89. Change of oscillation amplitude and phase at a change of a force gradient

The coefficients before $\Delta F'_z$ determine the sensitivity of peak and phase measurement methods. The sensitivity maximum is achieved at the certain frequencies of cantilever excitation. For amplitude measurements this frequency is:

$$\omega_A = \omega_0 \sqrt{1 - F'_{z0} / k}\ (1 \pm \frac{1}{\sqrt{8Q}}),$$

Thus $A'_{F'_z}(\omega_A, F'_{z0}) = -\dfrac{8\sqrt{2}}{\sqrt{27}} \dfrac{Q^2}{k}$.

For phase measurements the sensitivity maximum is achieved, when the frequency of cantilever excitation coincides with the resonant frequency of a tip-sample system:

$$\omega_F = \omega_0 \sqrt{1 - F'_{z0} / k},$$

Thus $\varphi'_{F'_z}(\omega_F, F'_{z0}) = \dfrac{Q}{k}$.

The MFM images of a surface of the magnetic disk, acquired with the help of various techniques, are presented as an example on Fig. 90.

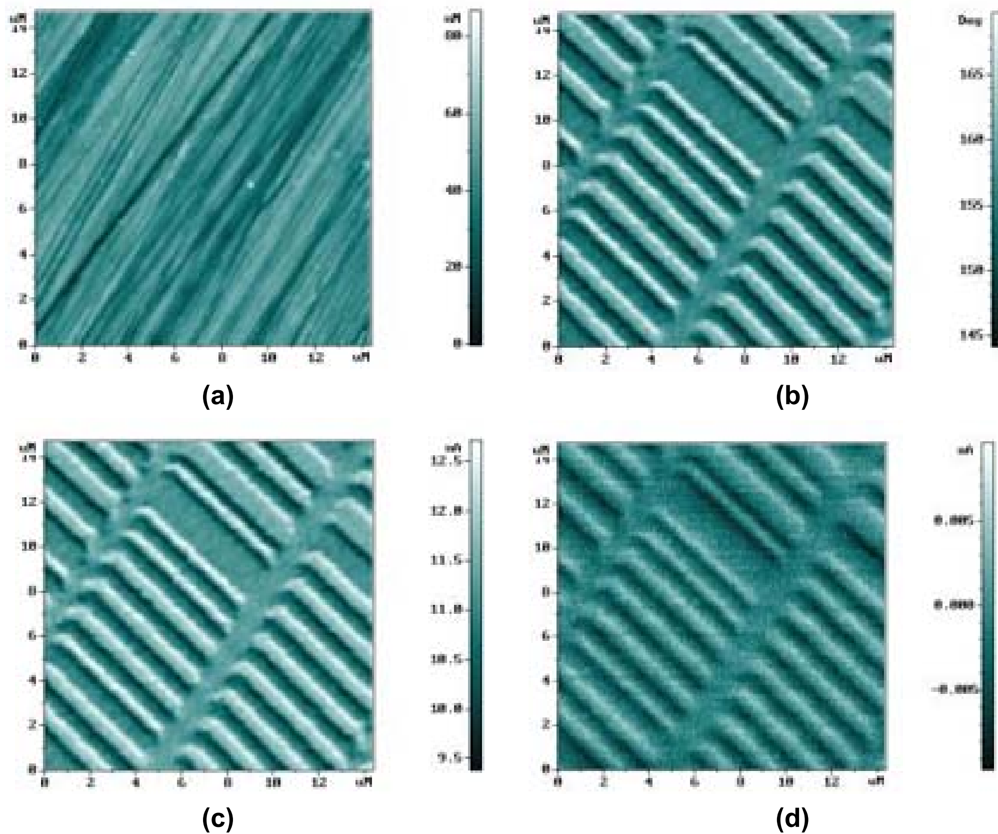

Fig. 90. MFM research of a magnetic disk surface:
(a) –AMF image of a surface topography;
(b) – MFM image of a phase contrast;
(c) – MFM image of an amplitude contrast;
(d) – MFM image of distribution of tip- surface force interaction

Contrast on MFM images is connected, after all, to the magnetization distribution in a sample. The specifics of formation of the MFM images of magnetic structures can be illustrated with the help of model calculations in approximation of a dipole-dipole interaction. In this case the magnetic sample is split into elementary volumes, magnetization of which is described by magnetic dipoles $\vec{m}_s^j$ (Fig. 91). The tip in the elementary case can be presented as a separate dipole $\vec{m}_p$. Then the Z-component of a force gradient will be written down as follows:

$$\frac{\partial}{\partial z} F_z(\vec{r}) = \sum_j ((\vec{m}_P \vec{\nabla}) \frac{\partial}{\partial z} H_z^j(\vec{r} - \vec{r}_S^j),$$

where magnetic field of the *j-th* dipole of a sample in the point of the apex of the tip is equal to [Lit. 45]

$$H_z^j(\vec{r} - \vec{r}_s^j) = \frac{3(z - z_s^j)(\vec{m}_s^j \cdot (\vec{r} - \vec{r}_s^j))}{\left|\vec{r} - \vec{r}_s^j\right|^5} - \frac{m_{sz}^j}{\left|\vec{r} - \vec{r}_s^j\right|^3}.$$

Moving the tip above the magnetic structure at some height and calculating in every point the $\Delta\varphi = \frac{QF_z'}{k}$ phase shift, it is possible to model the MFM image.

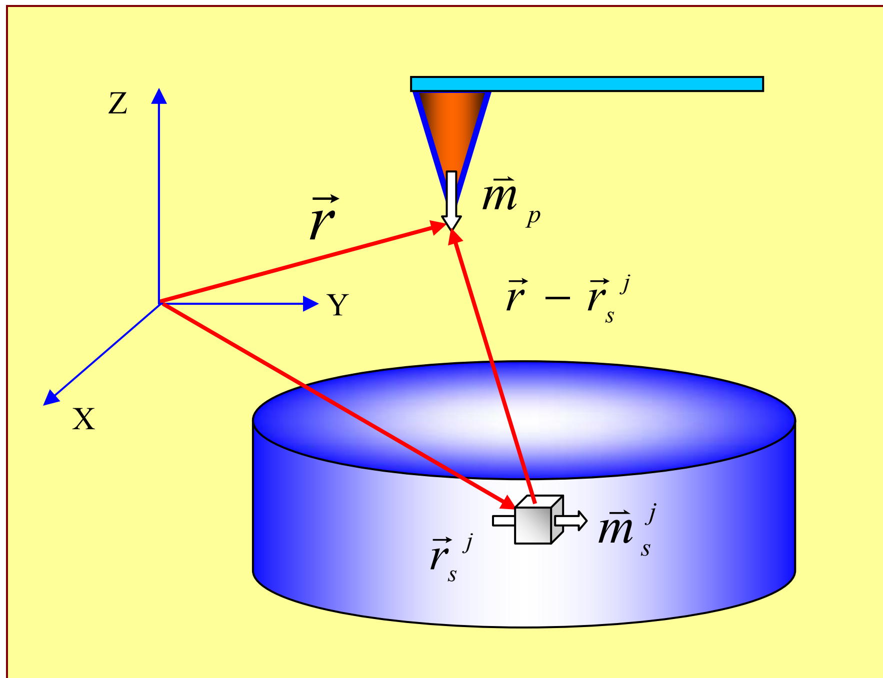

Fig. 91. Interaction of a tip with a sample in a dipole approximation

The results of modeling calculations of the MFM image for a homogeneously magnetized particle in form of an elliptic cylinder are presented on Fig. 92 as an example.

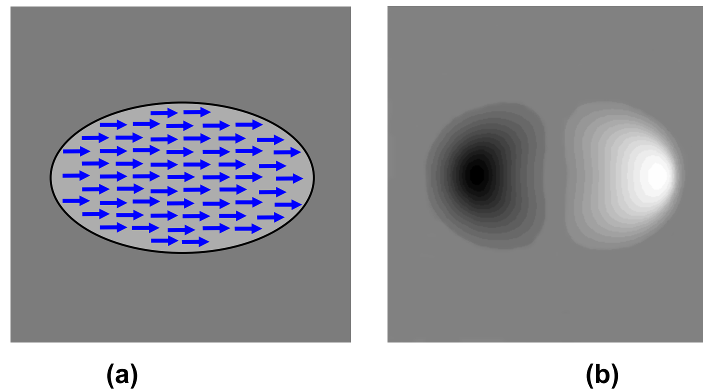

(a) (b)

Fig. 92. Modeling of the MFM image of a homogeneously magnetized particle:
(a) – magnetization distribution in a particle;
(b) – corresponding MFM image

The experimental MFM image of the organized array of magnetic particles of elliptic form is presented on Fig. 93.

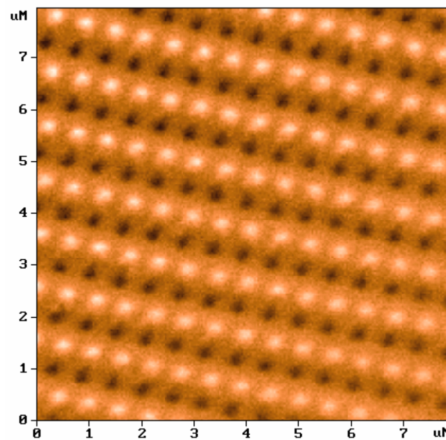

Fig. 93. The MFM image of an array of magnetic nanoparticles,
formed by the interferential laser annealing of Fe-Cr films method [Lit. 46]

AFM, EFM, MFM control system (oscillatory techniques)

The simplified circuit of the AFM, EFM, MFM control system is presented on Fig. 94. Electronic keys K1 – K5 are controlled by the voltages supplied from the output register (OR) and serve for configuration of control systems. The generator (G) forms harmonic signals for excitation of cantilever oscillations. The amplitude and frequency values of a generator signal are set with the help of a two-channel DAC-G converter. Mechanical cantilever oscillations are excited by the piezo-vibrator (PV). The amplitude and the phase of these oscillations are detected with the help of a synchronous detector (SD).

At the first stage the amplitude-frequency characteristics (AFC) and phase response (ФЧХ) of a cantilever in a free state (far from surface) are measured. For this purpose the K2 key is closed, and the sine wave voltage from the generator is applied to the piezo-vibrator and simultaneously to the synchronous detector as a base voltage. Cantilever oscillations end in that the current of the photo diode contains a variable component with the excitation frequency. With help of the DAC-G the sawtooth control voltage is formed, readjusting the frequency of the generator in the range selected by the operator. The voltage from the photo diode is amplified by the preliminary amplifier and supplied to the synchronous detector. The amplitude and the phase of a signal (synchronously with the DAC-G voltage) are recorded by the ADC in a computer memory. Then AFC and phase response are visualized on the monitor by means of computer graphics.

The AFM images of a surface in contactless and "semi-contact" modes of cantilever oscillation are formed as follows. The generator (G) sets the forced oscillation frequency of a cantilever in a vicinity of resonance. The amplitude of these oscillations is detected by the synchronous detector, and the U voltage proportional to the amplitude, is received on the input of the comparison circuit (CC). The U_0 voltage, set by the operator with help DAC-Set, is supplied to another input of the comparison circuit corresponding to the oscillation amplitude, which must be kept by the feedback system ($U_0 < U$). During feedback loop closing the scanner moves the sample towards the tip until the cantilever oscillation amplitude decreases so that the U voltage becomes equal to U_0. During sample scanning the oscillation amplitude is kept at the set level, and the control voltage in a feedback circuit is recorded as the AFM image in a computer memory. As it has been shown above, the oscillation amplitude decreases due to the AFC shift caused by a gradient of the interaction force of a tip with a surface. Therefore the AMF image obtained during sample scanning in a constant cantilever oscillation mode represents a surface of a constant force gradient, which, in absence of electric and magnetic interactions, is determined by van der Waals forces and coincides to a high accuracy with the topography of a surface. The phase of fluctuations cantilever is frequently registered simultaneously with the topography of a surface. This allows to plot AFM images of phase contrast and to analyze the elastic properties of a surface at a “semi-contact” mode of cantilever oscillations.

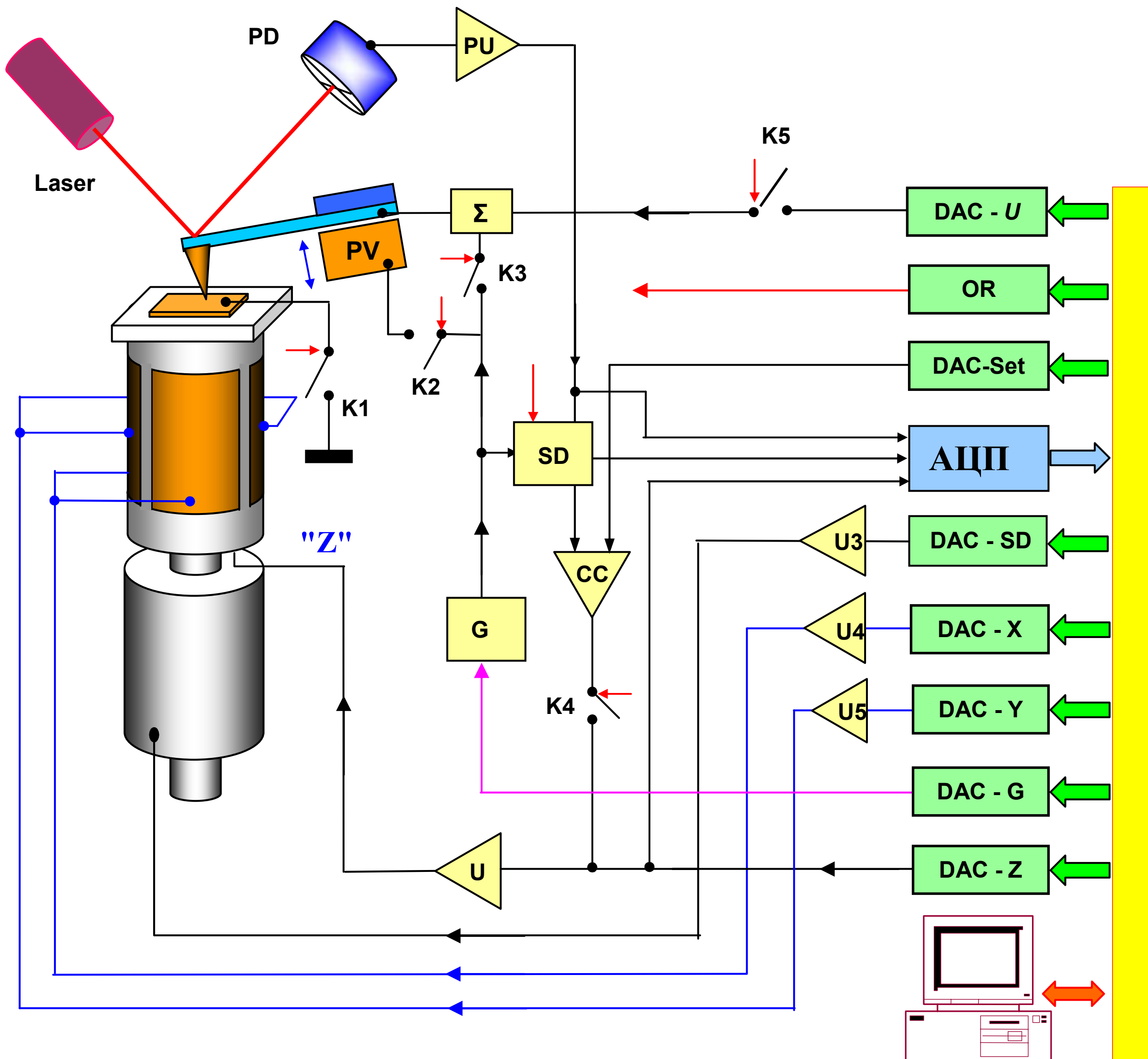

Fig. 94. Simplified schematic of the AFM, EFM, MFM control system

Research of magnetic samples is performed with the help of special tips with a magnetic coating. The two-pass technique is applied to obtain magnetic images. During the first pass the topography of a surface is registered in each scanning line in a “semi-contact” mode of cantilever oscillation. On the second pass the feedback is broken, and during scanning with help of the DAC-Z the probe is moved above a sample at some height with a trajectory repeating the topography of the given area of a surface. Since the average distance between a tip and a sample is constant in every point, changes of amplitude and phase of cantilever oscillation will be connected only to the change of a gradient of the magnetic force acting between a tip and a surface.

Application of conducting tips allows to investigate the local electric properties of samples in the EFM mode. In this case a variable voltage from the generator (G) and a constant voltage from *DAC-U* are summarized and supplied to a tip. The sample is grounded with the help of K1 key. Cantilever oscillations are excited under influence of a periodic electric force between a tip and a sample. The amplitude and the phase of oscillations with the frequency of excitation and on the double frequency are detected by the synchronous detector. The two-pass techniques also are applied during research of irregularity of electric interaction of a tip with a sample. During the first pass the topography of a given surface area is registered. On the second pass the tip moves with a trajectory corresponding to the topography, on some distance above the surface. Herewith the signal amplitude change from the photo diode on the double frequency is recoded in a computer memory as the $C_z'(x,y)$ distribution of an electric capacity derivative of a tip-sample system. For determination of a local surface potential using Calvin method the constant voltage component is changed by the *DAC-U* in every point of scanning until the oscillation amplitude with the frequency of excitation (analyzed by a computer) becomes equal to zero. The voltage corresponding to the given condition is recorded in memory for formation of the $\varphi(x,y)$ surface potential distribution file.

2.5. Near-field optical microscopy

Traditional modes of objects optical images acquisition have essential restrictions connected to the light diffraction. One of the basic laws of optics is the existence of a so-called diffraction limit that sets the minimal size *(R)* of an object, which image can be constructed by an optical system at use of a light with the λ length of a wave:

$$R \approx \frac{\lambda}{2n},$$

where n - environment index of refraction. For the optical range of wave-lengths the limit size is about 200÷300 nanometer. Other principles of object image construction are used in the near-field optical microscopy. These principles allow overcome the difficulties connected to diffraction of light and realize the spatial resolution at a level of 10 nanometers and better.

The near-field optical microscope (SNOM) was invented by Dieter Paul (IBM Laboratory, Zurich, Switzerland) in 1982 immediately after invention of a tunnel microscope. The principle of operation of this device is based on the phenomenon of light passage through sub wave diaphragms (apertures with a diameter that is much less than a wave-length of incident radiation).

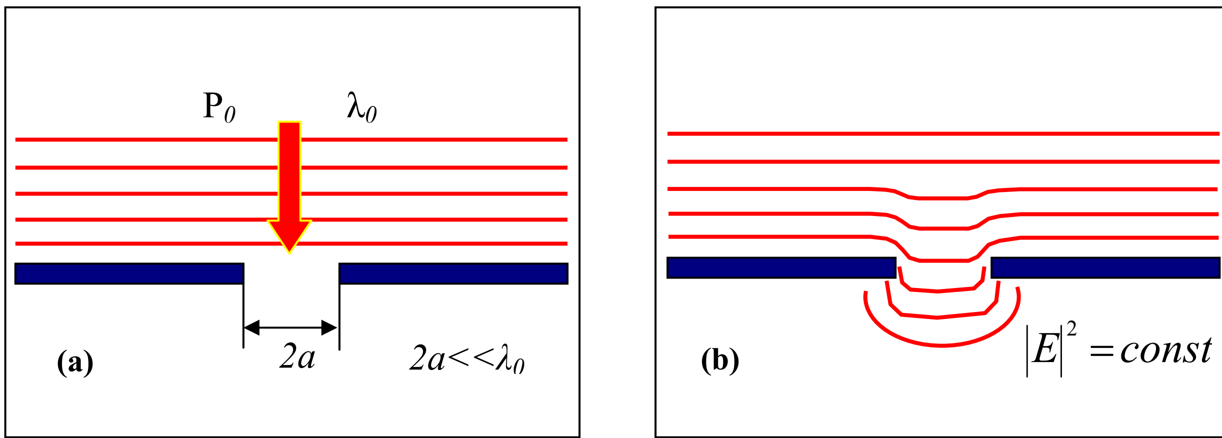

Fig. 95. (a) - Passage of light through an orifice in the screen with the sub wave aperture, (b) - Lines of constant intensity of optical radiation in sub wave aperture area

During the passage of light through a sub wave aperture a number of features are observed [Lit. 47, Lit. 48]. The electromagnetic field in the diaphragm area has a complex structure. The so-called near-field region is located directly behind an aperture within the range of Z < 100 a, where the electromagnetic field exists in general as evanescent (not propagating) modes localized near to the diaphragm surface. Within the range of Z > 100 a the far-field region is located where only radiating modes are observed. Radiation power behind a sub wave diaphragm in a far-field region can be estimated with the following formula [Lit. 48]:

$$P_{tr} = \frac{128}{27\pi} k^4 a^6 W_0 \ ,$$

where k – wave vector, W_0 – incident radiation power density. Estimations show that for radiation with a wave-length of the λ = 500 nanometers order and diaphragms with the aperture of ~ 5 nanometers the radiation power in a far-field region is about 10^{-10} order-of-magnitude of the incident radiation power. Therefore, at first sight it seems that the use of small apertures for construction of raster optical images of samples under study is practically impossible. However, if the investigated object is placed directly behind an aperture in a near-field region, then due to the interaction of evanescent modes with the sample, the part of energy of an electromagnetic field transforms into radiating modes, which intensity can be registered by an optical photodetector. Thus, the near-field image is formed during scanning of the test sample by a diaphragm with a subwave aperture and is registered as the distribution of intensity of optical radiation depending on the $I(x,y)$ diaphragm position. The SNOM images contrast is determined by processes of reflection, refraction, absorption and dispersion of light, which in turn depend on the local optical properties of a sample.

SNOM tips on the basis of an optical fiber

Currently there are several schemes of realization of a near-field optical microscope. SNOM with tips on the basis of the optical fiber representing an axially-symmetrical optical waveguide from materials with differing refractive indexes have found the widest application (Fig. 96).

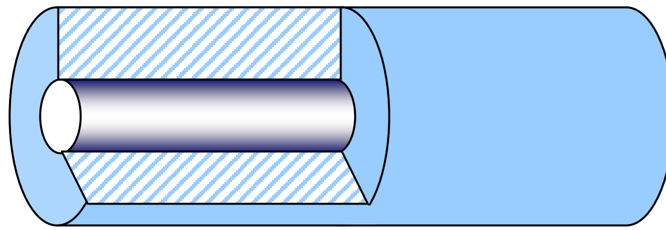

Fig. 96. Schematic drawing of an optical fiber structure

The optical fiber consists of a core and cladding. From the outside the fiber is covered by a protective layer. As a rule, the core and the cladding are made of a special quartz glass. In this case the glass that is used for cladding has a lesser refractive index than the glass for a core. (In practice the refractive index of glass is adjusted by addition elements so refractive indexes of core and cladding differ on about 1 %). Due to the phenomenon of total internal reflection, such system allows to localize optical radiation in the core area and to transport it on the big distances practically free of losses.

Tips for the SNOM are made as follows [see for example Lit. 49]. The end of an optical fiber with a removed protective layer is immersed in a solution consisting of two immiscible liquids – mixture of HF, NH4F, H2O, which is an etching agent for quartz and a liquid with lesser density (for example, toluene). Toluene settles down atop the etching agent and serves for formation of a meniscus on the “toluene-etching agent-fiber” border (Fig. 97 (a)). According to the etching the thickness of fiber decreases, resulting in reduction of a meniscus height. As a result, formation of a cone-shaped apex on the end of a fiber occurs during process of etching (Fig. 91 (b)). This apex has characteristic sizes of less than 100 nanometers. Then the apex of the tip is coated with a thin layer of metal. The overcoating is made by vacuum spraying at the angle of about 30º to the fiber axis so that the small aperture area remains uncovered on the apex in the shadow area. This area is the near-field source of radiation. The optimum angle at the apex of the tip is about 20º.

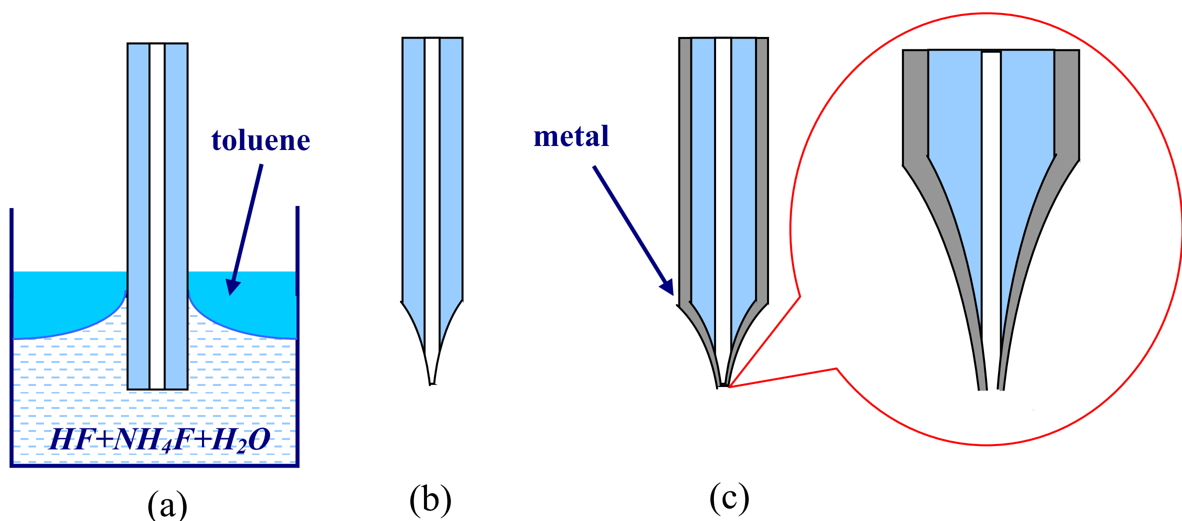

Fig. 97. Manufacturing of SNOM tips on the basis of an optical fiber:

(a) - chemical etching of fiber;
(b) – appearance of a fiber apex after etching;
(c) –thin metal film evaporation.

"Shear-force" mode of monitoring of tip–surface distance in a near-field optical microscope

During SNOM operation it is necessary to keep the tip above a surface on distances of about 10 nanometers and less. There are various solutions of the given problem; however the prevailing solution uses the SNOM with a so-called "shear force" mode of monitoring of a tip-sample distance.

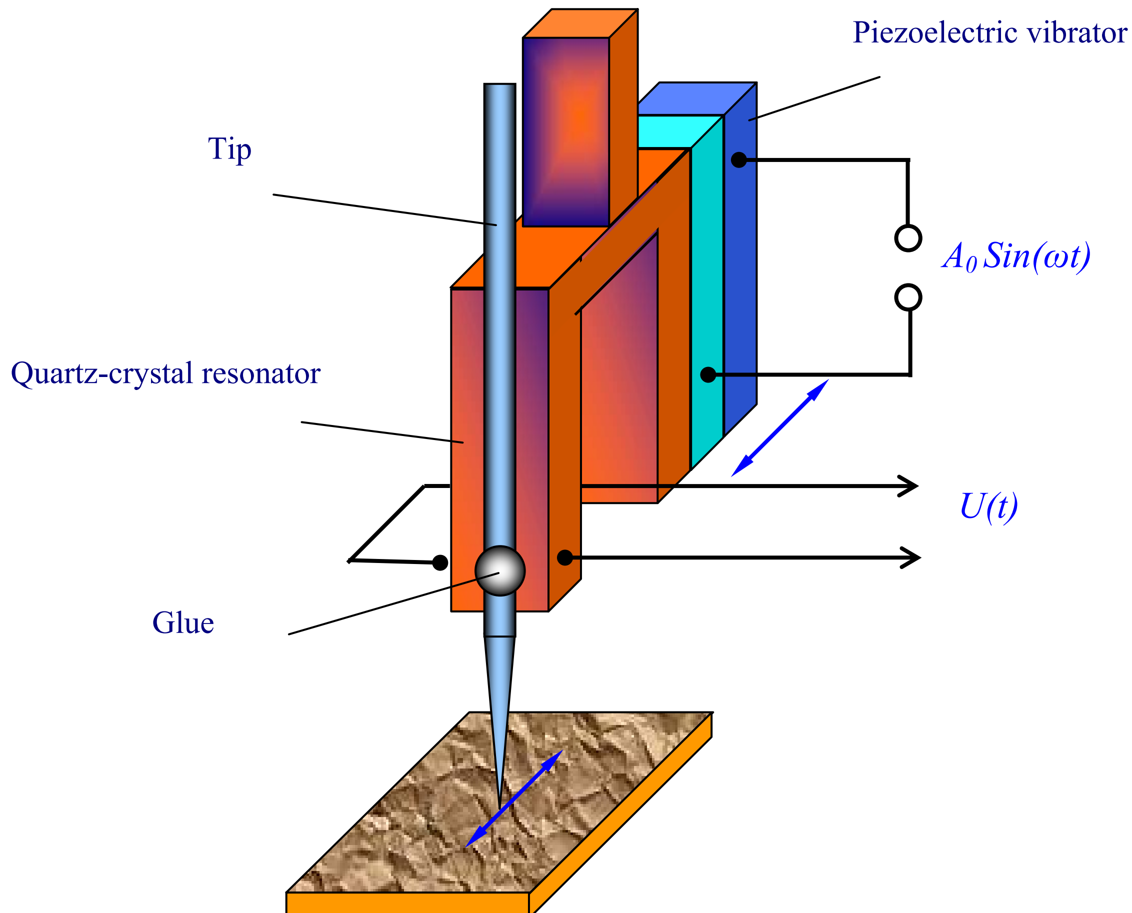

Fig. 98. "Shear-force" scheme of a tip-surface distance probe on the fork basis

Most often the "shear-force" control circuits using piezoelectric transducer are applied on the fork basis (Fig. 98). The SNOM tip is fixed to the quartz-crystal resonator with the glue. The forced oscillations of a fork with a frequency close to the resonant frequency of a "tip-quartz resonator" system are induced by an additional piezoelectric vibrator. Thus the tip makes oscillatory movements in parallel with the surface of a sample. Measurement of the interaction force of a tip with a surface is made by registration of a change of amplitude and phase of bending vibrations of the quartz-crystal resonator with the excitation frequency (with respect to the U (*t*) voltage variable component on the resonator electrodes). The theory of "shear force" control is complex enough, so here we come to nothing more than only qualitative reasons. During approach of a tip to a sample several effects are observed. Firstly, the additional dissipative interaction of a tip with a surface appears due to the forces of viscous friction (in a thin layer of air adjoining to the surface and in a thin layer of adsorbed molecules on a surface of a sample).

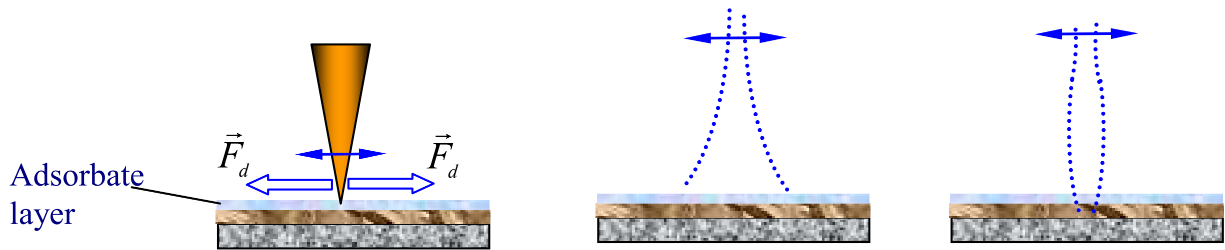

Fig. 99. Dissipative forces affecting the tip, and change of an oscillations mode of the tip near to the surface of a sample

This results in reduction of the quality of system, and consequently, to reduction of the amplitude of oscillations and widening of the amplitude-frequency characteristic and the phase response of the tip-resonator system on the resonance frequency. Secondly, the change of an oscillations mode in the tip-resonator system occurs at small tip-surface distances. The oscillation mode in a free state corresponds to oscillations of a rod with a free end, while at approach with a sample (in extreme case - at a contact of the tip with a surface) it transforms into oscillations of a rod with a fixed end. It results in increase of the resonance frequency in the tip-resonator system, i.e. the amplitude-frequency characteristic shift towards higher frequencies. These phenomena were experimentally observed in works [Lit. 50, Lit. 51]. Changes of amplitude and phase of bending vibrations in the tip-resonator system are used as feedback signals for control of the tip-surface distance in near-field optical microscopes.

SNOM configurations

Several constructive circuits of a near-field optical microscope are used [Lit. 52] in practice. Main SNOM configurations are shown schematically on Fig. 100. The circuit in which optical radiation of the laser is localized in space by a fiber tip is realized most often. Such circuit allows to receive the maximal emission power in the subwave aperture area and allows to investigate the samples both on reflection (Fig. 100 (a)), and on gleam (Fig. 100 (b)). The emission reflected from a sample or passed through a sample is gathered on a photodetector by a focusing mirror or a lens to increase the sensitivity. Besides that, this SNOM configuration is widely used in near-field optical lithography experiments.

In experiments, when high levels of optical pumping are required (as for example during research of local nonlinear properties of samples), a scheme is realized, in which powerful laser radiation is directed on a research structure, and reception is performed by a near-field tip (Fig. 100 (c), (d)).

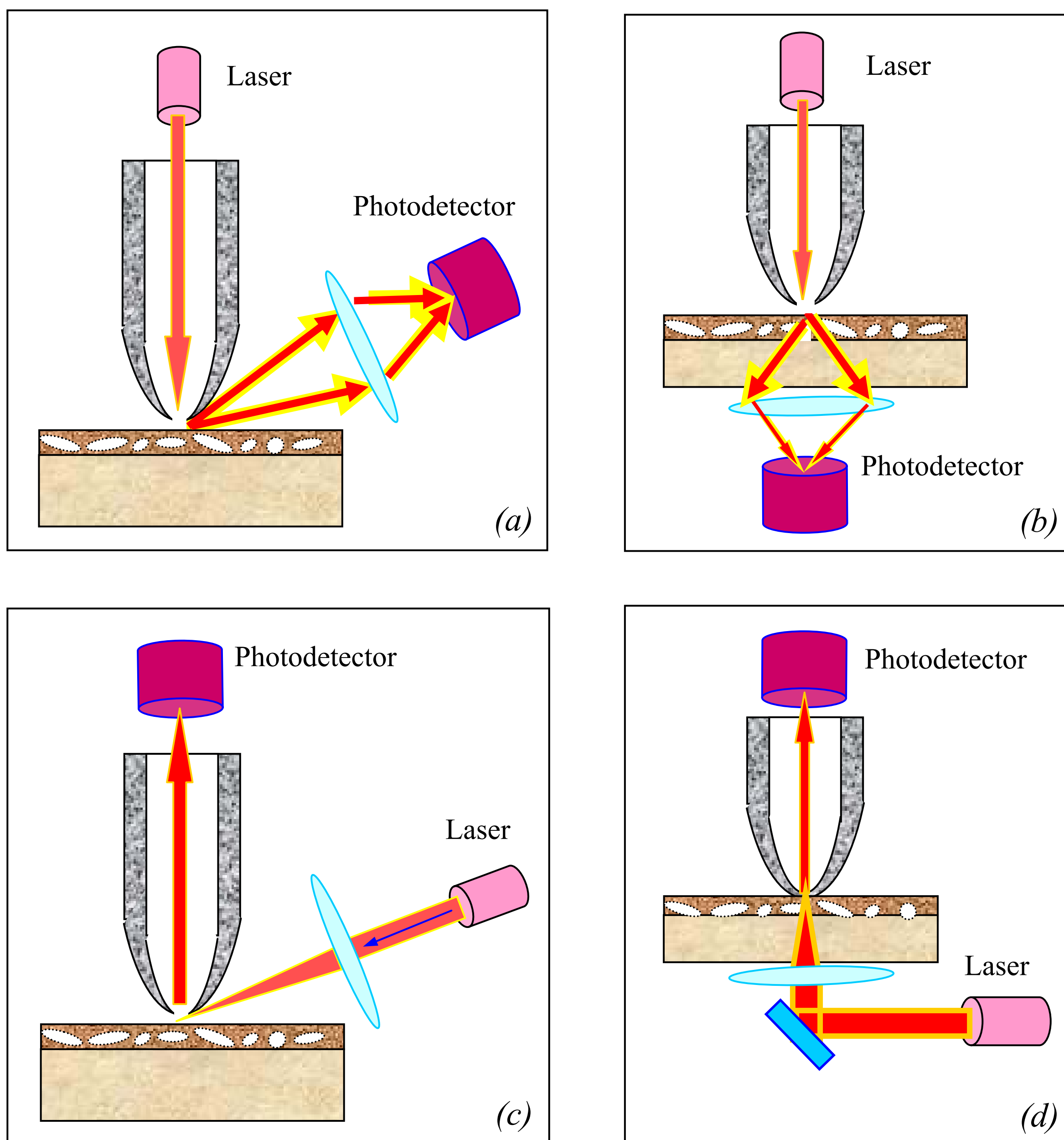

Fig. 100. Possible configurations of a near-field optical microscope

The AFM/SNOM image of the InAs/GaAs semi-conductor structure with quantum dots acquired by a microscope working on the scheme shown on Fig. 100 (a) [Lit. 12] is presented as an example on Fig. 101. The HeCd laser (λ = 442 nanometers) was used in the experiment. The near-field optical image of a sample represents the accumulation of the radiation reflected from a surface of the sample and the luminescent emission that corresponds to the transition between levels of dimensional quantization in InAs dots.

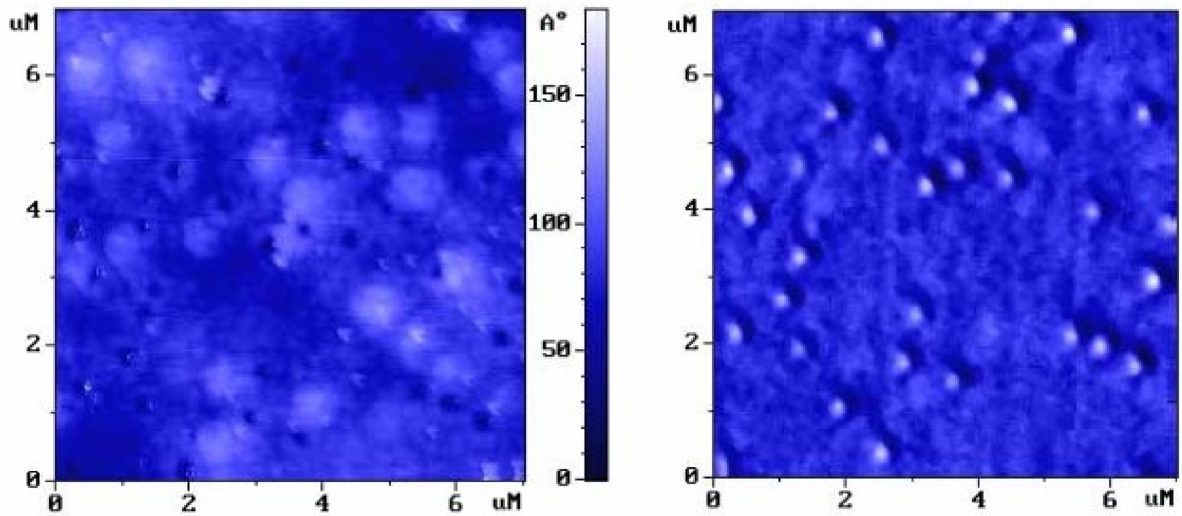

Fig. 101. “Shear force” AFM image of the topography of a surface (left) and the near-field optical image of a sample with InAs quantum dots (right) [Lit. 12]

Challenging, but a less widespread scheme, where excitation of the structure and reception of the near-field emission are carried out through the tip of a microscope, is presented on Fig. 102.

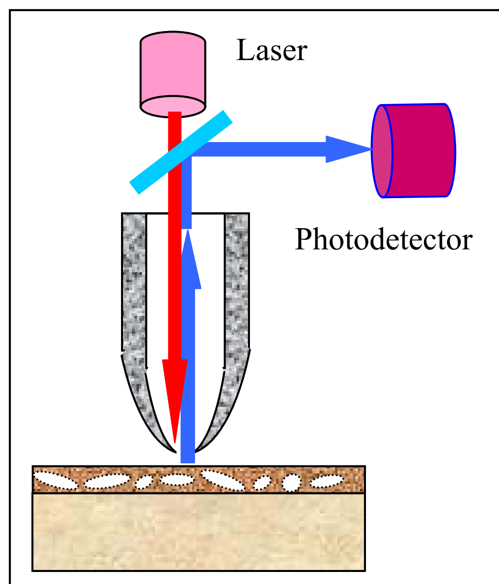

Fig. 102. The SNOM scheme where light-striking of a sample and reception of emission are carried out by the same tip

Such combination of a near-field source with a near-field receiver is rather a promising method providing very high spatial resolution. However, in the emission passes twice in this scheme through a subwave aperture. As a result, the signal coming on a photodetector has a very low intensity, and hence high-sensitivity methods of its registration are required. Integration of the SNOM with an optical monochromator allows to carry out local spectroscopic researches of samples. The basic fields of application of near-field optical microscopes are the research of local optical and photoelectric properties of semi-conductor photosensitive structures, research of biological objects, nanotechnology.

Conclusion

Thus, fundamentals of the scanning probe microscopy – one of the advanced methods of research of surface properties are briefly stated in this study guide. Principles of operation of the basic types of probe microscopes, most widely used in scientific researches, are described (scanning tunnel microscope, atomic-force microscope, electro-force microscope, magnetic-force microscope, near-field optical microscope). Unfortunately, there is a number of other devices working on the STM principles left outside the scope of this book, and a big number of research techniques with application of probe microscopes.

Partial the concept of the STM development basic stages can be acquired from the chronological table [Lit. 53] that is shown on the next page of the book. Today the scanning probe microscopy is a rapidly developing surface research technique with the high spatial resolution and is the powerful tool for the solution of nanotechnology problems – technology of creation of submicronic instrument structures.

Basic stages of STM development

1981 - Scanning tunnel microscopy. G. Binnig, H Rohrer.
The atomic resolution on conducting samples.

1982 - Scanning near-field optical microscope. D. W. Pohl.
The resolution of 50 nanometers in the optical image of a surface.

1984 - Scanning capacitive microscope. J. R. Matey, J. Blanc.
The resolution of 500 nanometers in the capacitive image is realized.

1985 - Scanning thermal microscope. C. C. Williams, H. K. Wickramasinghe.
The resolution of 50 nanometers in the thermal image of a surface.

1986 - Atomic-force microscope. G. Binnig, C. F. Quate, Ch. Gerber.
The atomic resolution on non-conducting (and conducting) samples.

1987 - Magnetic-force microscope. Y. Martin, H. K. Wickramasinghe.
The resolution of 100 nanometers in the magnetic image of a surface.
- Microscope on friction forces. C. M. Mate, G. M. McClelland, S. Chiang.
The image of lateral forces on nuclear scales.
- Electric force microscope. Y. Martin, D. W. Abraham, H. K. Wickramasinghe.
Detecting of unit charges on a surface of samples.
- Non-elastic tunnel STM spectroscopy. D. P. E. Smith, D. Kirk, C. F. Quare.
Registration of phonon spectra of molecules in STM.

1988 - Microscope on the basis of ballistic emission of electrons. W. J. Kaiser.
Research of Schottky barriers with nanometer resolution.
- Inverted photoemissive microscope.
J. H. Coombs, J. K. Gimzewski, B. Reihl J. K. Sass, R. R. Schlittler
Registration of luminescence spectra on nanometer scales.

1989 – Near-field acoustic microscope.
K. Takata, T. Hasegawa, S. Hosaka, S. Hosoki. T. Komoda
Low-frequency acoustic measurements with the resolution of 10 nanometers.
- Scanning noise microscope. R. Moller A. Esslinger, B. Koslowski.
Registration of a tunnel current without applying of voltage.
- Scanning microscope recording spin precession.
Y. Manassen, R. Hamers, J. Demuth, A. Castellano.
Visualization of spin in a paramagnetic with the resolution of 1 nanometer.
- Scanning microscope on ionic conductivity.
P. Hansma, B. Drake, O. Marti, S. Gould, C. Prater.
Reception of the image of a surface in electrolyte with the resolution of 500 nanometers.
- Scanning electrochemical microscope.
O. E. Husser, D. H. Craston, A. J. Bard.

1990 - Microscope recording changes of chemical potential.
C. C. Williams, H. K. Wickramasinghe

- STM recording photo-e.m.f. R. J. Hamers, K. Markert.
Registration of distribution of photo-e.m.f. with nanometer resolution.

1991 - Scanning tip microscope based on Calvin method.
N. Nonnenmacher, M. P. O'Boyle, H. K. Wickramasinghe.
Measurements of surface potential with the resolution of 10 nanometers.

1994 – Nonaperturate near-field optical microscope.
F. Zenhausern, M. P. O'Boyle, H. K. Wickramasinghe.
Optical microscopy with the resolution of 1 nanometer.

REFERENCES

- Lit. 1. D. Sarid - "Exploring scanning probe microscopy with "Mathematica"", John Wiley& Sons, Inc., New York, 1997, 262 p.
- Lit. 2. V.I. Panov – Scanning tunnel microscopy and spectroscopy of a surface. // UPS, vol.155, # 1, p. 155 – 158 (1988).
- Lit. 3. V. S. Edelman – Scanning tunnel microscopy. // Pribory i tehnika eksperimenta (Devices and technical equipment of experiment), # 5, p. 25 – 49 (1989).
- Lit. 4. V. S. Edelman – Development of scanning tunnel and force microscopy. // Pribory i tehnika eksperimenta (Devices and technical equipment of experiment), # 1, p. 24 – 42 (1991).
- Lit. 5. S. N. Magonov – Scanning force microscopy of polymers and related materials. // Vysokomolekulyarnye soedineniya (High-molecular compounds), vol. 38, # 1, p. 143 – 182 (1996).
- Lit. 6. V. A. Bykov, M. I. Lazarev, S. A. Saunin - Scanning probe microscopy for a science and industry. // Elektronika: nauka, tehnologiya, biznes (Electronics: science, technology, business), # 5, p. 7 – 14 (1997).
- Lit. 7. “Scanning probe microscopy of biopolymers” (Edited by I. V. Jaminskiy), M.: Nauchnyy mir (“Scientific world”), 1997, 86 p.
- Lit. 8. A.P.Volodin – New in scanning microscopy. // Pribory i tehnika eksperimenta (Devices and technical equipment of experiment), # 6, p. 3 – 42 (1998).
- Lit. 9. V.K.Nevolin – “Fundamentals of tunneling probe nanotechnology”: Textbook, Moscow, MGIET (TU), 1996, 91 p.
- Lit. 10. S.A.Rykov – “Scanning probe microscopy of semi-conductor materials and nanostructures”, SpB, Nauka, 2001, 53 p.
- Lit. 11. R.Z.Bahtizin, R.R.Galljamov – “Physical fundamentals of the scanning probe microscopy”, Ufa, RIO BashGU, 2003, 82 p.
- Lit. 12. Internet site of "NT-MDT" company: http: // www.ntmdt.ru/
- Lit. 13. Internet site of teaching and scientific centre “Bionanoskopiya”: http: // www.nanoscopy.org

- Lit. 14. G.Binnig, H.Rohrer - Scanning tunneling microscopy. // Helvol. Phys. Acta, vol. 55, # 6, p. 726 – 735 (1982).
- Lit. 15. G. Binnig, H. Rohrer, Ch. Gerber, E. Weibel - Tunneling through a controllable vacuum gap. // Appl. Phys. Lett., vol. 40, p. 178 (1982).
- Lit. 16. “Ultrasound. The small encyclopedia”. (Edited by I. P. Goljamina) // M.: “Sovetskaya entsiklopediya”, 1979, 400 p.
- Lit. 17. P.M. Williams, K.M. Shakesheff et al. – Blind reconstruction of scanning probe image data. // J. Vac. Sci. Technol. B 14 (2) p. 1557-1562 (1996).
- Lit. 18. A.A. Buharaev, N.V. Berdunov, D.V. Ovchinnikov, K.M.Salihov – “SFM metrology of micro- and nano-structures”. // Mikroelektronika (“Miscroelectronics”), vol. 26, # 3, p. 163-175 (1997).
- Lit. 19. D.I. Blohintsev – “Fundamentals of quantum mechanics”, Moscow, Nauka, 1983.
- Lit. 20. L. D. Landau, E.M.Lifshits – "Theoretical physics, vol. 3 - Quantum mechanics ", M.: "Fizmatlit", 2001, 804 p.
- Lit. 21. J.G.Simons – Generalized formula for the electric tunnel effect between similar electrodes separated by a thin insulating film // J. Appl. Phys., 34, 1793 (1963).
- Lit. 22. J.G.Simons-Electric tunnel effect between dissimilar electrodes separated by a thin insulating film // J. Appl. Phys., 34, 2581 (1963).
- Lit. 23. J. Tersoff and D. R. Hamann – Theory and application for scanning tunneling microscope. // Phys. Revol. Lett. vol. 50, p. 1998-2001 (1983).
- Lit. 24. J. Tersoff and D. R. Hamann - Theory of the scanning tunneling microscope. // Phys. Revol. B, vol. 31 (2), 805-813 (1985).
- Lit. 25. J. Tersoff – Method for the calculation of scanning tunneling microscope images and spectra. // Phys. Revol. B, vol. 40 (17), 11990-11993 (1989).
- Lit. 26. G.E.Pikus – “Fundamentals of the theory of semi-conductor devices”, M.: Nauka, 1965, 448 p.
- Lit. 27. C.B.Duke - "Tunneling in solids", Academic Press, New York, 1969, 353 p.

- Lit. 28. “Tunnel phenomena in solid bodies”, edited by E. Burnshtejn and S. Lundkvist. Moscow, Mir, 1973, 422 p.
- Lit. 29. R.M.Feenstra, V.Ramachandran, H.Chen – “Recent development in scanning tunneling spectroscopy of semiconductor surfaces”. // Appl. Phys., A 72, p. 193 – 199 (2001).
- Lit. 30. A.Rouz-Ins, E.Rederik “Introduction in physics of superconductivity”, M.: Mir, 1972, 272 p.
- Lit. 31. G.Binnig, C.F.Quate, Ch. Gerber – “Atomic force microscope”. // Phys. Revol. Lett., vol. 56, #9, p. 930 – 933 (1986).
- Lit. 32. J.S.Barash – “Van der Waals forces”, M: Nauka, 1988, 344 p.
- Lit. 33. M.Saint Jean, S.Hudlet, C.Guthmann, J.Berger – “Van der Waals and capacitive forces in atomic force microscopies”. // J. Appl. Phys., vol. 86 (9), p. 5245 – 5248 (1999).
- Lit. 34. I.A. Birger, B.F. Shorr, G.B. Iosilevich – “Calculation on strength of details of machines”. // M.: Mashinostroenie, 1979, 702 p.
- Lit. 35. S.N.Magonov, V.Elings, M.-H.Whangbo – “Phase imaging and stiffness in tapping-mode atomic force microscopy”. // Surf. Sci., 375, L385 – L391 (1997).
- Lit. 36. J.P. Cleveland, B. Anczykowski, A.E. Schmid, V.B. Elings – “Energy dissipation in tapping-mode atomic force microscopy”. // Appl. Phys. Lett. V. 72 (20), 2613 – 2615 (1998).
- Lit. 37. J.Tamayo, R.Garcia – “Relationship between phase shift and energy dissipation in tapping-mode atomic force microscopy”. // Appl. Phys. Lett. V. 73 (20), 2926 – 2928 (1998).
- Lit. 38. J.Tamayo – “Energy dissipation in tapping-mode atomic force microscopy with low quality factors”. // Appl. Phys. Lett. V. 75 (22), 3569 – 3571 (1999).
- Lit. 39. J.R.Matey, J.Blanc – “Scanning capacitance microscopy”. // J. Appl. Phys., vol. 57, # 5, p. 1437 – 1444 (1985).
- Lit. 40. M.Nonnenmacher, M.P.O'Boyle, H.K.Wikramasinghe – “Kelvin probe force microscopy”. // Appl. Phys. Lett., 58 (25), 2921 – 2923 (1991).
- Lit. 41. B. Stiller, P. Karageorgiev, et al. – “Scanning Kelvin microscopy as a tool for visualization of optically induced molecular switching in azobenzene self assembling films”. // Surf. Interface Anal. 30, 549-551, (2000).

- Lit. 42. Y. Martin and H. K. Wickramasinghe – “Magnetic imaging by "force microscopy" with 1000 Å resolution”. // Appl. Phys. Lett. vol. 50, # 20, p. 1455-1457 (1987).

- Lit. 43. D.Rugar, H.Mamin, P.Guethner et al. – “Magnetic force microscopy: General principles and application to longitudinal recording media”. // J. Appl. Phys., vol. 68, # 3, p.1169 – 1182 (1990).

- Lit. 44. I.E.Tamm – "Fundamentals of the electricity theory", M.: Nauka, 1976, 616 p.

- Lit. 45. L.D.Landau, E.M.Lifshits - "Theoretical physics vol. 2 – field theory ", M.: "Nauka", 1973, 504 p.

- Lit. 46. A.M. Alexeys, J.V.Verevkin, N.V.Vostokov, V.N.Petrjakov, N.I.Polushkin, A.F.Popkov, N.N.Salashchenko – “Observation of laser-induced local modifications of the magnetic order in layers of transitive metals” // Letters in JETPh, 73, 214 (2001).

- Lit. 47. D.W.Pohl, W.Denk, M.Lanz – “Optical spectroscopy: image recording with resolution λ/20”. // Appl. Phys. Lett., vol. 44, p. 651 – 653 (1984).

- Lit. 48. U.Durig, D.W.Pohl, F.Rohrer – “Near-field optical-scanning microscopy”. J.Appl. Phys. 593318-3327, 1986.

- Lit. 49. V.F.Drjahlushin, A.J.Klimov, V.V.Rogov, S.A.Gusev – “Scanning near-field optical microscope probe”. // Pribory i tehnika eksperimenta (Devices and technical equipment of experiment), # 2, p. 138-139 (1998).

- Lit. 50. P.K.Wei, W.S.Fann – “The probe dynamics under shear force in near-field scanning optical microscopy”. // J. Appl. Phys., vol. 83, # 7, p. 3461 – 3468 (1998).

- Lit. 51. D.G.Volgunov, A.V.Buryukov, S.V.Gaponov, V.L.Mironov – “Probe - surface interaction in the piezo-resonator "shear force" microscope”. // Physics of Low – Dimensional Structures, # 3/4, p. 17-23 (2001).

- Lit. 52. D.Courjon, C.Bainier – “Near field microscopy and near field optics”. Rep. Prog. Phys. 57, p. 989 – 1028, (1994).

- Lit. 53. H.K.Wickramasinghe – “Progress in scanning probe microscopy”. // Acta materialia, 48, p. 347-358 (2000).